UAV-Enabled Wireless Powered Communication Networks

Saif Najmeddin

A Thesis

in

The Department

of

Electrical and Computer Engineering

Presented in Partial Fulfillment of the Requirements

For the Degree of

Doctor of Philosophy (Electrical and Computer Engineering) at

Concordia University

Montréal, Québec, Canada

September 2021

CONCORDIA UNIVERSITY

Division of Graduate Studies

This is to certify that the thesis prepared

By: **Saif Najmeddin**

Entitled: **UAV-Enabled Wireless Powered Communication Networks**

and submitted in partial fulfilment of the requirements for the degree of

Doctor of Philosophy (Electrical and Computer Engineering)

complies with the regulations of this University and meets the accepted standards with respect to originality and quality.

Signed by the final examining committee:

_____ Dr. Chun-Yi Su

_____ Dr. Ha Nguyen

_____ Dr. Amr Youssef

_____ Dr. Wahab Hamou-Lhadj

_____ Dr. Dongyu Qiu

_____ Dr. Sonia Aïssa

_____ Dr. Sofiène Tahar

Approved by _____

Dr. Yousef R. Shayan, Chair of the ECE Department

August 24, 2021 _____

Dr. Mourad Debbabi, Dean, Faculty of Engineering and Computer Science

ABSTRACT

UAV-Enabled Wireless Powered Communication Networks

Saif Najmeddin, Ph.D.

Concordia University, 2021

Unmanned aerial vehicles (UAVs), popularly known as drones, have emerged as a promising solution for providing reliable and cost-effective wireless communications. The use of UAVs as aerial wireless power transmitters (UAV-WPT), with additional flexibility and 3D mobility, is expected to provide efficient wireless power supplies to low-power and hard-to-reach devices. Due to their adjustable altitude and mobility, efficient line-of-sight (LoS) between UAVs and ground nodes (GNs) could be established, thus mitigating signal blockage and shadowing. Based on this feature, UAVs can be good candidates to charge battery-limited or hard-to-reach devices through radio frequency (RF) wireless power transfer (WPT), which will significantly improve the wireless charging efficiency compared to conventional ground charging stations at fixed locations. Although the deployment of UAVs as wireless power transmitters is promising, it comes with many design challenges and reliability problems. For instance, the energy efficiency (EE) of UAVs requires careful consideration as it significantly impacts the performance of UAV-WPT systems. Thus, there is a need for a comprehensive framework to optimize such networks, where the devices are wirelessly powered via UAVs to enable uplink data transmission. In this thesis, we propose a detailed methodology to optimize the performance of the UAV-enabled WPT networks with different topologies and applications. We provide the required steps to be

followed for most applicable networks, where specific considerations have to be considered for each case. The optimization problem's solution has two main steps; firstly, the path loss of the air-to-ground channels is minimized by optimizing the UAV position depending on the GNs' service demands. Secondly, using the optimized positioning and a closed-form expression for the EE, a resource allocation aiming to maximize EE is developed using Lagrangian optimization and gradient-descent methods.

We present five different system models, which reflect different practical cases and setups considering single and multiple UAV scenarios. These models are: UAV-enabled wireless powered communications network (UAV-WPCN), UAV-enabled wireless information and power transfer network (UAV-WIPT), UAV-enabled simultaneous wireless information and power transfer network (UAV-SWIPT), multiple UAV-enabled wireless powered communications network (UAVs-WPCN), and multiple UAV-enabled simultaneous wireless information and power transfer network (UAVs-SWIPT). The results of applying the proposed scheme show significant enhancement in the EE for the non-orthogonal multiple access (NOMA) scheme compared to the orthogonal multiple access (OMA) scheme in most of the scenarios. However, the topology and distribution of the ground nodes play a vital role in figuring out the suitable access scheme to be used, where OMA or hybrid NOMA/OMA schemes could perform better.

In loving memory of my father, grandfather and grandmother,

To my mother Saeda,

To my brother Samer,

To my wife Sundos,

To my little man Bassel.

ACKNOWLEDGEMENTS

In the name of Allah, the Most Gracious and the Most Merciful.

All praises to Allah and His blessing for the completion of this thesis. I thank God for all the opportunities, trials and strength that have been showered on me to finish writing the thesis. Indeed, my prayer, my rites of sacrifice, my living and my dying are for Allah, Lord of the worlds. My humblest gratitude to the holy Prophet Muhammad (Peace be upon him) whose way of life has been a continuous guidance for me.

First, I would like to thank my supervisors, Dr. Sonia Aïssa and Dr. Sofiène Tahar, for their help, guidance and continuous support throughout my PhD thesis. Their insights and deep research expertise have strengthened this work significantly. I really appreciate their great efforts during my PhD journey, I have learned a lot from my discussions with them. I would like to express my gratitude to Dr. Ha Nguyen for accepting to serve as my external PhD thesis examiner. I am sincerely grateful to Dr. Amr Youssef, Dr. Dongyu Qiu, and Dr. Wahab Hamou-Lhadj for serving on my advisory thesis committee.

Many thanks to my friends and colleagues at the Hardware Verification Group (HVG) and INRS, especially Mahmoud Masadeh, Hassnaa Elderhalli, Yassmeen Elderhalli, Mbarka Soualhia, Alain Aoun, and Ali Bayat, for being kind and supportive. Their company has made my journey fruitful and unforgettable. I would also like to thank my friends in Palestine, Saudi Arabia and Canada for being caring, supportive and encouraging.

I am deeply grateful to my mother; without her continuous and unconditional love and support, I could not reach this milestone in my life. I am also thankful

to my father, who passed away during my PhD, and to my grandmother, who also passed away during my PhD; she was like my mother and I am profoundly missing her. I would sincerely like to thank my wife, Sundos, for her love, encouragement and patient throughout my PhD study. I am also grateful to my grandfather, my brother Samer and his kids, my father-in-law, my mother-in-law and my friend Suhaib for their endless love and support.

I can't also forget my brothers and sisters in Palestine who are still resisting the Zionist occupation. My deepest gratitude goes to each one of them; their sacrifice and dignity keep me always strong, focused and proud.

TABLE OF CONTENTS

List of Figures

LIST OF ACRONYMS

3D	Three Dimensions
5G	Fifth Generation
A2G	Air to Ground
AF	Amplify and Forward
AS	Access Scheme
BPP	Binomial Point Process
BS	Base Station
CSI	Channel State Information
D2D	Device to Device
EE	Energy Efficiency
EH	Energy Harvesting
ER	Energy Receiver
FAA	Federal Aviation Administration
FDMA	Frequency Division Multiple Access
G2A	Ground to Air
G2G	Ground to Ground
GN	Ground Node
HAP	High Altitude Platform
HDNUO	Hybrid Downlink NOMA Uplink OMA
HDOUN	Hybrid Downlink OMA Uplink NOMA
IR	Information Receiver
IoT	Internet of Things
KKT	Karush-Kuhn-Tucker

LAP	Low Altitude Platform
LoS	Line of Sight
LTE	Long Term Evolution
MEC	Mobile Edge Computing
MRC	Maximum Ratio Combining
MIMO	Multiple Input Multiple Output
MUAV	Multiple UAVs
NLoS	Non-Line of Sight
NOMA	Non-Orthogonal Multiple Access
OMA	Orthogonal Multiple Access
PR	Power Receiver
PT	Power Transmitter
QoS	Quality of Service
RF	Radio Frequency
ROI	Region of Interest
SINR	Signal to Interference plus Noise Ratio
SNR	Signal to Noise Ratio
SWIPT	Simultaneous Wireless Information and Power Transfer
SIC	Successive Interference Cancellation
TDMA	Time Devision Multiple Access
UAV	Unmanned Aerial Vehicle
UE	User Equipment
ULI	User Location Information
WET	Wireless Energy Transfer
WIT	Wireless Information Transfer

WIPT	Wireless Information and Power Transfer
WPCN	Wireless Powered Communication Network
WPT	Wireless Power Transmitter

Chapter 1

Introduction

In this chapter, we first present the motivation of this PhD thesis and the problem statement. Then, we explain the basic concepts and components of the UAV-based wireless networks. We present the most relevant related work, followed by our proposed methodology to achieve the primary goal of this thesis. Finally, we outline the main contributions and the organization of this thesis.

1.1 Motivation

Unmanned aerial vehicles (UAVs), with their high agility and affordable cost, have been receiving significant attention for many applications, including weather forecasting, traffic control, cargo transport, site fire detection, emergency and rescue situations, and communication systems [1]. Multiple reports from the federal aviation administration (FAA) showed that the number of UAVs will be increasing rapidly in the coming years [2].

In general, UAVs can be classified according to their altitudes: high altitude platforms (HAPs) and low altitude platforms (LAPs) [3]. HAPs have altitudes around 20 km and are typically quasi-stationary with long endurance. On the other hand, LAPs can fly at altitudes up to a few kilometers, with more flexible and fast deployment, however, with shorter flying time [4]. Another classification of the UAVs is based on their types, i.e., fixed-wing and rotary-wing UAVs. Fixed-wing UAVs have more weights, higher speed, and have to move forward in order to maintain their flying heights. In contrast, rotary-wing can hover and remain stationary for a specific time over a given area [5].

For each application, a suitable type of UAV has to be chosen to meet many requirements imposed by the application, environment, and governmental regulations [6]. Actually, different factors like UAV capabilities, velocity, and flying altitudes, need to be taken into account for various applications. Among the wide range of applications enabled by UAVs, their use for different communication applications is predicted to be an essential part in wireless systems of the future [7]. Along with massive multiple-input multiple-output (MIMO), energy harvesting (EH), and millimeter wave (mmWave) communications, it is expected that the use of UAVs will be one of the most important concepts for the upcoming fifth generation (5G) and beyond, where high data rates shall be provided with better reliability, lower latency, and decreased power consumption compared to the state-of-the-art [8]. With the rise of online shopping and the introduction of new distance working environments, the use of UAVs has emerged as a promising solution for providing reliable and cost-effective transportation, monitoring, and communication activities. For wireless communication applications, the use of UAVs has gained a tremendous attention for its appealing and flexible solutions [9]. UAV-based aerial base stations can be deployed to enhance

the wireless capacity and coverage at temporary events or hotspots, such as sport stadiums and outdoor events [10]. In some regions or countries, deploying UAVs is highly beneficial as it removes the need for expensive towers and infrastructure deployment that terrestrial cellular systems consume [11]. Drones can also be operated as aerial user equipments (UEs), known as cellular-connected UAVs, along with ground users. They can also be used in public safety scenarios to support disaster relief activities and to enable communications when conventional terrestrial networks are damaged [12]. Another important application of UAVs is in the context of Internet of Things (IoT) [13], in which the devices have small transmit power and may not be able to communicate over a long range [14]. Moreover, UAVs can be efficiently used as wireless power transmitters (WPT) for battery-limited or hard to reach devices [15]. The global UAV payload market, including all types of equipment used by UAVs such as sensors, cameras, communications equipment, and all other devices, is expected to expand rapidly in the coming few years [16]. Therefore, the interest from the academia and industry in UAV-based solutions has become significant. A substantial number of research projects have studied many different aspects and details related to the UAV-based networks [17]. Moreover, many large corporations started testing UAVs on their platforms. For instance, the possibility of deploying HAP-UAVs for Internet connectivity in remote areas has been investigated by Facebook and Google [18]. Furthermore, Qualcomm is exploring the integration of LAP-UAVs in current long term evolution (LTE) and future 5G cellular applications [19]. Also, Ericsson has started multiple projects for the integration of UAVs in the broadband communication services. For example, Ericsson and China Mobile jointly established a time division LTE network in some areas of China which successfully provided broadband communication services through multiple UAVs and terrestrial base stations (BSs) [20].

On top of that, many other companies started working on deploying UAVs as power transmitters to charge ground or aerial devices. For instance, Amazon implemented a method for charging electrical vehicles through drones [21]. Moreover, some other companies like Festo and SkyCharge are using UAVs as power transmitters in the area of agriculture and farming to charge ground sensors [22].

1.2 UAV as Wireless Power and Information Transmitter

Mobile devices (such as low-power sensors) usually are energy-constrained since their lifetimes are limited by the battery capacity. Energy harvesting (EH) techniques based on radio frequency (RF) signals have been considered as promising solutions for extending the lifetime of battery-limited wireless devices [23]. In conventional WPT systems, dedicated power transmitters (PTs) are usually deployed at fixed locations to send RF signals to charge distributed power receivers (PRs), such as low-power sensors or IoT devices. The goal of the WPT is to meet the need of the device for transmitting its data to the target receiver by using the harvested energy [24].

UAVs as aerial power transmitters, with additional flexibility and 3D mobility, are expected to provide efficient wireless power supply to low power and hard to reach devices. Due to their adjustable altitude and mobility, efficient line-of-sight (LoS) between UAVs and ground nodes (GNs) could be established, and thus mitigating signal blockage and shadowing. By this feature, UAVs promise to be an interesting solution to charge battery-limited or hard-to-reach devices through RF WPT. This will significantly improve the wireless charging efficiency compared to the conventional ground charging stations at fixed locations and reduce the number of required PTs [25].

The UAV-WPT network mainly consists of UAVs as wireless power transmitters, where they could be extended to be power and information transmitters, as shown in Figure 1.1. The number of UAVs depends on the application of the network, the covered area, and the required quality of service. In addition, it contains the ground nodes (GNs), which can be an information receiver (IR) or an energy receiver (ER) or both at the same time. As a hybrid solution with terrestrial network, UAV-WPT networks can have terrestrial BSs in their setups, which can be used for receiving the information from GNs at any time in the process. There are three main transferring operations in such network, namely, downlink data transfer, downlink power transfer, and uplink data transfer. The downlink transfers are basically from the UAVs to their connected GNs, where the uplink could be towards the UAV (same or different) or towards the terrestrial BS. In many use-cases, UAVs are called to not only charge devices, but also to send and/or collect information from them [26]. Using the concept of wireless power and information transfer (WIPT) or simultaneous WIPT (SWIPT), where the transmitter sends power and information signals towards ERs and IRs, UAVs can be deployed to provide efficient WPT along with reliable data services when and where needed. Therefore, the use of UAVs to enable WIPT/SWIPT becomes more efficient, interesting, and promising to provide stable energy along with reliable data services for ERs and IRs.

By using different access schemes like non-orthogonal multiple access (NOMA) or orthogonal multiple access (OMA), the transceiver can separate the data of the users in the uplink or in the downlink. The superiority of one access scheme over other is still debatable and cannot be generalized for all cases and applications. Nonetheless, NOMA recently received significant attention for its promising performance. However, this comes with additional complexity, where successive interference cancellation (SIC)

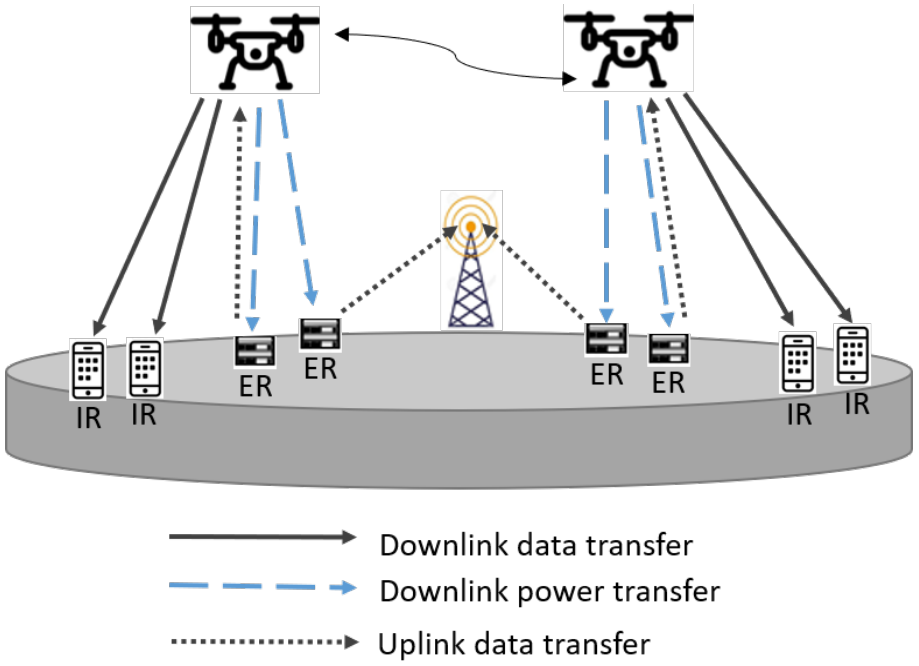

Figure 1.1: General UAV wireless powered communication network (UAV-WPCN).

is performed for reliable uplink and downlink transmissions. [27]. In the downlink, the user with strong channel condition (i) receives the NOMA signal; (ii) decodes the symbol of higher power from the received signal; (iii) subtracts it from the received NOMA signal; and (iv) continues to decode its own symbol. On the other hand, for the uplink NOMA, messages from different users are combined together and SIC is conducted at the receiver [28].

1.3 Energy Efficiency for UAV-based Networks

Although the deployment of UAVs in communication networks is promising, it comes with a lot of design challenges and reliability problems. For instance, since different network topologies are possible due to the mobility of UAVs, effective coordination schemes should be put in place to ensure the reliability of the network connections. Thus, new communication protocols should be designed accordingly [29]. Moreover,

one of the most critical challenges is the management of the limited on-board energy resources. In fact, the energy consumption of the UAV mainly originates from transmission, mobility, control, data processing and payloads purposes [30]. Thus, the flight duration of the drones is typically short and insufficient for providing long-term, and continuous wireless errands. The energy consumption of the UAV also depends on the role/mission of the UAV, weather conditions, and the traveling path.

In wireless communication systems, EE can be quantitatively measured by the bits of information reliably transferred to a receiver per unit of consumed energy at the transmitter [31]. Due to its significant impact on the performance of UAV-communication systems, EE, in the UAV-based communication networks, requires careful consideration. In fact, the limited on-board energy of UAVs is a key constraint for deployment and mobility of UAVs in various applications. Therefore, the allocation of the resources should be studied in such a way that the overall energy usage becomes more efficient. However, one must optimize the performance of UAV-WPT networks under power, time, and position constraints of UAVs and many other constraints according to the application. Having said that, there is a need for a framework to analyze and optimize the performance of UAV-WPT networks. The main idea is to efficiently allocate the available resources for reliable downlink/uplink communications using UAVs. Mostly, this kind of problem, with EE, throughput, and related constraints, is non-convex and thus difficult to be solved [32]. In this PhD thesis, we are interested in the optimization of the available resources in UAV-WPT networks, basically on the UAV side, through the maximization of EE.

1.4 Related Work

In this section, we briefly review the most relevant literature in the area of UAV-based wireless networks in different categories with more focus on UAV-enabled WPT networks. Several works in the literature investigate the resource allocation to enhance the performance of UAV-assisted networks, mainly in the wireless information transmission (WIT) networks [33–36], and network coverage extensions [37–40]. For instance, the authors of [36] suggested a model to characterize the capacity region over a given UAV flight duration. This was done by jointly optimizing the UAV's trajectory and transmit power/rate allocations over time aiming to send independent information to two users at different fixed locations on the ground. On the other side, a placement algorithm is suggested in [39] to efficiently use the UAV transmit power and maximize the coverage of GNs. Optimizing the throughput of a relay-based UAV system is considered in [41] by jointly controlling the UAV trajectory and the source/relay transmit powers. The authors of [42], explored the uplink coverage performance of an underlay drone cell for temporary events. In addition, [43] investigates how UAVs can be used to reinforce the communication infrastructure in emergency and public safety situations during which the existing terrestrial network is damaged or not fully operational. Also, by exploiting the perfect user location information (ULI), the authors of [44] and [45], use UAV placements to directly maximize the system throughput. On the other hand, with no ULI, the authors of [46] investigate the downlink coverage performance, where maximum ground coverage and minimum required transmit power for a single small cell drone are derived. Moreover, the authors of [47] optimize the UAV's trajectory, altitude, velocity, and data links with ground users to minimize the total mission time while enhancing the data collection.

Few existing works focus on the resource allocation to enhance the performance of UAV-assisted power transmission networks. For instance, the work in [48] suggests a design based on optimization of the UAVs trajectory to enhance throughput while taking into consideration the energy consumption of the UAV which tries to maximize the amount of energy transferred to the GNs during a finite charging period. Throughput maximization of UAV-powered device-to-device (D2D) communication is investigated in [49], by jointly optimizing the time and power assuring the energy causality constraint on the transmitter side. A slightly different scenario has been considered in [50], which focuses on the maximization of the system throughput exploiting trajectory design, jointly with the wireless resource allocation optimization, where a single UAV is used to transfer power to multiple ERs ground nodes on a specific time by changing its position periodically. Moreover, the uplink transmission of IoT devices, which is enabled through WPT by a single UAV has been investigated in [51]. The authors formulate and address a secure EE optimization problem to find the optimal transmit power and location for the UAV. Furthermore, the authors of [52] consider a UAV-enabled mobile edge computing (MEC) system, where a UAV powers the IoT nodes via WPT. A new time division multiple access (TDMA) based workflow model is proposed, which allows parallel transmissions and executions to minimize the total energy consumption of the UAV.

In addition to that, few studies have investigated the performance of NOMA and OMA for UAV based communication system. The authors in [53] suggested a multiple access mode selection (NOMA/OMA) based on the outage probability for the ground nodes in a system, where a fixed-wing UAV is used to support coverage for ground nodes located outside the coverage of BS. The minimization of energy consumption of mobile nodes with accepted quality of service of the offloaded mobile

application has been analyzed in [54], where offloading is enabled by uplink and downlink communications between the nodes and the UAV via NOMA or OMA schemes. UAV constrained coverage expansion methodology, facilitated by NOMA user rate gain has been proposed in [55]. Moreover, the authors of [56] proposed a cooperative NOMA scheme and suggested to maximize the weighted sum-rate of the UAV and ground users through optimizing the power allocations and UAV's rate. The authors of [57] focused on the optimization of the altitude of a rotary-wing UAV-BS aiming to maximize the individual rate for a two users NOMA scenario. An optimal resource allocation algorithm was proposed through the maximization of the throughput of a two ground users, which are enabled via NOMA transmission of UAV-assisted relaying systems [58]. The authors of [59] optimized the max-min rate problem for a large number of ground users served by a single-antenna UAV-BS and NOMA technique. A path-following algorithm was developed to solve the non-convex problem by jointly optimizing the UAV's flying altitude, the transmit antenna beamwidth, the amount of power and the bandwidth. Furthermore, the authors of [60] proposed a MIMO-NOMA aided UAV framework, where a multi-antenna UAV communicates with multiple users equipped with multiple antennas.

A few works have studied the performance of SWIPT for UAV based communication system. For instance, a resource allocation problem has been studied in an UAV-assisted SWIPT system with the existence of multiple eavesdroppers [61], where the secrecy rate has been maximized by jointly optimizing the trajectory and transmit power of the UAV. Also, the authors of [62] have investigated the joint optimization of power allocation and trajectory design of the UAV to support infrastructure-starved IoT services by maximizing the minimum energy harvested among the IoT devices. Moreover, the end-to-end cooperative throughput maximization problem for

the amplify-and-forward (AF) protocol for UAV-SWIPT systems has been investigated in [63] by optimizing the decision profile, power profile and trajectory.

In addition to the above mentioned works, a few studies have investigated the performance of multiple-UAV communication systems. For instance, the authors of [64] investigated the download coverage probability for a network of multiple UAVs modeled as a uniform binomial point process (BPP) at the same altitude. The authors in [65] investigated the stochastic modelling of UAV base stations, where different coverage models were suggested. Moreover, [66] studied the maximization of the minimum data rate of GNs by jointly optimizing the 3D locations, user association, and power allocation in multiple-UAV networks. In addition, [67] investigated the maximization of the minimum throughput over all ground users in the downlink communication by optimizing the multiuser communication scheduling and association jointly with the UAV's trajectory and power control.

Most of the aforementioned works, have some limitations and there is a huge potential for enhancement and development. For example, many works, e.g. [33, 34, 39, 59], consider single antenna UAV for their models, which basically degrades the ability of the UAV to meet the goals of the GNs for simultaneous transmissions. Furthermore, some systems, e.g. [35,40,41,49,52], are based only on the OMA scheme, and there is no consideration for NOMA. Moreover, many works, e.g. [50,56,63,66,67], ignored the most important aspect in this particular setup, i.e., energy efficiency, which is extremely important since we are dealing with power transfer. Some works, e.g. [36, 53, 55], consider one or two GNs for getting more insights to the problem, which is reasonable, however, more general examples have to be introduced. On top of that, the very general scenario including multiple UAVs to enable SWIPT for a general number of ERs and IRs for NOMA/OMA schemes has not been address by

any of the publicly available related work.

1.5 Proposed Methodology

Motivated by the need for a comprehensive framework to deal with the optimization of UAV wireless powered communication networks (UAV-WPCN). The main objective of this thesis is to develop the analytical foundations and algorithms to be able to exploit the available UAV-WPCN resources efficiently while maximizing the system's EE. To meet this goal, we propose a detailed methodology, as shown in Figure 1.2, which is general enough to deal with different topologies and applications. We provide the required steps to be followed for all applicable networks, where specific considerations have to be accounted for in each case.

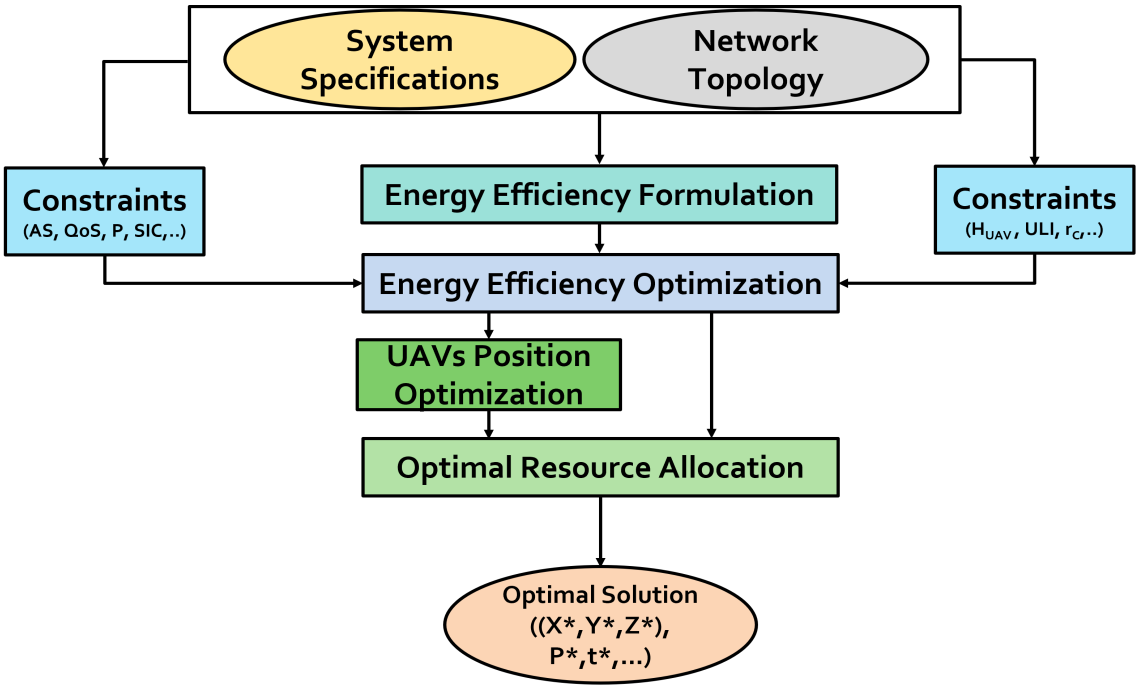

Figure 1.2: Proposed methodology

The inputs of this methodology are: network topology and system specifications, from which we construct the system EE and the related constraints. The constraints

related to the network topology are mainly about user location information (ULI), the maximum and minimum allowable height of the UAV (H_{UAV}), the radius of each cluster in the network (r_{C}), etc. On the other hand, the constrains related to the system specifications are basically pertained to the type of access scheme (AS), quality of service (QoS), SIC thresholds, transmit power (P), etc. We then construct the respective EE formula subject to the related constraints of the system specifications and network topology. After that, we conduct the optimization process, where we figure out the suitable strategies to be taken into account depending on the application and its constraints. Hence, this kind of problem with multiple highly coupled variables in the objective function and constraints is mainly non-convex and hard to be solved directly.

As a general understanding of the UAV-WPT networks, we propose first to optimize the positions (paths) of the UAVs before any transmission steps. Thereafter, we optimize the available resources; transmit power towards GNs and the switching/charging time. Both optimization steps will require the construction of algorithms depending on the system parameters and derived formulations. We construct these algorithms efficiently through conventional optimization methods which are suitable to handle such problems after relaxation. At the end, the optimal positions (X^*,Y^*,Z^*), transmit power (P^*) and time (t^*) will be obtained for the given setup.

To reach to the final general configuration, we investigated four main scenarios (see Figure 1.3) that will collectively provide a comprehensive study for the UAV-enabled WPT networks:

- Single UAV-enabled wireless powered communications network (UAV-WPCN).
- Single UAV-enabled simultaneous wireless power and information transfer network (UAV-SWIPT).

- Multiple UAV-enabled wireless powered communications network (MUAV-WPCN).
- Multiple UAV-enabled simultaneous wireless power and information transfer network (MUAV-SWIPT).

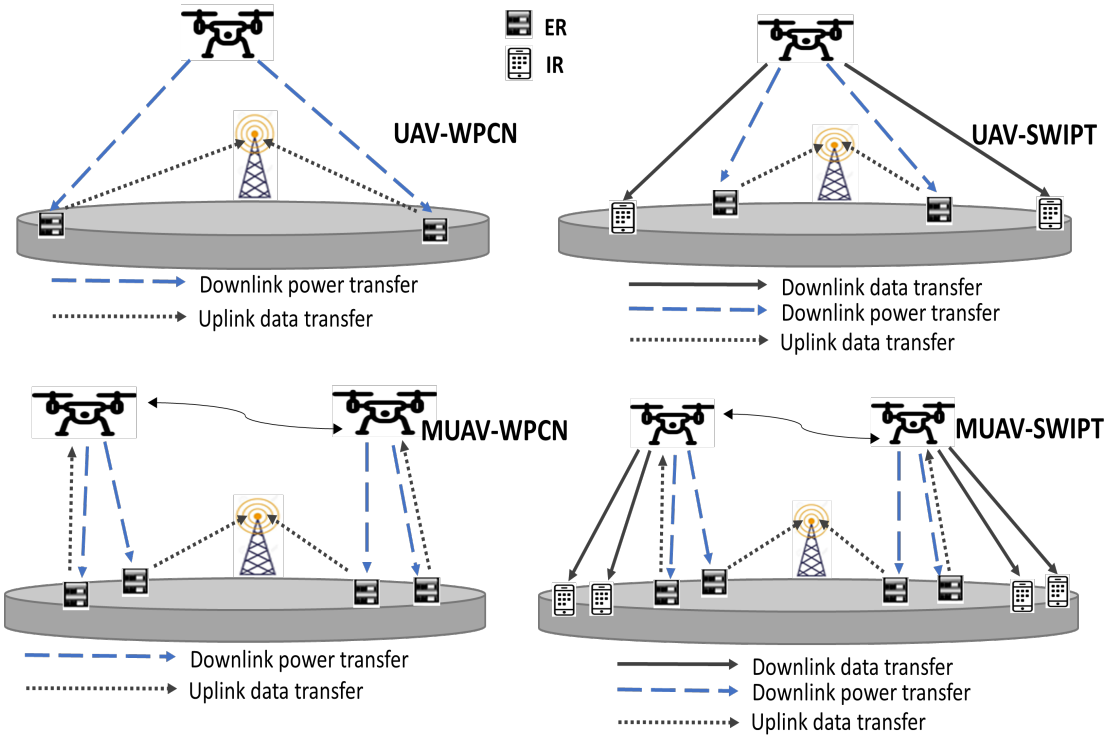

Figure 1.3: Proposed topologies

It is worth mentioning that the single UAV scenarios can be considered as special cases for the multiple UAV scenario, however, one can consider each scenario as an independent deployment that can reflect a practical setup, where the number of UAVs could vary according to the requirements. For example, it can be used to serve in a sports stadium with different gates where the sensors (light, humidity, etc.) around the stadium need to be charged by the UAVs and the UAVs also have to send ticketing information to the electronic gates around the stadium (one scenario is to have the

number of UAVs as the number of gates). Another possible application is to use the UAVs in the context of serving hard-to-reach devices like sensors on bridges and at the same time sending information to some advertising screens that are fixed on those bridges (one scenario is to have the number of UAVs reflecting the required sides of the bridge that need to be served). Note that for applications, where the area to be covered is small or the load can be handled without a need for multiple UAVs, one of the proposed single UAV scenario can be deployed.

1.6 Thesis Contributions

Unmanned aerial vehicles are becoming more reachable and available to be used in numerous applications. One of the most appealing and interesting application is the use of UAVs as wireless power transmitters for low-power or hard-to-reach devices to enable their communications using the harvested energy. However, this comes with many challenges related to the limited power budget, the UAV placement, the quality of service, and many other complexities. Intuitively, many other challenges are added when using multiple UAVs, which is becoming essential in many cases in order to enhance the coverage of the network. Therefore, the main objective of this thesis is to develop the analytical foundations and algorithms to be able to exploit the available UAV-WPT-based networks resources efficiently while maximizing the system's EE. In the following, we list the main contributions of this thesis along with references to related publications provided in the Biography section at the end of this document.

- A design and optimization of a UAV-WPCN assisted terrestrial network. The proposed design uses a multiple-antenna UAV for charging ground nodes through RF WPT to assist their uplink data communication with a terrestrial BS. We

formulate and solve the optimization problem by exploiting the movement flexibility of the UAV, which allows minimizing the path loss on the A2G channels according to the nodes' demands, and optimizing the transmit powers towards the maximization of the system's EE. [Bio-Cf3].

- An energy-efficient resource allocation scheme for NOMA-based UAV-WIPT networks. We propose a system model where a fixed position single UAV deploys information and power transfer towards co-located IRs and ERs to enable downlink and uplink data transmission through NOMA scheme. We propose an algorithm, which jointly takes into account the downlink and uplink stages using Lagrangian optimization and gradient decent methods. [Bio-Cf2].

- A general framework for maximizing the system's EE of UAV-SWIPT networks through different access schemes. We construct the system's EE and develop a general optimization problem that considers a general number of ERs and IRs for two main scenarios; linear and circular. We propose two different hybrid access schemes depending on the NOMA and OMA schemes, namely, hybrid downlink OMA uplink NOMA (HDOUN) and hybrid downlink NOMA uplink OMA (HDNUO). We derive the optimization formulation for transmitting the power towards each ER and IR and provide comprehensive comparisons between several combinations of the suggested scenarios and schemes [Bio-Jr1].

- A general setup of MUAV-WPCN systems for partial ULI of a general number of ERs. The proposed setup consists of multiple UAVs that deploy WPT towards several ERs to enable their uplink data transmissions through NOMA scheme. We consider different cases depending on the ERs' service demands. We develop two algorithms to handle the 3D position optimization of the UAVs, and the

transmit power allocation towards each ER [Bio-Cf1].

- A general framework for optimizing the MUAV-SWIPT networks for a general number of ERs and IRs. We address the optimization of the EE of a wireless network, where multiple-antenna UAVs serve as simultaneous power and information transmitters towards ERs and IRs, respectively. We consider the partial ULI approach of ERs and IRs, and we present accordingly a user distribution and association model for each cluster in the network. We also propose collision avoidance constraints to avoid UAVs' collisions as they move to enhance the links for the ERs and IRs. We finally consider the required QoS of the ERs as well as IRs on the downlink, and the uplink thresholds to enable SIC. [Bio-Jr2]

1.7 Thesis Organization

The rest of the thesis is organized as follows: In Chapter 2, we present the design and the optimization of the UAV-WPCN. We detail its system and channel models and discuss the simulation results by comparing different setups. In Chapter 3, we introduce the integration of the NOMA scheme in the UAV-WIPT networks. We present the formulation and the optimization of the system's EE and conduct a comparison between the performance of OMA and NOMA schemes. In Chapter 4, we extend the approach of Chapter 3 to handle the position optimization along with the resource allocation for the UAV-SWIPT networks. We describe different scenarios and propose several access schemes.

In Chapter 5, we detail the system and channel models of the MUAV-WPCN systems. We describe the distribution of the ERs within each cluster and explain the

steps for maximizing the system's EE. In Chapter 6, we present the details of the general scenario of MUAV-SWIPT. We explain the constructions of the system's EE and the formulation of the optimization problem. We present the suggested collision avoidance constraints to avoid UAVs' collisions and discuss the several constraints on the main system parameters. Finally, we conclude the thesis in Chapter 7 and provide future research directions.

Chapter 2

Single UAV-Enabled Wireless Powered Communication Networks

This chapter presents the system and channel models details for the first suggested topology, i.e., UAV-WPCN scenario. In this scenario, we consider two ERs that receive energy signals from a single UAV to allow its uplink communications toward a terrestrial BS. We formulate and describe the optimization problem within the suggested methodology that we presented in Chapter 1. First, the path loss of the air-to-ground channels is minimized by optimizing the position of the UAV depending on the ground nodes' service demands. Then, using the optimized positioning and a closed-form expression for the energy efficiency, a resource allocation aiming at maximizing the energy efficiency is developed. To this end, two algorithms are proposed using Lagrangian optimization and gradient descent methods.

2.1 UAV-WPCN System Model

The hovering UAV, equipped with N_u antennas, transmits power wirelessly to ERs during a duration τ which is repeated every time slot T. For simplicity, the 2-user case is considered in this work. From a time slot to the other, the position of the UAV can vary according to the demands of the ERs. Within a time slot, each ER harvests energy from the UAV during time τ, and by applying the *harvest-then-transmit* protocol consumes the harvested energy to transmit its always-available data to the BS during the remaining slot time of $T - \tau$, according to a TDMA-based OMA scheme, as shown in Figure 2.1. The BS is equipped with a massive antenna array of N_b elements, and its position is denoted (X_b, Y_b, h_b). Without loss of generality, the positions of the ERs are set to $(X_1, Y_1, h_1) = (\mathrm{R}/2, 0, 0)$ and $(X_2, Y_2, h_2) = (-\mathrm{R}/2, 0, 0)$, as shown in Figure 2.1. d_1 and d_2 are the distances between the UAV and each ER, respectively. A quantized level of minimum required rate on the uplink is sent from the ER to the UAV to initiate the link and to indicate its power demand. Based on this side information, the UAV determines the relative demand of each ER, denoted μ_j, such that $\sum_j \mu_j = 1$. Here, if ER_j has a larger value of μ_j, then it has a higher rate demand which means a higher priority in the WPT.

2.1.1 Channel Models

Let $\mathbf{h}_j$ and $\mathbf{g}_j$, $j = 1, 2$, be the complex channel vectors corresponding to the UAV-ER_j and ER_j-BS links, respectively. $\mathbf{h}_j$ is a row vector and $\mathbf{g}_j$ is a column vector. On the UAV side, we have $\mathbf{h}_j = \mathbf{h}'_j/\sqrt{L_{d,j}}$, where $L_{d,j}$ and $\mathbf{h}'_j = [h'_{j,1}, h'_{j,2}, \ldots, h'_{j,N_u}]$ denote the average path-loss and the normalized channel fading vector corresponding to UAV-ER_j link, respectively. For the case of Rician fading, the normalized channel

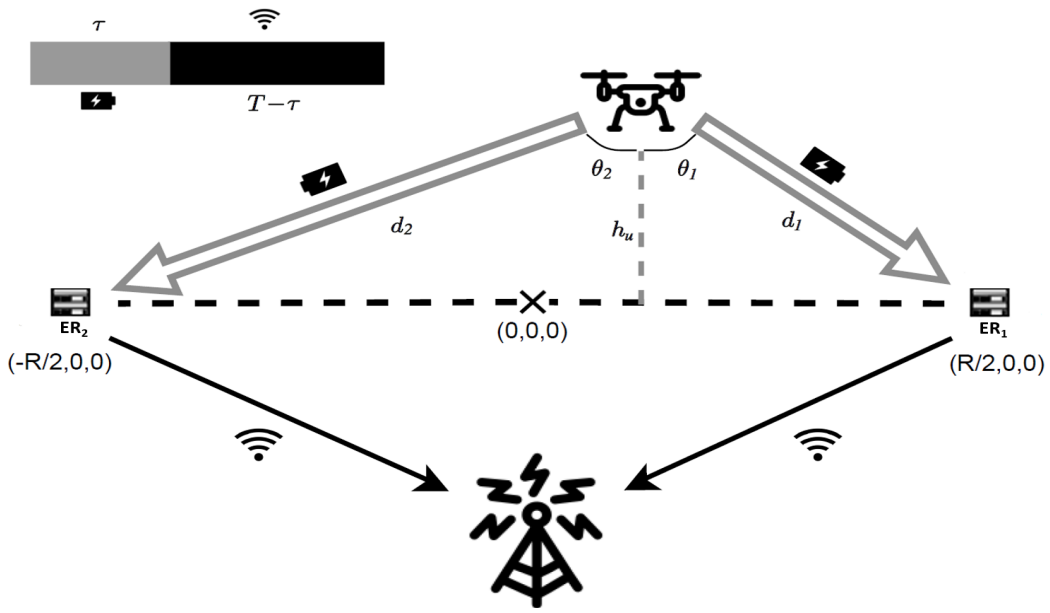

Figure 2.1: UAV-WPCN system model.

vector $\mathbf{h}'_j$ can be written as [68]

$$\begin{aligned}\mathbf{h}'_j &= \mathbf{h}_{\mathrm{LoS},\,j} + \mathbf{h}_{\mathrm{NLoS},\,j} \\ &= \sqrt{\frac{K}{K+1}}\mathbf{1}_{1\times N_u} + \sqrt{\frac{1}{K+1}}\mathbf{h}_{w,j},\end{aligned} \tag{2.1}$$

where K denotes the Rice factor, $\mathbf{1}_{1\times N_u}$ denotes a unity row vector, $\mathbf{h}_{w,j}$ is a row vector whose elements are independent and identically distributed (i.i.d.) complex Gaussian random variables with zero mean and unit variance; and it is assumed that the UAV antennas are sufficiently apart for the no spatial correlation assumption to hold in defining $\mathbf{h}_{\mathrm{NLoS},\,j}$'s [69]. Further, the average air-to-ground (A2G) free-space distance-dependent path loss of ERs, $L_{d,j}$ in dB, is obtained as follows [70]:

$$L_{d,j} = p_{\mathrm{LoS},\,j}\, L_{\mathrm{LoS},\,j} + (1 - p_{\mathrm{LoS},\,j})\, L_{\mathrm{NLoS},\,j}, \tag{2.2}$$

where the LoS and NLoS path losses are given by

$$L_{\mathrm{LoS},\,j} = 10\ n\ \log_{10}\left(\frac{4\pi f d_j}{c}\right) + \xi_{\mathrm{LoS},\,j}, \tag{2.3}$$

$$L_{\mathrm{NLoS},\,j} = 10\ n\ \log_{10}\left(\frac{4\pi f d_j}{c}\right) + \xi_{\mathrm{NLoS},\,j}, \tag{2.4}$$

where n denotes the path loss exponent, f is the carrier frequency, c denotes the speed of light; and $\xi_{\mathrm{LoS},\,j}$ and $\xi_{\mathrm{NLoS},\,j}$ are the average environment-dependent excessive path losses in dB [71] corresponding to ER_j. $p_{\mathrm{LoS},\,j}$ in (2.2) denotes the probability that the UAV has a LoS to ER_j, and is given by [72]

$$p_{\mathrm{LoS},\,j} = \frac{1}{1 + a\exp\left(-b\ \left(\frac{180}{\pi}\theta_j - a\right)\right)}, \tag{2.5}$$

where a and b are constant values related to the environment, and θ_j is the elevation angle in radian related to node ER_j. We have $\theta_j = \arccos(h_u/d_j)$, where h_u is the altitude of the UAV and d_j is the Euclidean distance between the UAV and ER_j (see Figure 1). Using (2.2)–(2.5), we obtain

$$L_{d,j} = \frac{\xi_{\mathrm{LoS},\,j} - \xi_{\mathrm{NLoS},\,j}}{1 + a\exp\left(-b\ \left(\frac{180}{\pi}\theta_j - a\right)\right)} + 20\log\left(\frac{4\pi f d_j}{c}\right) + \xi_{\mathrm{NLoS},\,j}, \tag{2.6}$$

where the distance d_j is given by

$$d_j = \sqrt{(X_u - X_j)^2 + (Y_u - Y_j)^2 + (h_u - h_j)^2}, \tag{2.7}$$

where (X_u, Y_u, h_u) indicates the position of the UAV in sky.

2.1.2 Energy and Information Transmissions

The unmodulated transmit signal vector $\mathbf{x}(t)$ from the N_u UAV antennas is $\mathbf{x}(t) = \Re\{\sum_{j=1}^{J} \sqrt{P_j}\mathbf{w}_j e^{i2\pi ft}\}$, where $\mathbf{w}_j$ is the energy beamforming complex vector with unit norm—assuming availability of perfect channel state information (CSI) on the UAV side—and P_j is the transmit power destined for ER_j, where $P = \sum_{j=1}^{J} P_j$ is the transmit power of the UAV. The maximum harvested energy by ER_j from the UAV during τ dedicated for WPT operation is given by

$$E_j = \eta_j P|\mathbf{h}_j\mathbf{w}_j^{\star}|^2\tau = \eta_j P\|\mathbf{h}_j\|^2\tau = \eta_j \frac{P}{L_{d,j}}\|\mathbf{h}_j'\|^2\tau, \tag{2.8}$$

where $0 < \eta_j \leq 1$ is the energy-harvesting circuit efficiency [73]. The optimal weight vector $\mathbf{w}_j^{\star}$ is equal to $\mathbf{h}_j^{\dagger}/\|\mathbf{h}_j\|$ with $\dagger$ denoting Hermitian transposition; thus leading to the energy expression as in (2.8).

The ground nodes use the harvested energy for the uplink communication with the BS. Without loss of generality, we assume that the time slot duration T is unity. The received data signal at the BS from node j is given by

$$\mathbf{y}_j = \sqrt{\frac{E_j/L_{b,j}}{1-\tau}}\,\mathbf{g}_j\, s_j + \mathbf{n}_j, \tag{2.9}$$

where $s \in \mathbb{C}$ is the normalized data symbol with zero mean and unit magnitude, $\mathbf{y}_j \in \mathbb{C}^{N_b \times 1}$, and $\mathbf{n}_j \in \mathbb{C}^{N_b \times 1}$ is the additive Gaussian noise with zero mean and covariance matrix $\mathbb{E}\{\mathbf{n}_j\mathbf{n}_j^{\dagger}\} = \sigma_j^2\mathbf{I}_{N_b}$. Further, $\mathbf{g}_j$ denotes the normalized uplink small-scale fading channel vector distributed as $\mathcal{CN} \sim (0, \mathbf{I}_{N_b})$, and $L_{b,j}$ is the distance-dependent path loss of the ER_j-BS link. With perfect CSI at the BS, maximum ratio combining (MRC) is implemented [74]. Assuming that the channel coefficients

$\mathbf{h}_j$ and $\mathbf{g}_j$ are constant during each time slot, the transmission rate related to ER_j, considering the OMA scheme, is given by

$$\begin{aligned} R_j(P_j, \tau, d_j, \theta_j) &= \frac{1-\tau}{2} W_j \log_2 \left(1 + \frac{2E_j \|\mathbf{g}_j\|^2 / L_{b,j}}{(1-\tau)\Gamma_j \sigma_j^2}\right) \\ &= \frac{1-\tau}{2} W_j \log_2 \left(1 + \frac{2\eta_j P_j \|\mathbf{h}'_j\|^2 \|\mathbf{g}_j\|^2 \tau}{L_{b,j} L_{d,j} (1-\tau)\Gamma_j \sigma_j^2}\right) \end{aligned} \tag{2.10}$$

where W_j is the bandwidth related to ER_j, $\Gamma_j > 1$ is the signal-to-noise ratio (SNR) gap to account for the lower performance of physically realizable encoding systems compared to the ideal Shannon-capacity reaching ones. Note that $L_{d,j}$ is itself a function of d_j and θ_j as per (2.6). The UAV can also adjust its charging power P_j and charging time duration τ.

Exploiting the idea of channel hardening [75], namely that $\lim_{N_b \to \infty} \frac{\|\mathbf{g}_j\|^2}{N_b} = 1$ in large-scale MIMO, (2.10) becomes

$$R_j(P_j, \tau, d_j, \theta_j) = \frac{1-\tau}{2} W_j \log_2 \left(1 + \frac{2\eta_j P_j \|\mathbf{h}'_j\|^2 N_b \tau}{L_{b,j} L_{d,j} (1-\tau)\Gamma_j \sigma_j^2}\right). \tag{2.11}$$

By using the Jensen's inequality, we can write

$$\begin{aligned} &\mathbb{E}\left[\frac{1-\tau}{2} W_j \log_2 \left(1 + \frac{2\eta_j P_j \|\mathbf{h}'_j\|^2 N_b \tau}{L_{b,j} L_{d,j} (1-\tau)\Gamma_j \sigma_j^2}\right)\right] \\ &\leq \frac{1-\tau}{2} W_j \log_2 \left(1 + \frac{2\eta_j P_j \mathbb{E}\left[\|\mathbf{h}'_j\|^2\right] N_b \tau}{L_{b,j} L_{d,j} (1-\tau)\Gamma_j \sigma_j^2}\right) \\ &\overset{\text{(a)}}{=} \frac{1-\tau}{2} W_j \log_2 \left(1 + \frac{2\eta_j P_j N_b \tau}{L_{b,j} L_{d,j} (1-\tau)\Gamma_j \sigma_j^2}\right), \end{aligned} \tag{2.12}$$

where (a) in (2.12) gives an upper-bound for the average transmission rate of ER_j.

Let us define the throughput as the sum-rate of the system:

$$R(\mathbf{P}, \tau, \mathbf{d}, \boldsymbol{\theta}) = \sum_{j=1}^{2} R_j(P_j, \tau, d_j, \theta_j). \tag{2.13}$$

where $\mathbf{P} = [P_1, P_2]$, $\mathbf{d} = [d_1, d_2]$, and $\boldsymbol{\theta} = [\theta_1, \theta_2]$.

2.2 Energy Efficiency Maximization

The energy efficiency of the wireless powered communication system can be evaluated by defining the energy efficiency coefficient

$$\rho_E = \frac{R(\mathbf{P}, \tau, \mathbf{d}, \boldsymbol{\theta})}{P_0\tau + P\tau}, \tag{2.14}$$

where P_0 is the constant power consumption of the UAV which significantly includes the electrical power to keep the UAV moving in air, and $P = P_1 + P_2$ is the transmit power. Having assumed spherical coordinates (d_j, θ_j, ϕ_j) and noticing that $L_{d,j}$ does not depend on ϕ_j, we try to solve the below optimization problem to decide first on the optimized position of the UAV in the sky according to the demand parameters, μ_1 and μ_2. Then, optimization of the transmit powers, P_1, P_2, and the harvesting time τ by both nodes is tackled. The problem is formulated as follows:

$$\begin{aligned}
\max_{P,\tau,d_j,\theta_j} \quad & \rho_E \\
\text{subject to:} \quad & P_1 + P_2 \leq P_{u,\max}, \\
& \frac{E_j}{1-\tau} \leq P_{ER_j,\max}, \quad j = 1, 2, \\
& \tau < 1, \\
& r_{j,\min} \leq R_j(P_j, \tau, d_j, \theta_j), \quad j = 1, 2,
\end{aligned}$$

$$h_{u,\min} \leq d_j \cos(\theta_j), \quad j = 1, 2, \tag{2.15}$$

where $P_{\mathrm{ER}_j,\max}$ and $P_{u,\max}$ are the maximum transmit power of ER_j and the UAV, respectively; $r_{j,\min}$ denotes the minimum expected transmission rate of node ER_j during each time slot, and $h_{u,\min}$ is the minimum allowed height for the UAV. Note that $d_j \cos(\theta_j) = h_u$.

We split the optimization problem into two sub-problems. In the first one (OP1), we aim to find the optimum position of the UAV, i.e., the optimal distances and elevation angles with respect to the ERs according to their demands. In the second problem (OP2), and after getting the optimum position of the UAV, we determine the optimal power and switching time.

2.2.1 UAV Position Optimization

In OP1, we care about θ_j and d_j which are given in (2.6) for both nodes at the same time. This can be achieved by connecting the path losses for two A2G channels related to each node by the parameters pertaining to the nodes' demands. So, OP1 will be as follows:

$$\begin{aligned} \text{OP1:} \quad & \min_{d_j,\theta_j} \quad \mu_1 L_{d,1} + \mu_2 L_{d,2} \\ & \text{subject to:} \quad h_{u,\min} \leq d_j \cos(\theta_j), \quad j = 1, 2. \end{aligned} \tag{2.16}$$

This optimization problem can be solved by introducing the vector of Lagrangian multipliers $\boldsymbol{\lambda} = [\lambda_1, \lambda_2]$. The objective function then becomes

$$\mathcal{L}_1(\boldsymbol{\lambda}, \mathbf{d}, \boldsymbol{\theta}) = \mu_1 L_{d,1} + \mu_2 L_{d,2} - \lambda_1 h_{u,\min} - \lambda_2 h_{u,\min}$$

$$- \lambda_1 d_1 \cos(\theta_1) - \lambda_2 d_2 \cos(\theta_2). \tag{2.17}$$

Exploiting the Karush–Kuhn–Tucker (KKT) conditions [76], one can get the optimal position of the UAV by solving the first derivatives of $\mathcal{L}_1$ with respect to d_j and θ_j, respectively, as follows:

$$\begin{aligned}\frac{\partial \mathcal{L}_1}{\partial d_j} &= \mu_j \frac{\partial L_{d,j}}{\partial d_j} - \lambda_j \\ &= \frac{20\,\mu_j}{d_j \ln(10)} - \lambda_j \cos(\theta_j) \\ &= 0, \quad j \in \{1, 2\},\end{aligned} \tag{2.18}$$

$$\begin{aligned}&\frac{\partial \mathcal{L}_1}{\partial \theta_j} = \frac{\partial L_{d,j}}{\partial \theta_j} + \lambda_j d_j \sin(\theta_j) \\ &= \frac{ab\dfrac{180}{\pi}(\xi_{\mathrm{LoS},\,j} - \xi_{\mathrm{NLoS},\,j}) \exp\left(-b\,(\frac{180}{\pi}\theta_j - a)\right)}{\left(1 + a \exp\left(-b\,(\frac{180}{\pi}\theta_j - a)\right)\right)^2} \\ &+ \lambda_j d_j \sin(\theta_j) \\ &= 0, \quad j \in \{1, 2\}.\end{aligned} \tag{2.19}$$

The new value of λ_j can be simply calculated using the gradient decent method as follows [77]:

$$\lambda_j(i+1) = [\lambda_j(i) - \triangle_{\lambda_j}(h_{u,\min} - d_j \cos(\theta_j))]^+, \tag{2.20}$$

where $\lambda_j(i)$, $j \in \{1, 2\}$, is the value of λ_j at the i^{th} iteration, $\triangle_{\lambda_j}$ is the iteration step, and $[x]^+ = \max(0, x)$. As a starting point, we set $\lambda_j = 0$ for $j \in \{1, 2\}$ as mentioned in Algorithm 2.1 and then update it in each iteration. The output of the optimization will be the optimum position of the UAV, i.e. θ_j^* and d_j^*, corresponding to ER_j, $j \in \{1, 2\}$. Algorithm 2.1 summarizes the procedure for finding the optimal

positioning of the UAV. Notice that the position of the ERs are known. The results will be used in the second optimization problem.

Algorithm 2.1. 3D Position Optimization (X_u^*,Y_u^*,h_u^*)

Input: $[X_j,Y_j,h_j]$, μ_j, $\xi_{\text{LoS},j}$, $\xi_{\text{NLoS},j}$ for $j \in \{1,2\}$; a, b, $h_{u,\min}$, f.
Output: $[X_u^*,Y_u^*,h_u^*]$
Initialization : $[X_{u0},Y_{u0},h_{u0}]$, $\lambda_j = 0$ for $j \in \{1,2\}$.
1: Update λ_j's according to (2.20).
2: Solve (2.18) for d_j, $j \in \{1,2\}$.
3: Solve (2.19) for θ_j, $j \in \{1,2\}$.
4: Compute the optimal $[X_u^*,Y_u^*,h_u^*]$ by solving (2.16)

2.2.2 Energy-Efficient Resource Allocation

In OP2, we eliminate the last constraint in (2.15) which is already covered by OP1. With the remaining constraints, the optimization problem is formulated as follows:

$$\begin{aligned}
\text{OP2:} \quad & \max_{P_1,P_2,\tau} \quad \rho_E \\
& \text{subject to:} \quad P_1 + P_2 \le P_{u,\max}, \\
& \qquad \frac{E_j}{1-\tau} \le P_{\text{ER}_j,\max}, \quad j = 1,2, \\
& \qquad \tau < 1, \\
& \qquad r_{j,\min} \le R_j(P_j,\tau,d_j^*,\theta_j^*), \quad j = 1,2.
\end{aligned} \tag{2.21}$$

From the first and second constraints in (2.21), and by substituting (2.8) in the second constraint in (2.21); and assuming that both ERs have the same maximum transmit power $P_{\text{ER,max}}$ and energy-harvesting efficiency η, we can deduce that $\tau \le \tau_{\max}$, where

$$\tau_{\max} = \frac{P_{\text{ER,max}} L_{d,1} L_{d,2}}{\eta P_{u,\max}(\mu_1 L_{d,2} + \mu_2 L_{d,1}) + L_{d,1} L_{d,2} P_{\text{ER,max}}}. \tag{2.22}$$

It is obvious that the objective function of OP2 is a fractional optimization problem with variables P_1, P_2, and τ, which is generally non-convex. Exploiting the idea in [78], the fractional programming problem is transformed into a convex problem by introducing the variable z^* as the optimal energy efficiency when we have the optimal powers and optimal switching time, P_1^*, P_2^* and τ^*, respectively. Thus, OP2 is now described as

$$\begin{aligned} \text{OP2}^*: \quad \max_{P,\tau} \quad & R(\mathbf{P}, \tau, \mathbf{d}^*, \boldsymbol{\theta}^*) - z^*(P_0\tau + P\tau) \\ \text{subject to:} \quad & P_1 + P_2 \leq P_{u,\max}, \\ & \tau \leq \tau_{\max}, \\ & \tau < 1, \\ & R_j(P_j, \tau, d_j^*, \theta_j^*), \quad j = 1, 2, \end{aligned} \tag{2.23}$$

Basically OP2* can be efficiently proved to be a convex optimization problem by assuring that the second derivatives of $R(\mathbf{P}, \tau, \mathbf{d}^*, \boldsymbol{\theta}^*)$ with respect to P_j and τ, are less than zero.

By introducing $\vartheta \geq 0$, $\varsigma \geq 0$, $\varepsilon \geq 0$, $\varphi_1 \geq 0$, and $\varphi_2 \geq 0$ as the Lagrange multipliers associated with the four constraints in OP2*, respectively, the Lagrangian function of OP2* can be formulated as

$$\begin{aligned} \mathcal{L}_2(\vartheta, \varsigma, \varepsilon, \varphi_1, \varphi_2, P_1, P_2, \tau) = {} & R_1(P_1, \tau, d_1^*, \theta_1^*) + R_2(P_2, \tau, d_2^*, \theta_2^*) \\ & - z^*(P_0\tau + P\tau) - \vartheta(P_1 + P_2) + \vartheta P_{u,\max} \\ & - \varsigma\tau + \varsigma\tau_{\max} - \varepsilon\tau + \varepsilon - \varphi_1 r_{1,\min} - \varphi_2 r_{2,\min} \\ & + \varphi_1 R_1(P_1, \tau, d_1^*, \theta_1^*) + \varphi_2 R_2(P_2, \tau, d_2^*, \theta_2^*). \end{aligned} \tag{2.24}$$

To find the optimal transmit powers P_1^* and P_2^* from the UAV towards ER_1 and ER_2, respectively, we assume that the UAV will use its maximum power during the WPT period, which simply means that $P_2^* = P_{u,\max} - P_1^*$. Our aim now is to get P_1^* which also implicitly means P_2^* and the optimal WPT time τ^*. Taking into consideration that OP2* is a nonlinear programming problem, this can be done through derivation of the Lagrangian function with respect to P_1 and τ, respectively, as follows:

$$\begin{aligned}
&\frac{\partial \mathcal{L}_2(\vartheta, \varsigma, \varepsilon, \varphi_1, \varphi_2, P_1, \tau)}{\partial P_1} \\
&= (1+\varphi_1)\frac{\partial R_1(P_1, \tau, d_1^*, \theta_1^*)}{\partial P_1} + (1+\varphi_2)\frac{\partial R_2(P_1, \tau, d_2^*, \theta_2^*)}{\partial P_1} \\
&- z^*\tau - \vartheta \\
&= \frac{(1+\varphi_1)(1-\tau)W_1}{2P_1 \ln 2} - \frac{(1+\varphi_2)(1-\tau)W_2 P_1}{2(P_{u,\max} - P_1)\ln 2} \\
&- z^*\tau - \vartheta \\
&= 0,
\end{aligned} \tag{2.25}$$

$$\begin{aligned}
&\frac{\partial \mathcal{L}_2(\vartheta, \varsigma, \varepsilon, \varphi_1, \varphi_2, P_1, \tau)}{\partial \tau} \\
&= (1+\varphi_1)\frac{\partial R_1(P_1, \tau, d_1^*, \theta_1^*)}{\partial \tau} + (1+\varphi_2)\frac{\partial R_2(P_1, \tau, d_2^*, \theta_2^*)}{\partial \tau} \\
&- z^* P_{u,max} - z^* P_0 - \varsigma - \varepsilon \\
&= \frac{(1+\varphi_1)W_1}{2}\left(\frac{(1-\tau)}{\tau \ln 2} - \log_2\left(\frac{\eta_1 P_1 N_b \tau}{L_{b,1} L_{d,1}(1-\tau)\Gamma_1 \sigma_1^2}\right)\right) \\
&+ \frac{(1+\varphi_2)W_2}{2}\left(\frac{(1-\tau)}{\tau \ln 2} - \log_2\left(\frac{\eta_2 (P_{u,\max} - P_1) N_b \tau}{L_{b,2} L_{d,2}(1-\tau)\Gamma_2 \sigma_2^2}\right)\right) \\
&- z^* P_{u,\max} - z^* P_0 - \varsigma - \varepsilon \\
&= 0.
\end{aligned} \tag{2.26}$$

The updating of the Lagrangian variables ϑ, ς , ε, φ_1 and φ_2 can be done using the

gradient method as follows:

$$\vartheta(i+1) = [\vartheta(i) - \triangle_{\vartheta}(P_{u,\max} - P)]^{+} \tag{2.27}$$

$$\varsigma(i+1) = [\varsigma(i) - \triangle_{\varsigma}(\tau_{\max} - \tau)]^{+} \tag{2.28}$$

$$\varepsilon(i+1) = [\varepsilon(i) - \triangle_{\varepsilon}(1 - \tau)]^{+} \tag{2.29}$$

$$\varphi_1(i+1) = [\varphi_1(i) - \triangle_{\varphi_1}(R_1(P_1, \tau, \theta_1^*, d_1^*) - r_{1,\min})]^{+} \tag{2.30}$$

$$\varphi_2(i+1) = [\varphi_2(i) - \triangle_{\varphi_2}(R_2(P_1, \tau, \theta_2^*, d_2^*) - r_{2,\min})]^{+}, \tag{2.31}$$

where i is the iteration index, and the $\triangle_{\vartheta}$, $\triangle_{\varsigma}$, $\triangle_{\varepsilon}$, $\triangle_{\varphi_1}$, and $\triangle_{\varphi_2}$ are the iteration steps.

The solution of OP2, by depending on the expressions (2.21)–(2.31) and the output of Algorithm 2.1, is summarized in Algorithm 2.2.

Algorithm 2.2. Energy-Efficient Resource Allocation

Input: Output of Algorithm (2.1) $[X_u^*, Y_u^*, h_u^*]$, $[X_1, Y_1, h_1]$, $[X_2, Y_2, h_2]$, $[X_b, Y_b, h_b]$, $h_{u,\min}$, a, b, $\xi_{LoS,j}$, $\xi_{NLoS,j}$, f, N_u, N_b, $L_{d,j}$, $L_{b,j}$, η_j, Γ_j, σ_j, $r_{1,\min}$, $r_{2,\min}$, $\triangle_{\vartheta}$,$\triangle_{\varsigma}$, $\triangle_{\varepsilon}$, $\triangle_{\varphi_1}$, $\triangle_{\varphi_2}$, and z^*.

Output: $[P_1^*, P_2^*, \tau^*]$.

Initialization: $[P_{1_0}, \tau_0]$, $\vartheta = 0$, $\varsigma = 0$, $\varepsilon = 0$, $\varphi_1 = 0$, $\varphi_2 = 0$.

1: Update ϑ, ς , ε, φ_1, and φ_2 based on (2.27), (2.28), (2.29), (2.30), and (2.31), respectively.
2: Solve (2.25) and (2.26) jointly to obtain P_1 and τ.
3: Compute the optimal $[P_1^*, P_2^*, \tau^*]$ by solving (2.23).

2.2.3 Complexity Analysis

In the proposed methodology, we decomposed the problem into two sub-problems and were able to solve them efficiently through two algorithms. Both algorithms depend on the gradient descent method where the worst complexity of such method

is $\mathcal{O}(n \times \frac{1}{\epsilon})$ [79], where n is the number of optimization variables, and ϵ is the solution accuracy. Thus, for Algorithm 2.1, the complexity depends on the 3D plane size that the UAV considers for moving, i.e., $(X \times Y \times (h_{\max} - h_{\min}))$, where the $(h_{\max} - h_{\min})$ is the allowable altitude range for moving. This could be eliminated to $(X \times Y)$ only as the UAV will mostly hover at the minimum allowable height to provide better links to the ERs and IRs. For Algorithm 2.2, the complexity depends on the number of ERs (J). Accordingly, the total complexity for both algorithms is $\mathcal{O}(X \times Y \times (h_{\max} - h_{\min}) \times \frac{1}{\epsilon}) + \mathcal{O}((J) \times \frac{1}{\epsilon})$.

2.3 Simulation Results

In the simulations, we assume the propagation parameters to correspond to an urban environment [72], unless stated otherwise. We choose $a = 9.6$, $b = 0.28$, $\xi_{LoS,j} = 1$ dB, $\xi_{NLoS,j} = 20$ dB, $f = 2$ GHz, $\Gamma_j = 1.2$, $W_j = 200$ kHz, $\eta_j = 0.8$, $\sigma_j^2 = 1$; for $j = 1, 2$. The coordinates of ER_1, ER_2 and the BS are set to [500 0 0], [-500 0 0] and [0 100 25], respectively. The UAV position is the output of OP1 with $h_{u,\min} = 100$ m. Moreover, we set $P_0 = 10$ Watt, $P_{u,\max} = 3$ Watt, $N_u = 5$ and $N_b = 100$, unless stated otherwise.

2.3.1 3D Position of the UAV

The proposed algorithm for finding the optimal 3D position of the UAV, i.e., Algorithm 2.1, efficiently converges to the optimal position with respect to d_j and θ_j where $j = 1, 2$, after no more than 10 iterations for different initial settings. Afterwards, this output is used in OP2.

With two ERs, we have three cases: (i) the demand of ER_1 is larger than the demand of ER_2, i.e., $\mu_1 > \mu_2$; (ii) the demand of ER_2 is larger than that of ER_1, i.e.,

$\mu_2 > \mu_1$; and (iii) both have the same demand, i.e., $\mu_1 = \mu_2$. These three cases are clearly illustrated in Figure 2.2, which represents the optimal horizontal location of the UAV depending on the values of μ_1 and μ_2. For instance, when $\mu_1 = 0.8$ and $\mu_2 = 0.2$, the UAV hovers at the position of [300 0 100]. In the extreme case where the demand of one ER is at most whereas the other has no demand, the path loss will be on its minimum with respect to the former node and to the maximum with respect to the latter. For example, when ER_1 has maximum demand, $\mu_1 = 1$, then the UAV will hover directly on top of it, i.e. at the position [500 0 100]. In the case of same demands, where $\mu_1 = \mu_2 = 0.5$, the path losses will be the same for both nodes and the UAV will be at the medium point [0 0 100] between the nodes.

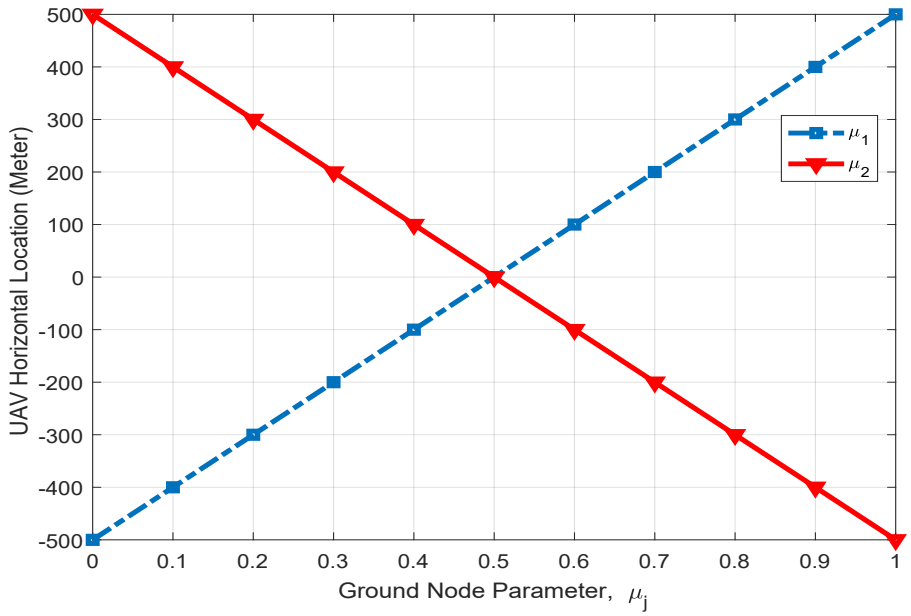

Figure 2.2: UAV position according to the nodes' demands.

2.3.2 Energy Efficiency with Optimal Power and Charging Time

Figure 2.3 shows the transmit powers from the UAV towards the ERs, as a function of the demand parameter of ER_1, i.e., μ_1. The figure compares P_1^* and P_2^* when the UAV takes the demand parameters of the ERs into consideration and when not. It is clear that the UAV transmit power will be divided equally among the ERs and that the UAV will hover in the middle between them when demand parameters are not taken into account. For instance, when $\mu_1 = 0.7$ and the UAV takes the ER demands into account, a power of $P_1^* = 2.45$ Watt and $P_2^* = 1.35$ Watt will be allocated towards ER_1 and ER_2, respectively. On the other hand, when the UAV does not take the demands into consideration,the power levels will be fixed to 1.5 Watt regardless of the nodes' requirements for the data communication on the uplink.

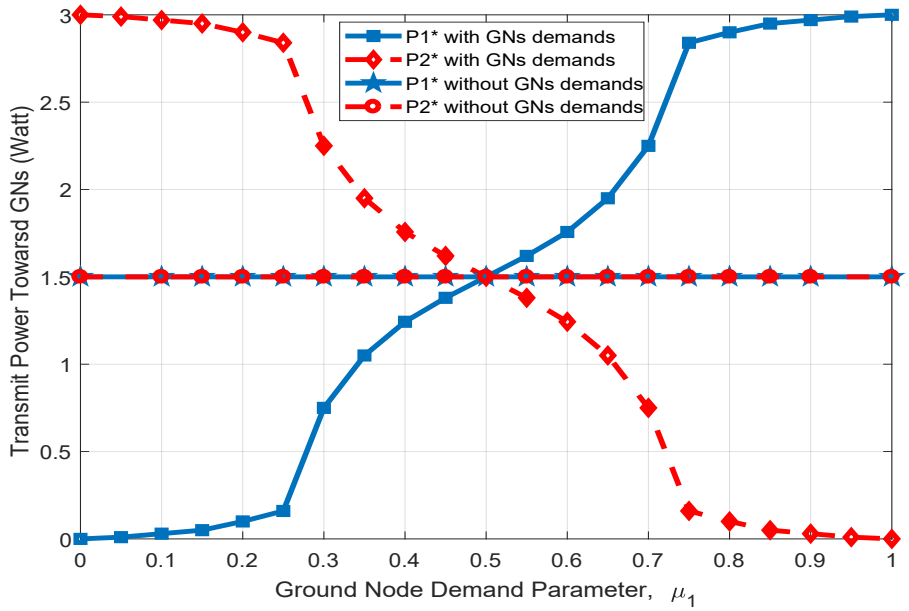

Figure 2.3: Transmit power towards ERs versus demand parameter of ER_1.

Figure 2.4 shows the optimal normalized harvesting time, τ^*/T, for different

demand values, which also means for the different optimized positions of the UAV. The results are plotted as a function of μ_1, while recalling that the demands are normalized such such that $\mu_1 + \mu_2 = 1$. The figure illustrates the usefulness of optimizing the UAV position according to the ERs' demands. It is clear that in all cases, except when the ERs have equal demands, the WPT time will be lower when the UAV takes the ERs' demands into consideration. For example, when $\mu_1 = 0.8$, i.e., $\mu_2 = 0.2$, the normalized harvesting time is almost 0.3 while it is around 0.6 when ERs' demands are not taken into account. With the ensuing time savings, the UAV can be used for other missions

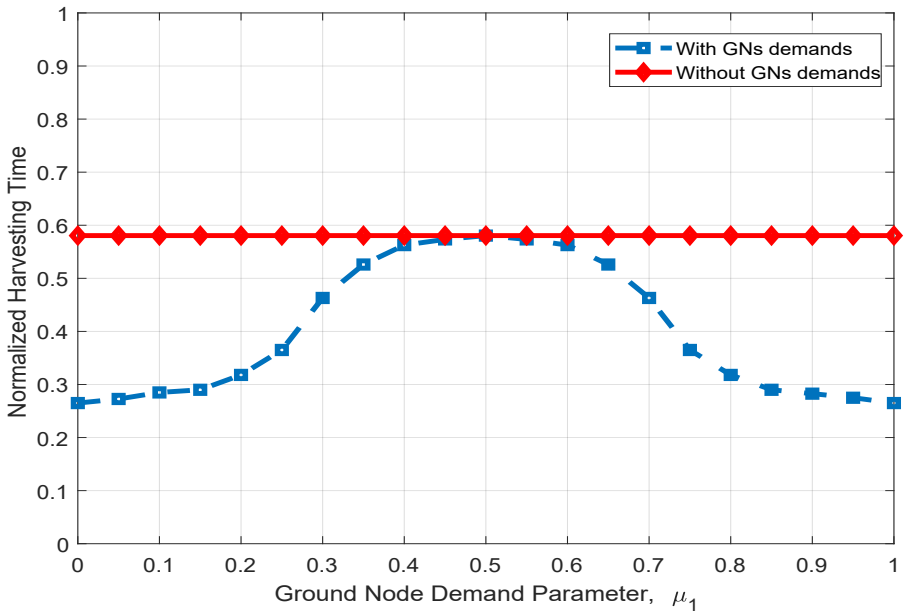

Figure 2.4: Normalized harvesting time versus demand parameter of ER_1.

Figure 2.5 displays the effect of varying demands on the energy efficiency of the system. Similar to Figure 2.4, results are plotted as a function of μ_1. The energy efficiency, when the optimization of the UAV position does not take into account the ERs' demands will be fixed. The energy efficiency with optimized UAV position based on the ERs' demands will be better in all cases. Obviously, the result is the same when

the ERs have the same demand. For instance, when $N_b = 100$ and $\mu_1 = 0.75$, there is a considerable difference in the energy efficiency when ERs' demands are taken into account and when not. Note that by increasing the number of antennas of the BS, the energy efficiency increases in all cases.

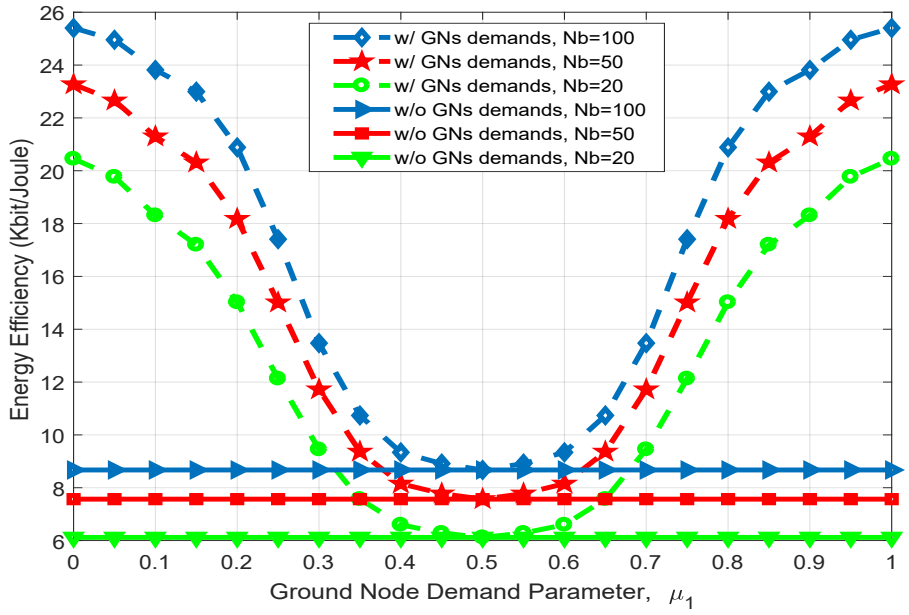

Figure 2.5: Energy efficiency versus demand parameter of ER_1.

2.4 Summary

In this chapter, we presented the resource allocation problem in the UAV-WPCN, where a multiple-antenna UAV is deployed for charging ground nodes through RF wireless power transfer to assist their uplink data communication with a terrestrial base station. The optimization problem was solved by exploiting the movement flexibility of the UAV, which allows minimizing the path loss on the air-to-ground channels according to the nodes' demands, and optimizing the transmit powers towards the maximization of the energy efficiency of the system. The results show that significant EE can be achieved by the proposed allocation scheme. In particular, the

results showed that less wireless power transfer time will be needed from the UAV to simultaneously charge GNs when their demands are taken into account. However, this scenario covers only a system, where the UAV is used to send energy signal towards the ERs and uses the OMA scheme for uplink transmissions, where in many use-cases, the UAVs are called to not only charge devices but also to send and/or collect information to/from them. Using the concept of WIPT/SWIPT, where the transmitter sends power and information signals towards ERs and IRs, the UAVs can be deployed to provide efficient WPT along with reliable data services when and where needed. The use of such a concept needs to meet the radio resource sharing of 5G and beyond 5G systems, where non-orthogonal multiple access (NOMA) will highly likely be replacing the conventional OMA. The details of such a scenario, i.e., using UAV to enable WIPT scenario based on NOMA scheme, will be discussed in the next chapter.

Chapter 3

Single UAV-Enabled Wireless Information and Power Transfer

In Chapter 2, we presented the UAV-WPCN scenario, where the primary use of the UAV is limited to charge ERs to enable their uplink transmissions via conventional OMA scheme. Therefore, in this chapter, we propose a wireless communication network in which a UAV deploys information and power transfer towards co-located IRs and ERs to enable downlink and uplink data transmission through the NOMA scheme. We present the details of the UAV-WIPT scenario and apply the suggested methodology to maximize the EE by optimally allocating the available resources.

3.1 UAV-WIPT System and Channel Models

The UAV serves K single-antenna IRs and J single-antenna ERs in each time slot T (Figure 3.1). The total number of antennas at the UAV is $N = N_E + N_I$, with N_E used for the ERs, and N_I dedicated to the IRs. The time slot is divided into two phases. In

the first phase, αT $(0 < \alpha < 1)$, the UAV transmits energy signals to the ERs. In the second phase, $(1-\alpha)T$, the ERs make use of the harvested energy to transmit their always-available data to the UAV. Simultaneously, the UAV transmits information to the IRs. The data transmissions on the uplink (U) and downlink (D) are performed according to the NOMA protocol. Without loss of generality, the time slot duration T is set to unity. The position of the UAV is denoted $(X_{\mathrm{UAV}}, Y_{\mathrm{UAV}}, h_{\mathrm{UAV}})$, the one of ER_j is $(X_{\mathrm{ER}_j}, Y_{\mathrm{ER}_j}, h_{\mathrm{ER}_j})$, and that of IR_k is $(X_{\mathrm{IR}_k}, Y_{\mathrm{IR}_k}, h_{\mathrm{IR}_k})$. In this work, we focus on the system operation once the UAV starts hovering in a specific position, i.e., $(X_{\mathrm{UAV}}, Y_{\mathrm{UAV}}, h_{\mathrm{UAV}})$, for serving the ground devices.

For the channel models, channels are of two types: air-to-ground (A2G) from the UAV to IRs and ERs, and ground-to-air (G2A) from ERs to the UAV. The complex channel vector of link UAV-IR_k is denoted $\mathbf{h}_k \in \mathbb{C}^{1\times N_I}$, $k = 1, \cdots, K$. For ER_j, $j = 1, \cdots, J$, the complex channel vector of the A2G link is denoted $\mathbf{g}_j \in \mathbb{C}^{1\times N_E}$, and the one of the G2A is $\mathbf{z}_j \in \mathbb{C}^{N_E\times 1}$. First, we have $\mathbf{g}_j = \mathbf{g}'_j/\sqrt{L^{\mathrm{D}}_{\mathrm{ER}_j}}$, where $L^{\mathrm{D}}_{\mathrm{ER}_j}$ is the average path-loss, and $\mathbf{g}'_j = [g'_{j,1}, g'_{j,2}, \ldots, g'_{j,N_E}]$ is the normalized channel fading vector. Assuming Rician fading, $\mathbf{g}'_j$ can be written as [80]:

$$\mathbf{g}_j{}' = \sqrt{\frac{\mathcal{K}}{\mathcal{K}+1}}\mathbf{1}_{1\times N_E} + \sqrt{\frac{1}{\mathcal{K}+1}}\tilde{\mathbf{g}}_j, \tag{3.1}$$

where $\mathcal{K}$ is the Rice factor, $\mathbf{1}_{1\times N_E}$ is a unity row vector, and the non-line-of-sight (NLoS) fading component $\tilde{\mathbf{g}}_j$ is a row vector whose elements are i.i.d. complex Gaussian random variables with zero mean and unit variance, i.e., $\mathcal{CN}(0,1)$. The average A2G free-space distance-dependent path loss of ER_j, $L^{\mathrm{D}}_{\mathrm{ER}_j}$ in dB, is given by

$$L^{\mathrm{D}}_{\mathrm{ER}_j} = p_{\mathrm{LoS},j}\, L_{\mathrm{LoS},j} + (1 - p_{\mathrm{LoS},j})\, L_{\mathrm{NLoS},j}, \tag{3.2}$$

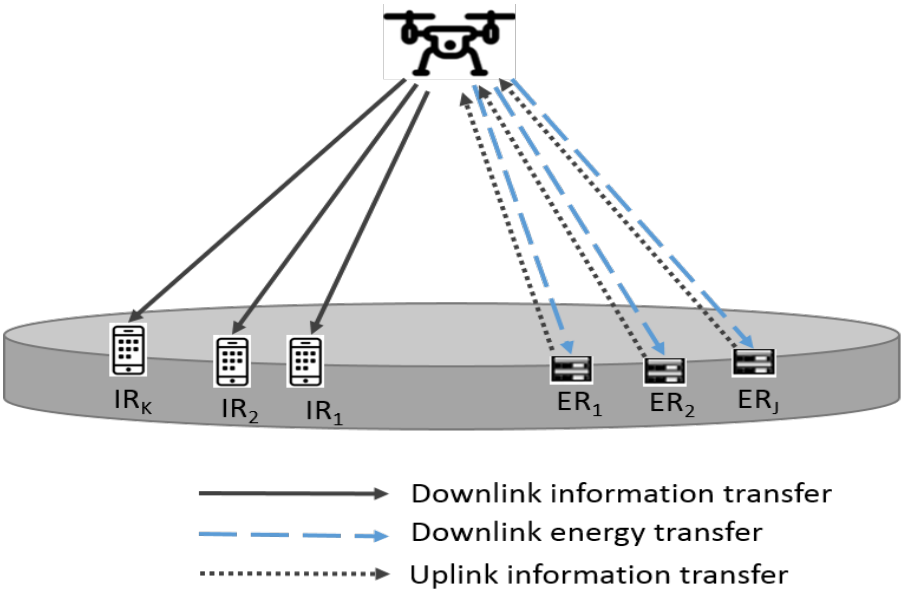

Figure 3.1: UAV-WIPT system model.

where the LoS and NLoS path losses are given by as in (2.3) and (2.4), respectively. The probability that the UAV has LoS with ER_j ,$p_{\text{LoS},j}$, can be given as in (2.5), and the Euclidean distance is given as in (2.7).

The A2G channel model described above w.r.t. ERs ($\mathbf{g}$) applies to the IRs ($\mathbf{h}$) by replacing k with j and IR with ER in (2.3)-(2.7) and (3.1)-(3.2). For the channel between ER_j and UAV, $\mathbf{z}_j$, we also consider a Rician model as for $\mathbf{g}_j$, with $\mathbf{z}_j = \mathbf{z}'_j/\sqrt{L^{\text{U}}_{\text{ER}_j}}$ and $L^{\text{U}}_{\text{ER}_j}$ being the average G2A distance-dependent path-loss.

3.2 Energy Transmission

The UAV transmits energy signal $\mathbf{x}_1 \in \mathbb{C}^{N_E \times 1}$, which consists of J energy beams, one for each ER, i.e.,

$$\mathbf{x}_1 = \sum_{j=1}^{J} \sqrt{P_j^{\text{D}}}\, \mathbf{w}_j s_j^{\text{ER}}, \tag{3.3}$$

where P_j^{D} is the transmit power destined for ER_j, $s_j^{\mathrm{ER}} \in \mathcal{CN}(0,1)$ denotes the energy-carrying signal, and $\mathbf{w}_j \in \mathbb{C}^{N_E \times 1}$ is the corresponding energy beamforming vector. For the j^{th} ER, the received signal is given by

$$y_j^{\mathrm{ER}} = \mathbf{g}_j \sum_{i=1}^{J} \sqrt{P_i^{\mathrm{D}}}\, \mathbf{w}_j s_j^{\mathrm{ER}} + n_j^{\mathrm{ER}}, \tag{3.4}$$

where $n_j^{\mathrm{ER}} \sim \mathcal{CN}(0, \sigma^2)$ is the AWGN noise. Without loss of generality, we assume equal noise powers for all ERs, i.e., σ^2. It is assumed that the harvested energy is the result of the energy signal, and that noise does not take part in it. Assuming the availability of perfect CSI, the optimal weight vector $\mathbf{w}_j^{\star}$ is $\mathbf{g}_j^{\dagger}/\|\mathbf{g}_j\|$. Hence, energy that is harvested by ER_j during the first phase is given by

$$E_j = \zeta_j \alpha |\mathbf{g}_j \mathbf{w}_j^{\star}|^2 \sum_{i=1}^{J} P_i^{\mathrm{D}} \; = \zeta_j \alpha \frac{\|\mathbf{g}_j'\|^2}{L_{\mathrm{ER}_j}^{\mathrm{D}}} P^{\mathrm{D}}, \tag{3.5}$$

where $0 < \zeta_j \leq 1$ is the energy-harvesting circuit efficiency [73], assumed the same for all ERs, and P^{D} is the total power destined to ERs.

3.3 Information Transmission

In the second phase, ERs use the harvested energy for their uplink communication with the UAV, simultaneously with the downlink transmission from the UAV to the IRs.

3.3.1 Uplink Information Transmission

The transmit power from the j^{th} ER is $P_j^{\mathrm{U}} = \frac{E_j}{1-\alpha}$. The UAV receives the superposed message signal of J ERs, and applies SIC to decode each device's message. The

received signal at the UAV, is given by

$$\mathbf{y}_{\text{UAV}} = \sum_{j=1}^{J} \sqrt{P_j^{\text{U}}}\, \mathbf{z}_j\, \mathbf{o}_j s_j^{\text{UAV}} + \mathbf{H}_{\text{SI}} \sum_{k=1}^{K} \sqrt{Q_k^{\text{D}}}\, \mathbf{v}_k s_k^{\text{IR}} + \mathbf{n}, \tag{3.6}$$

where $\mathbf{o}_j \in \mathbb{C}^{1\times N_E}$ is the beamforming vector of the j^{th} ER, and $s_j^{\text{UAV}} \in \mathcal{CN}(0,1)$ is the normalized data symbol of ER_j towards the UAV. Further, $\mathbf{H}_{\text{SI}} \in \mathbb{C}^{N_I\times N_E}$ is the self interference (SI) channel due to the full-duplex process, i.e., simultaneous uplink and downlink transmissions [81], Q_k^{D} is the transmit power for IR_k, $\mathbf{v}_k \in \mathbb{C}^{N_I\times 1}$ is the corresponding beamforming vector, $s_k^{\text{IR}} \in \mathcal{CN}(0,1)$ denotes the information-bearing signal for the k^{th} IR, and $\mathbf{n}$ is the AWGN with zero mean and covariance matrix $\mathbb{E}\{\mathbf{n}\mathbf{n}^\dagger\} = \sigma^2\mathbf{I}_{N_E}$, where $\mathbf{I}$ is the identity matrix. We assume that powerful SI cancellation is in place [82], thus its effect can be ignored.

3.3.2 Downlink Information Transmission

The data signal $\mathbf{x}_2 \in \mathbb{C}^{N_I\times 1}$ sent by the UAV to the IRs consists of K information beams, one for each IR. Hence, we have

$$\mathbf{x}_2 = \sum_{k=1}^{K} \sqrt{Q_k^{\text{D}}}\, \mathbf{v}_k s_k^{\text{IR}}. \tag{3.7}$$

Each IR encounters interference from the uplink signals of ERs towards the UAV, as well as interference from the downlink beams to other IRs. The received signal at IR_k is given by

$$y_k^{\text{IR}} = \mathbf{h}_k \sum_{i=1}^{K} \sqrt{Q_i^{\text{D}}}\, \mathbf{v}_i s_i^{\text{IR}} + \sum_{j=1}^{J} \sqrt{P_j^{\text{U}}}\, \mathbf{o}_j s_j^{\text{UAV}} + n_k^{\text{IR}}. \tag{3.8}$$

Since the interferences from the ERs to IR_k are small compared to the interferences from other IRs, their effect can be neglected. Hence, the signal-to-interference-plus-noise ratio (SINR) at the k^{th} IR is formulated as

$$\gamma_k = \frac{Q_k^{\mathrm{D}} \mathbf{v}_k^{\dagger} \mathbf{h}_k^{\dagger} \mathbf{h}_k \mathbf{v}_k}{\sum\limits_{i=1, i \neq k}^{K} Q_i^{\mathrm{D}} \mathbf{v}_i^{\dagger} \mathbf{h}_k^{\dagger} \mathbf{h}_k \mathbf{v}_i + \sigma^2}, \quad \forall k. \tag{3.9}$$

3.4 Energy Efficiency Maximization

3.4.1 Energy Efficiency Formulation

To formulate the EE of the UAV-WIPT system, we have to construct the throughputs of the downlink and uplink stages. For the downlink information NOMA setup, where the channel gains of IRs are increasing when closer to the UAV (channel gain of IR_1 is larger than IR_2, and so on until IR_K), the rate in *bps* related to a given IR can be expressed as [83]:

$$R_k^{\mathrm{D}} = (1-\alpha) W \log_2 \left(1 + \frac{\frac{Q_k^{\mathrm{D}} \|\mathbf{h}_k{}'\|^2}{L_{\mathrm{IR}_k}^{\mathrm{D}}(1-\alpha)}}{\sum\limits_{i=1, i \neq k}^{K-1} \frac{Q_i^{\mathrm{D}} \|\mathbf{h}_k{}'\|^2}{L_{\mathrm{IR}_i}^{\mathrm{D}}(1-\alpha)} + 1} \right), \tag{3.10}$$

where W is the bandwidth. According to the principles of power-domain NOMA, for a given IR, the strong interfering signals are mainly due to the transmissions to users with low channel gains. The weakest channel user, IR_K, which receives low interferences due to the relatively low powers of the messages of high channel gain users, cannot cancel any interferences. However, the highest channel gain user, IR_1, which receives strong interferences due to the relatively high powers of the transmissions to

weak users, can cancel all interfering signals [84]. On the other hand, for the uplink NOMA throughput, knowing that the channel gains are stronger when ERs are closer to the UAV (channel gain of ER_1 is larger than ER_2, and so on until ER_J), then based on (3.5) and (3.6), the rate related to a given ER can be expressed as [83]:

$$R_j^{\mathrm{U}} = (1-\alpha)W \log_2 \left(1 + \frac{\frac{\zeta P_j^{\mathrm{D}} \|\mathbf{g}_j'\|^2 \|\mathbf{z}_j'\|^2 \alpha}{L_{\mathrm{ER}_j}^{\mathrm{U}} L_{\mathrm{ER}_j}^{\mathrm{D}} (1-\alpha)}}{\sum_{l=j+1}^{J} \frac{\zeta P_l^{\mathrm{D}} \|\mathbf{g}_l'\|^2 \|\mathbf{z}_l'\|^2 \alpha}{L_{\mathrm{ER}_l}^{\mathrm{U}} L_{\mathrm{ER}_l}^{\mathrm{D}} (1-\alpha)} + 1} \right). \tag{3.11}$$

The signal of the highest channel gain user, ER_1, is decoded first at the UAV. As a result, ER_1 experiences interference from all other ERs. Then, the signal for the second highest channel gain user is decoded until the last one, ER_J, [85].

Define the downlink throughput as the sum-rate of all IRs, i.e., $R^{\mathrm{D}} = \sum_{k=1}^{K} R_k^{\mathrm{D}}$, and the uplink throughput as the sum-rate $R^{\mathrm{U}} = \sum_{j=1}^{J} R_j^{\mathrm{U}}$. The EE of the system is expressed as

$$\eta = \frac{\text{Total Throughput}}{\text{Total Consumed Energy}} = \frac{R^{\mathrm{D}} + R^{\mathrm{U}}}{P_{\mathrm{DC}} + P^{\mathrm{D}} + Q^{\mathrm{D}}(1-\alpha)}, \tag{3.12}$$

where P_{DC} is the constant power consumption of the UAV, and where $P^{\mathrm{D}} = \sum_{j=1}^{J} P_j^{\mathrm{D}} = \beta P$ and $Q^{\mathrm{D}} = \sum_{k=1}^{K} Q_k^{\mathrm{D}} = (1-\beta)P$ are the powers dedicated to the ERs and the IRs, respectively, i.e., $P = P^{\mathrm{D}} + Q^{\mathrm{D}}$, where β indicates the percentage of power destined to ERs and $(1-\beta)$ indicates to the percentage of power destined to IRs. Hence, a larger value of β means that higher priority is given to the WPT.

3.4.2 Energy-Efficient Resource Allocation

The optimization problem which aims to maximize EE is formulated as follows:

$$
\begin{aligned}
\mathrm{OP}_1: \quad & \max_{Q^{\mathrm{D}},P^{\mathrm{D}},\alpha,\beta} \quad \eta \\
& \text{subject to:} \quad P \le P_{\max}, \\
& \qquad\qquad\quad P_j^{\mathrm{U}} \le P_{j,\max}^{\mathrm{U}}, \quad \forall j, \\
& \qquad\qquad\quad \alpha < 1, \\
& \qquad\qquad\quad 0 \le \beta \le 1, \\
& \qquad\qquad\quad R_j^{\mathrm{U}} \ge R_{j,\min}^{\mathrm{U}}, \quad \forall j, \\
& \qquad\qquad\quad R_k^{\mathrm{D}} \ge R_{k,\min}^{\mathrm{D}}, \quad \forall k, \\
& \qquad\qquad\quad P_{\mathrm{thr}}^{\mathrm{U}} \le P_j^{\mathrm{U}} z_j - \sum_{l=j+1}^{J} P_l^{\mathrm{U}} z_l, \quad \forall j, \\
& \qquad\qquad\quad Q_{\mathrm{thr}}^{\mathrm{D}} \le \left(Q_k^{\mathrm{D}} - \sum_{m=1}^{k-1} Q_m^{\mathrm{D}} \right) h_{k-1}, \quad \forall k,
\end{aligned}
\tag{3.13}
$$

where $R_{j,\min}^{\mathrm{U}}$ and $R_{k,\min}^{\mathrm{D}}$ denote the minimum required rates of ER_j and IR_k, respectively, and where $P_{\mathrm{thr}}^{\mathrm{U}}$ and $Q_{\mathrm{thr}}^{\mathrm{D}}$ are the SIC detection thresholds of the uplink and downlink, respectively.

It is obvious that OP_1 is a fractional optimization problem with variables P^{D}, Q^{D}, and α, and is non-convex. Exploiting the idea in [78], the fractional programming problem can be transformed into a convex problem by introducing variable χ^* as the optimal EE when we have the optimal powers and optimal WPT fraction of time, α. Hereafter, for more tractability and to get a clearer insight into the system performance, we focus on the scenario with two ERs and two IRs.

Accordingly, (3.13) becomes

$$\begin{aligned}
\mathrm{OP}_2: \quad & \max_{Q^{\mathrm{D}},P^{\mathrm{D}},\alpha,\beta} \quad \sum_{k=1}^{2} R_k^{\mathrm{D}} + \sum_{j=1}^{2} R_j^{\mathrm{U}} \\
& \quad - \chi^*(P_{DC} + P_D^{ER} + Q_D^{IR}(1-\alpha)) \\
\text{subject to:} \quad & P \le P_{\max}, \\
& P_j^{\mathrm{U}} \le P_{j,\max}^{\mathrm{U}}, \quad j = 1,2, \\
& \alpha < 1, \\
& 0 \le \beta \le 1, \\
& R_j^{\mathrm{U}} \ge R_{j,\min}^{\mathrm{U}}, \quad j = 1,2, \\
& R_k^{\mathrm{D}} \ge R_{k,\min}^{\mathrm{D}}, \quad k = 1,2, \\
& P_{\mathrm{thr}}^{\mathrm{U}} \le P_j^{\mathrm{U}} z_j - \sum_{l=j+1}^{J} P_l^{\mathrm{U}} z_l, j = 1,2, \\
& Q_{\mathrm{thr}}^{\mathrm{D}} \le \left(Q_k^{\mathrm{D}} - \sum_{m=1}^{k-1} Q_m^{\mathrm{D}} \right) h_{k-1}, k = 1,2.
\end{aligned} \tag{3.14}$$

By introducing $\vartheta \ge 0$, $\varsigma_1 \ge 0$, $\varsigma_2 \ge 0$, $\varepsilon \ge 0$, $\varrho \ge 0$, $\varphi_1 \ge 0$, $\varphi_2 \ge 0$, $\lambda_1 \ge 0$, $\lambda_2 \ge 0$, $\mu \ge 0$, and $\phi \ge 0$, as the Lagrange multipliers associated with the constraints in OP_2, the Lagrangian function of OP_2 can be formulated as:

$$\begin{aligned}
& \mathcal{L}(\vartheta, \varsigma_1, \varsigma_2, \varepsilon, \varrho, \varphi_1, \varphi_2, \lambda_1, \lambda_2, \mu, \phi, \beta, Q_1^{\mathrm{D}}, Q_2^{\mathrm{D}}, P_1^{\mathrm{D}}, P_2^{\mathrm{D}}, \alpha) \\
& = \sum_{k=1}^{2} R_k^{\mathrm{D}} + \sum_{j=1}^{2} R_j^{\mathrm{U}} - \chi^*(P_{\mathrm{DC}} + \beta P + (1-\beta)(1-\alpha)P) \\
& - \vartheta(P - P_{\max}) - \varsigma_1(P_1^{\mathrm{U}} - P_{1,\max}^{\mathrm{U}}) - \varsigma_2(P_2^{\mathrm{U}} - P_{2,\max}^{\mathrm{U}}) \\
& - \varepsilon(\alpha - 1) - \varphi_1(R_{1,\min}^{\mathrm{U}} - R_1^{\mathrm{U}}) - \varphi_2(R_{2,\min}^{\mathrm{U}} - R_2^{\mathrm{U}}) \\
& - \varrho(\beta - 1) - \lambda_1(R_{1,\min}^{\mathrm{D}} - R_1^{\mathrm{D}}) - \lambda_2(R_{2,\min}^{\mathrm{D}} - R_2^{\mathrm{D}}) \\
& - \mu(P_{\mathrm{thr}}^{\mathrm{U}} - P_1^{\mathrm{U}} z_1 + P_2^{\mathrm{U}} z_2) - \phi(Q_{\mathrm{thr}}^{\mathrm{D}} - Q_2^{\mathrm{D}} h_1 + Q_1^{\mathrm{D}} h_1).
\end{aligned} \tag{3.15}$$

We assume that the UAV uses its maximum power, such that $\beta P_{\max} = P^{\mathrm{D}}$ and $(1-\beta)P_{\max} = Q^{\mathrm{D}}$. Our goal is to find β, Q_1^{D}, and hence $Q_2^{\mathrm{D}} = (1-\beta)P_{\max} - Q_1^{\mathrm{D}}$, as well as P_1^{D} which also implicitly means $P_2^{\mathrm{D}} = \beta P_{\max} - P_1^{\mathrm{D}}$, and the optimal WPT fraction of time (α^*). The optimization problem OP_2 is split into two stages. In the first stage, the aim is to determine the optimized value of β. In the second stage, the optimization problem OP_2 after obtaining β is split into two sub-problems. The first one corresponds to the downlink WIT, where the purpose is to find Q_1^{D} and Q_2^{D}, taking into account that the WIT takes place in the second phase of the process, with the constraints focused on the first, fifth, and eighth constraints of OP_2. In the second sub-problem, the aim is to optimize P_1^{D}, P_2^{D}, and α, where this accounts for the first, second, third, fifth, and seventh constraints. After getting the optimized parameters, we merge them together to find the optimized EE, which is the result of the optimized rates on both processes. Taking into account that OP_2 is a nonlinear programming problem, this can be done through derivation of the Lagrangian function (3.15) w.r.t. Q_1^{D}, P_1^{D}, and α, and setting them to zero, i.e.,

$$\frac{\partial \mathcal{L}}{\partial Q_1^{\mathrm{D}}} = 0, \quad \frac{\partial \mathcal{L}}{\partial P_1^{\mathrm{D}}} = 0, \quad \frac{\partial \mathcal{L}}{\partial \alpha} = 0, \tag{3.16}$$

where we dropped the arguments of the functional $\mathcal{L}(\vartheta, \varsigma_1, \varsigma_2, \varepsilon, \varrho, \varphi_1, \varphi_2, \lambda_1, \lambda_2, \mu, \phi, \beta, Q_1^{\mathrm{D}}, Q_2^{\mathrm{D}}, P_1^{\mathrm{D}}, P_2^{\mathrm{D}}, \alpha)$ for notational simplicity. The updating of the Lagrangian variables (ϑ, ς_1, ς_2, ε,ϱ, φ_1, φ_2, λ_1, λ_2 , μ, and ϕ) can be done using the gradient-decent method, according to

$$\vartheta(i+1) = [\vartheta(i) - \triangle_{\vartheta}(P_{\max} - P)]^{+}, \tag{3.17}$$

$$\varsigma_1(i+1) = [\varsigma_1(i) - \triangle_{\varsigma_1}(P_{1,\max}^{\mathrm{U}} - P_1^{\mathrm{U}})]^{+}, \tag{3.18}$$

$$\varsigma_2(i+1) = [\varsigma_2(i) - \triangle_{\varsigma_2}(P^{\mathrm{U}}_{2,\max} - P^{\mathrm{U}}_2)]^+, \tag{3.19}$$

$$\varepsilon(i+1) = [\varepsilon(i) - \triangle_{\varepsilon}(1-\alpha)]^+, \tag{3.20}$$

$$\varrho(i+1) = [\varrho(i) - \triangle_{\varrho}(1-\beta)]^+, \tag{3.21}$$

$$\varphi_1(i+1) = [\varphi_1(i) - \triangle_{\varphi_1}(R^{\mathrm{U}}_1 - R^{\mathrm{U}}_{1,\min})]^+, \tag{3.22}$$

$$\varphi_2(i+1) = [\varphi_2(i) - \triangle_{\varphi_2}(R^{\mathrm{U}}_2 - R^{\mathrm{U}}_{2,\min})]^+, \tag{3.23}$$

$$\lambda_1(i+1) = [\lambda_1(i) - \triangle_{\lambda_1}(R^{\mathrm{D}}_1 - R^{\mathrm{D}}_{1,\min})]^+, \tag{3.24}$$

$$\lambda_2(i+1) = [\lambda_2(i) - \triangle_{\lambda_2}(R^{\mathrm{D}}_2 - R^{\mathrm{D}}_{2,\min})]^+, \tag{3.25}$$

$$\mu(i+1) = [\mu(i) - \triangle_{\mu}(P^{\mathrm{U}}_1 z_1 - P^{\mathrm{U}}_2 z_2 - P^{\mathrm{U}}_{\mathrm{thr}})]^+, \tag{3.26}$$

$$\phi(i+1) = [\phi(i) - \triangle_{\phi}(Q^{\mathrm{D}}_2 h_1 + Q^{\mathrm{D}}_1 h_1 - Q^{\mathrm{D}}_{\mathrm{thr}})]^+, \tag{3.27}$$

where i is the iteration index, and the $\triangle$'s are the iteration steps.

The closed form of the optimized power fraction can be obtained by solving $\frac{\partial \mathcal{L}}{\partial \beta} = 0$, which leads to:

$$\begin{aligned}\beta = {} & \frac{\alpha\varphi_1 + \alpha}{\alpha\varphi_1 + \alpha\lambda_1 + 2\alpha} + \frac{((1-\alpha)\varphi_1 - \alpha + 1)L^{\mathrm{D}}_{\mathrm{IR}_1}}{(\alpha\varphi_1 + \alpha\lambda_1 + 2\alpha)\|\mathbf{h}_1{}'\|^2 P_{\max}} \\ & + \frac{((\alpha-1)\lambda_1 + \alpha - 1)L^{\mathrm{D}}_{\mathrm{ER}_1} L^{\mathrm{U}}_{\mathrm{ER}_1}}{(\alpha\varphi_1 + \alpha\lambda_1 + 2\alpha)\|\mathbf{g}_1{}'\|^2 \|\mathbf{z}_1{}'\|^2 P_{\max}\zeta} - \chi^* \alpha P_{\max} - \varrho \\ & - \frac{\zeta\alpha\|\mathbf{g}_1{}'\|^2 P_{\max}}{L^{\mathrm{D}}_{\mathrm{ER}_1}(1-\alpha)}.\end{aligned} \tag{3.28}$$

The solution of the optimization problem OP_2 is summarized in Algorithm 3.1, where $Q^{\mathrm{D}}_{1_0}$, $P^{\mathrm{D}}_{1_0}$, and α_0 denote the initial values for Q^{D}_1, P^{D}_1, and α, respectively.

Algorithm 3.1. Energy-Efficient Resource Allocation

Input: $(X_{\mathrm{UAV}}, Y_{\mathrm{UAV}}, h_{\mathrm{UAV}})$; $(X_{\mathrm{ER}_j}, Y_{\mathrm{ER}_j}, h_{\mathrm{ER}_j})$, $j = 1, 2$; $(X_{\mathrm{IR}_k}, Y_{\mathrm{IR}_k}, h_{\mathrm{IR}_k})$, $k = 1, 2$; a, b, β, ξ_{LoS}, ξ_{NLoS}, f, η, σ, $R^{\mathrm{U}}_{\min}$, $R^{\mathrm{D}}_{\min}$, $\triangle_{\varsigma_1}$, $\triangle_{\varsigma_2}$, $\triangle_{\varepsilon}$, $\triangle_{\varrho}$, $\triangle_{\varphi_1}$, $\triangle_{\varphi_2}$,$\triangle_{\lambda_1}$,$\triangle_{\lambda_2}$, $\triangle_{\mu}$,$\triangle_{\phi}$, and χ^*.

Output: $\left[\beta, Q^{\mathrm{D}}_1, Q^{\mathrm{D}}_2, P^{\mathrm{D}}_1, P^{\mathrm{D}}_2, \alpha\right]$.

Initialization: $\left[Q^{\mathrm{D}}_{1_0},\ P^{\mathrm{D}}_{1_0},\ \alpha_0\right]$, $\vartheta = 0$, $\varsigma_1 = 0$, $\varsigma_2 = 0$, $\varepsilon = 0$, $\varphi_1 = 0$, $\varphi_2 = 0$, $\lambda_1 = 0$, $\lambda_2 = 0$, $\mu = 0$, $\phi = 0$.

1: Calculate β as per (3.28).
2: Update ϑ, λ_1, λ_2 and ϕ based on (3.17), (3.24), (3.25), and (3.27), respectively.
3: Solve (3.16) to obtain Q^{D}_1.
4: Update ϑ, ς_1, ς_2, ε, φ_1, φ_2, and μ based on (3.17), (3.18), (3.19), (3.20), (3.22), (3.23), and (3.26), respectively.
5: Solve (3.16) to obtain P^{D}_1 and α.
6: Compute $\left[Q^{\mathrm{D}*}_1, Q^{\mathrm{D}*}_2, P^{\mathrm{D}*}_1, P^{\mathrm{D}*}_2, \alpha^*\right]$ by solving (3.14).

3.4.3 Complexity Analysis

As discussed in the previous chapter, the complexity is mainly depending on the deployed algorithms. For instance, in the UAV-WIPT case, the problem was solved based on an algorithm that is constructed through the gradient descent method. Accordingly, the worst complexity of such method is $\mathcal{O}(n \times \frac{1}{\epsilon})$ [79], where n is the number of optimization variables, and ϵ is the solution accuracy. Thus, for Algorithm 3.1, the complexity depends on the number of ERs (J) and IRs (K). Therefore, the complexity for this algorithm is $\mathcal{O}((J + K) \times \frac{1}{\epsilon})$.

3.5 Simulation Results

In the simulations, we set $a = 9.6$, $b = 0.28$, $\xi_{\mathrm{LoS}} = 1$ dB, $\xi_{\mathrm{NLoS}} = 20$ dB, $f = 2$ GHz, $W = 200$ kHz, $\eta = 0.8$, $\sigma^2 = 1$, and $N_E = N_I = 2$. The position of ER_1 is fixed at (1,0,0), and we vary the horizontal coordinate of ER_2 (x,0,0). The UAV is positioned at (0,0,10). Also, the position of IR_1 is set to (-1,0,0), and we vary the horizontal coordinate of IR_2 (-x,0,0). We set $Q^{\mathrm{D}}_{\mathrm{thr}} = P^{\mathrm{U}}_{\mathrm{thr}} = 0.05$ Watt, $P_{\mathrm{DC}} = 5$ Watt, $P_{\max} = 3$

Watt, and $R^{\mathrm{U}}_{\min} = R^{\mathrm{D}}_{\min} = 12$ Kbps.

As a first stage of the process, β is determined before starting the actual transmissions towards the ERs and IRs. According to the closed-form expression of β along with the symmetrical positions of ERs and IRs in our setup, the power among ERs and IRs is split equally. Once β is obtained, the transmissions towards the ERs and IRs start. Figure 3.2 shows the throughput of each IR along with the summation of those rates. It is clear that the throughput of IR_1 always outperforms that of IR_2, for

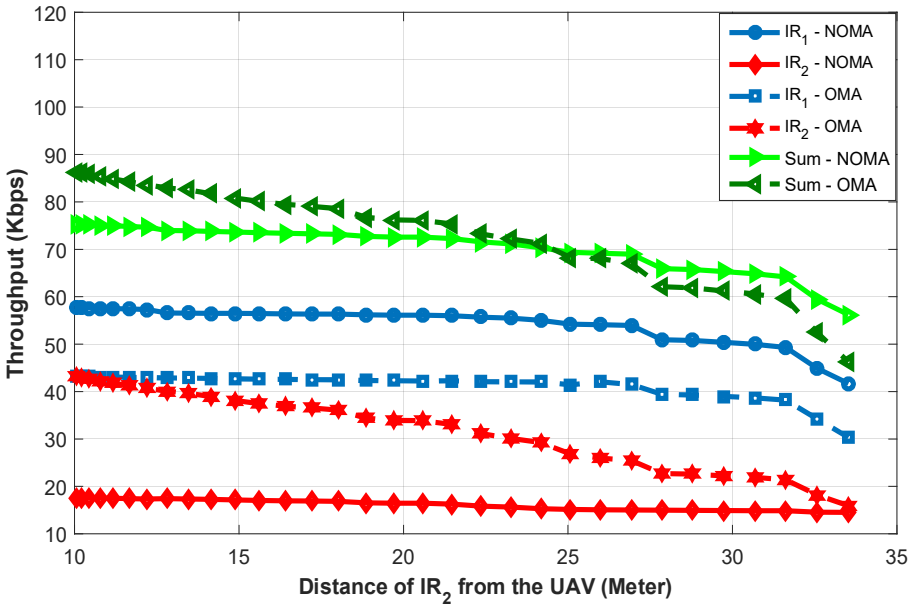

Figure 3.2: Downlink throughput.

both the OMA and NOMA schemes. With OMA protocol, the UAV sends the information separately by dedicating half of the transmission phase, $(1-\alpha)/2$, to each IR. The sum-rate with OMA is better than with NOMA for small distances of IR_2 w.r.t. the UAV, while NOMA starts to outperform OMA as the said distance increases and the link of IR_2 becomes much weaker compared to the link of the strong user.

Energy harvested by the ERs from the downlink WPT is used for their NOMA uplink communication with the UAV. Figure 3.3 illustrates the throughput of each

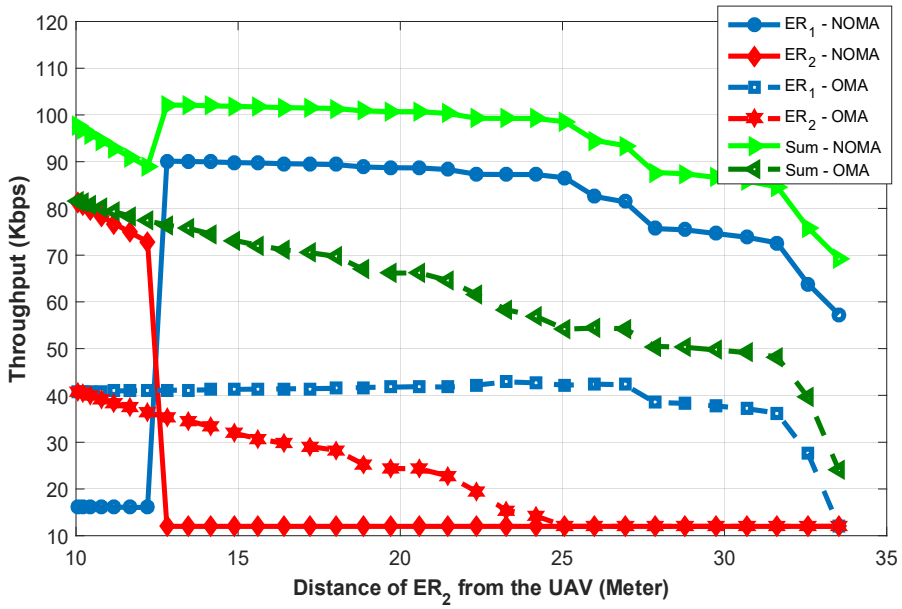

Figure 3.3: Uplink throughput.

ER along with the sum-rate. Results of conventional uplink OMA, where each ER sends its information to the UAV during half of the second phase, i.e., $(1-\alpha)/2$, are also provided. It is obvious that the throughput of ER_1 mostly outperforms the throughput of ER_2 in the OMA set-up. With NOMA, there are some variation and correlation between the rates of ER_1 and ER_2. As observed, the throughput of ER_1 decreases sharply when ER_2 becomes closer to the UAV, which implicitly means that its transmission increases the interference on the ER_1 signal. This can be clearly noticed when the distance of ER_2 is less than 13 meters, which means that it starts to have a strong connection with the UAV. In both OMA and NOMA schemes, the rate of ER_1 starts to decrease when the distance of ER_2 from the UAV increases, which is due to the minimum rate constraints in both schemes. As the rate of ER_2 must also satisfy the said constraints, and with decreasing channel gain with the distance, this is compensated by specifying more power towards ER_2 on the account of ER_1 in both OMA and NOMA. It is clear that the sum-rate of the NOMA based uplink is larger

compared to OMA, due to the simultaneous transmissions from the ERs.

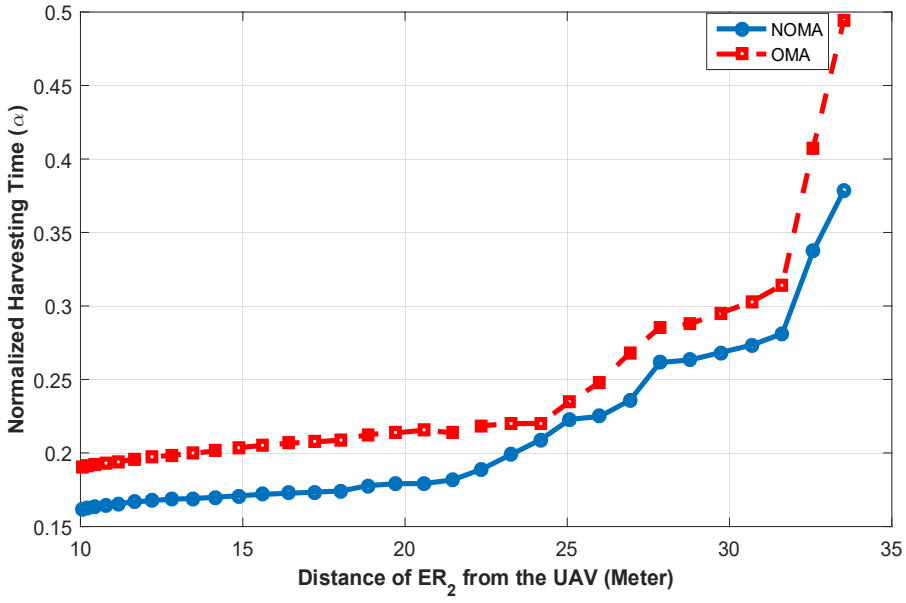

Figure 3.4: Normalized harvesting time.

Figure 3.4 shows the optimal normalized harvesting time, α^*, for different positions of ER_2, while the position of ER_1 remains fixed. The figure compares the fraction of time slot needed for the WPT to ERs to enable their uplink transmissions using NOMA or OMA. As observed, in all cases, the WPT time in the NOMA case is lower compared to OMA.

Figure 3.5 compares the effect of different access schemes, i.e., NOMA and OMA, on the EE of the system. Results are plotted as a function of the distance of ER_2 from the UAV, taking into account that the downlink throughput of IR_2 is constructed from the same distance of the uplink throughput of ER_2. The EE with the NOMA scheme is considerably better than that with OMA for different distances of ER_2 w.r.t the UAV, and the difference increases as the distance of ER_2 from the UAV increases. It is important to note that when the said distance is small and that the ERs and IRs are close to each other, then OMA and NOMA yield similar performance, due to the

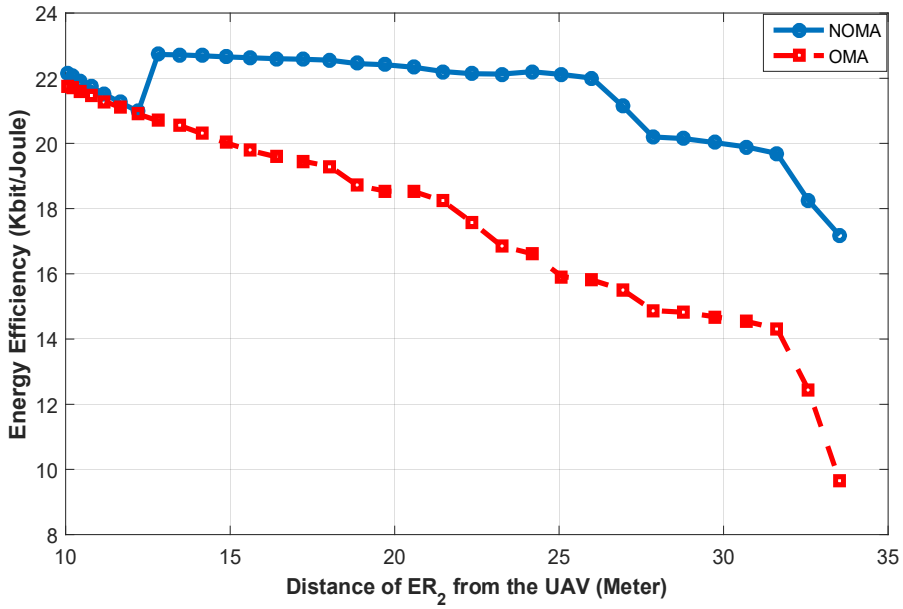

Figure 3.5: System energy efficiency.

loss of the required distinctions between users in NOMA.

3.6 Summary

In this chapter, we investigated the resource allocation in a multiple-antenna UAV deployed for transmitting data to IRs, as well as wireless power to ERs to assist their uplink data communication towards it through the NOMA protocol. The resource allocation problem was solved by optimizing the transmit powers towards the maximization of the EE. The results showed that significant EE can be achieved by the proposed allocation. In particular, it was shown that the EE of the NOMA-based system outperforms that of OMA in most cases w.r.t. the position of the weak user, and that reduced WPT time is needed at the UAV to power devices when NOMA is used for the data communication. The details of the optimization process in this chapter were limited to 2 ERs and 2 IRs with a given and fixed position of the UAV. However, it is very interesting and demanding to extend the process to handle a general number

of ERs and IRs and take into account the UAV trajectory. Although NOMA shows better performance compared to OMA, the superiority of one access scheme over the other cannot be generalized for all cases and applications. In the next chapter, we will introduce other hybrid access schemes, and extend the optimization process to handle general scenarios within two different practical setups.

Chapter 4

Single UAV-Enabled Wireless Simultaneous Information and Power Transfer

In this chapter, we investigate the optimization of the EE in a wireless communication network, where a UAV deploys simultaneous information and power transfer (SWIPT) towards different IRs and ERs to enable downlink and uplink data transmission through NOMA, OMA, or hybrid NOMA/OMA schemes. We present the system model of the UAV-SWIPT network, we formulate and solve the optimization problem for a general number of ERs and IRs aiming to maximize the system's EE while fulfilling the constraints related to the limited power budget of the UAV, the minimum required QoS and the acceptable SIC thresholds. We come up with two main scenarios, i.e., linear and circular, that provide different realizations of the suggested UAV-SWIPT scenario. We propose two different hybrid access schemes depending on the NOMA and OMA schemes, namely, hybrid downlink OMA uplink

NOMA (HDOUN) and hybrid downlink NOMA uplink OMA (HDNUO).

4.1 UAV-SWIPT System and Channel Models

The UAV serves K single-antenna IRs and J single-antenna ERs in each time slot T, in a known region of interest (ROI), as illustrated in Figure 4.1. The total number of antennas at the UAV is $N = N_E + N_I$, with N_E used for the ERs, and N_I dedicated to the IRs. The time slot is divided into two phases. In the first phase, αT $(0 \leq \alpha \leq 1)$, the UAV transmits energy signals to the ERs, while IRs also send uplink pilot signals to the UAV. In the second phase, $(1-\alpha)T$, the ERs make use of the harvested energy to transmit their always-available data to the UAV. Simultaneously, the UAV transmits information to the IRs. The data transmissions on the uplink (U) and downlink (D) are performed according to the NOMA scheme. Without loss of generality, the slot duration T is set to unity. Further, we assume that the positions of the ERs and IRs are perfectly known, the one of ER_j is $(x_{\mathrm{ER}_j}, y_{\mathrm{ER}_j}, h_{\mathrm{ER}_j})$, and that of IR_k is $(x_{\mathrm{IR}_k}, y_{\mathrm{IR}_k}, h_{\mathrm{IR}_k})$. This perfect ULI has been widely used in the literature [86]. The position of the UAV is denoted $(x_{\mathrm{u}}, y_{\mathrm{u}}, h_{\mathrm{u}})$. Besides, a quantized level of the required rate on the uplink is sent from each ER to the UAV to indicate its demand. Based on this side information, and knowledge of the rate requirements of the IRs, the UAV determines the relative demand of each ER and IR, denoted ϖ_j^U and ϖ_k^D, respectively, such that $\sum_{j,k} \varpi_j^U + \varpi_k^D = 1$. Here, a larger value of ϖ means a higher rate demand.

4.1.1 Channel Models

There are three types of channels: air-to-ground (A2G) from the UAV to IRs and ERs, ground-to-air (G2A) from the ERs and IRs to the UAV, and ground-to-ground

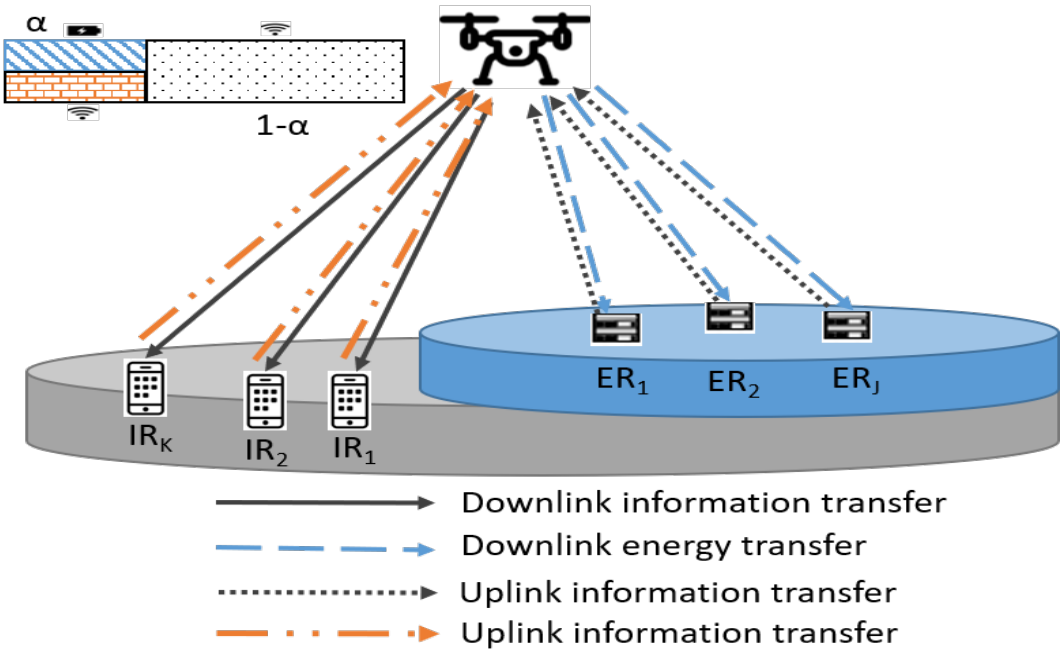

Figure 4.1: UAV-SWIPT system model.

(G2G) between the ERs and IRs. The complex channel vector of link UAV-IR$_k$ is denoted $\mathbf{h}_k \in \mathbb{C}^{1\times N_I}$, $k = 1, \cdots, K$. For ER$_j$, $j = 1, \cdots, J$, the complex channel vector of the A2G link is denoted $\mathbf{g}_j \in \mathbb{C}^{1\times N_E}$, and for the G2A related to ER and IR are $\mathbf{z}_j \in \mathbb{C}^{N_E\times 1}$ and $\mathbf{m}_k \in \mathbb{C}^{N_I\times 1}$, respectively. First, we have $\mathbf{g}_j = \mathbf{g}'_j/\sqrt{L^{\mathrm{D}}_{\mathrm{ER}_j}}$, where $L^{\mathrm{D}}_{\mathrm{ER}_j}$ is the average path-loss, and $\mathbf{g}'_j = [g'_{j,1}, g'_{j,2}, \ldots, g'_{j,N_E}]$ is the normalized channel fading vector. For Rician fading, $\mathbf{g}'_j$ can be written as in (3.1). The average A2G free-space distance-dependent path loss of ER$_j$, $L^{\mathrm{D}}_{\mathrm{ER}_j}$ in dB, is given by as in (3.2). where the LoS and NLoS path losses are given as in (2.3) and (2.4), respectively. The probability that the UAV has LoS with ER$_j$,$p_{\mathrm{LoS},j}$, can be given as in (2.5), and the Euclidean distance is given as in (2.7). The A2G channel model described above w.r.t. ERs ($\mathbf{g}$) applies to the IRs ($\mathbf{h}$) by replacing k with j, and IR with ER in (2.3)-(2.7) and (3.1)-(3.2). For the channel between ER$_j$ and UAV, $\mathbf{z}_j$, we also consider a Rician

model as for $\mathbf{g}_j$, with $\mathbf{z}_j = \mathbf{z}'_j/\sqrt{L^{\mathrm{U}}_{\mathrm{ER}_j}}$ and $L^{\mathrm{U}}_{\mathrm{ER}_j}$ being the average G2A distance-dependent path-loss. The G2A channel model described above w.r.t. ERs ($\mathbf{z}$) applies to the IRs ($\mathbf{m}$) by replacing k with j, and IR with ER. For the G2G channel, the complex channel of link ER_j-IR_k is denoted e_j, which includes the Rayleigh fading from the j$^{\mathrm{th}}$ ER to the the k$^{\mathrm{th}}$ IR along with the path loss, with no LoS component. In particular, $e_j = e'_j/\sqrt{L_{\mathrm{NLoS}_j}}$, where e'_j is the normalized channel fading, and L_{NLoS_j} is the average path-loss similar to (2.4) with the distance being between ER_j and IR_k.

4.1.2 Energy Transmission

The UAV transmits energy signal $\mathbf{x}_1 \in \mathbb{C}^{N_E \times 1}$, which consists of J energy beams, one for each ER is given as in (3.3). For the j^{th} ER, the received signal is given as in (3.4). Without loss of generality, we assume equal noise powers for all ERs, i.e., σ^2. It is assumed that the harvested energy is the result of the energy signal, and that noise does not take part in it. Assuming the availability of perfect CSI, the optimal weight vector $\mathbf{w}^\star_j$ is $\mathbf{g}^\dagger_j/\|\mathbf{g}_j\|$. Hence, the harvested energy by ER_j during the first phase is given by (3.5).

4.1.3 Information Transmission

In the second phase, exploiting the harvested energy gained in the first phase, ERs start their uplink communications with the UAV, simultaneously with the downlink transmission from the UAV to the IRs.

Uplink Information Transmission

The transmit power from the j^{th} ER is $P^{\mathrm{U}}_j = \frac{E_j}{1-\alpha}$. The UAV receives the superposed message signal of J ERs and applies SIC to decode each device's message. The received

signal at the UAV, $\mathbf{y}_{\text{UAV}} \in \mathbb{C}^{N_E \times J}$, is given as in (3.6).

Downlink Information Transmission

In the downlink information transfer, the data signal $\mathbf{x}_2 \in \mathbb{C}^{N_I \times 1}$ sent by the UAV to the IRs, consists of K information beams, one for each IR, and it is formulated as in (3.7). Each IR encounters interference from the uplink signals of ERs towards the UAV, as well as interference from the downlink beams to other IRs. The received signal at IR_k is given by (3.8) Since the interferences from the ERs to IR_k are small compared to the interferences from other IRs, their effect can be neglected. Hence, the signal-to-interference-plus-noise ratio (SINR) at the k^{th} IR is given as in (3.9).

4.1.4 Topology and Distribution

To reflect potential practical scenarios, we consider two setups, namely, linear, and circular, according to the topology and distribution of the ERs and IRs.

Linear Scenario

In the linear scenario, we consider that the ERs and IRs are distributed linearly, this could be a reflection of UAV charging ERs fixed on a bridge to collect data for the number of passing cars, while at the same time it sends data to the IRs of an advertising screen on the same line of the bridge, as shown in Figure 4.2.

Circular Scenario

In the circular scenario, we consider that all ERs are uniformly distributed on the circumference of the circle while all IRs are uniformly distributed on the circumference of a bigger circle. This scenario could be a reflection of a UAV charging ERs fixed on

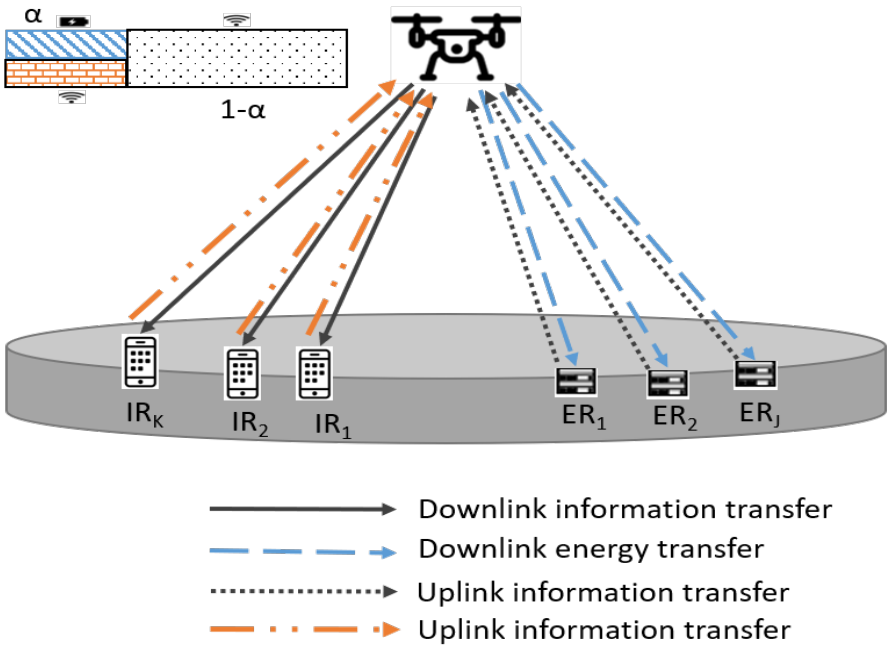

Figure 4.2: Linear scenario

top of a sport complex to collect data about humidity, temperature, light, or other data, while at the same time it sends data to the IRs about ticketing information on electronic gates around the complex, as shown in Figure 4.3.

4.2 Energy Efficiency Maximization

4.2.1 Energy Efficiency Formulation

The first step in the formulation of the system's EE is to construct the throughputs of the downlink and uplink stages. For the downlink information NOMA setup, where the channel gains of IRs are increasing when closer to the UAV (channel gain of IR_1 is larger than IR_2, and so on until IR_K), the rate in *bps* related to a given IR can be expressed as in (3.10). According to the principles of power-domain NOMA, for a given IR, the strong interfering signals are mainly due to the transmissions to users with

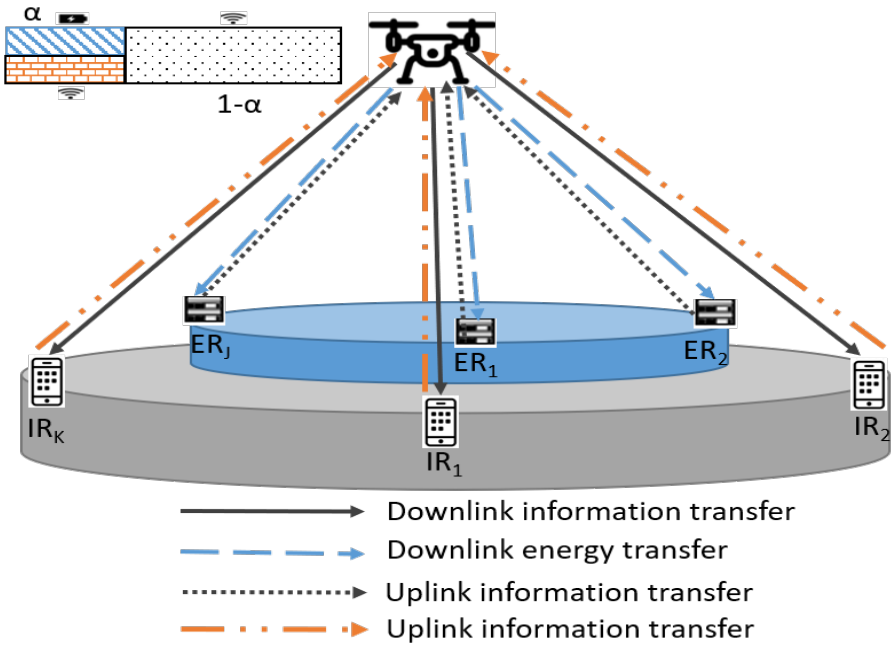

Figure 4.3: Circular scenario.

low channel gains. The weakest channel user, IR$_K$, which receives low interferences due to the relatively low powers of the messages of high channel gain users, cannot cancel any interferences. However, the highest channel gain user, IR$_1$, which receives strong interferences due to the relatively high powers of the transmissions to weak users, can cancel all interfering signals [85].

On the other hand, for the uplink NOMA throughput, knowing that the channel gains are stronger when ERs are closer to the UAV (channel gain of ER$_1$ is larger than ER$_2$, and so on until ER$_J$), then based on (3.5) and (3.6), the rate related to a given ER can be expressed as in (3.11). The signal of the highest channel gain user, ER$_1$, is decoded first at the UAV. As a result, ER$_1$ experiences interference from all other ERs. Then, the signal for the second highest channel gain user is decoded until the last one, ER$_J$, [85]. The same approach is suitable for both linear and circular scenarios, however, as the distances of the IRs from the UAV are the same in the circular

scenario, the gains and the path losses for all of them will be the same. Accordingly, the rate for IR_k becomes

$$R_k^{\mathrm{D}}=(1-\alpha)W\log_2\left(1+\frac{\frac{Q_k^{\mathrm{D}}\|\mathbf{h}_k'\|^2}{L_{\mathrm{IR}_k}^{\mathrm{D}}(1-\alpha)}}{((1-\beta)P-Q_k^{\mathrm{D}})\sum\limits_{i=1,i\neq k}^{K-1}\frac{\|\mathbf{h}_k'\|^2}{L_{\mathrm{IR}_i}^{\mathrm{D}}(1-\alpha)}+\sum\limits_{j=1}^{J}\frac{\zeta P_j^{\mathrm{D}}\|\mathbf{g}_j'\|^2\|\mathbf{z}_j'\|^2|e_j'|^2\alpha}{L_{\mathrm{ER}_j}^{\mathrm{U}}L_{\mathrm{ER}_j}^{\mathrm{D}}L_{\mathrm{NLoS}_j}(1-\alpha)}+1}\right) \tag{4.1}$$

On the other hand, the rate for ER_j can be rewritten as follows:

$$R_j^{\mathrm{U}}=(1-\alpha)W\log_2\left(1+\frac{\frac{\zeta P_j^{\mathrm{D}}\|\mathbf{g}_j'\|^2\|\mathbf{z}_j'\|^2\alpha}{L_{\mathrm{ER}_j}^{\mathrm{U}}L_{\mathrm{ER}_j}^{\mathrm{D}}(1-\alpha)}}{(\beta P-P_j^{\mathrm{D}})\sum\limits_{l=j+1}^{J}\frac{\zeta\|\mathbf{g}_l'\|^2\|\mathbf{z}_l'\|^2\alpha}{L_{\mathrm{ER}_l}^{\mathrm{U}}L_{\mathrm{ER}_l}^{\mathrm{D}}(1-\alpha)}+1}\right). \tag{4.2}$$

Let us define the downlink throughput as the sum-rate of all IRs, i.e., $R^{\mathrm{D}}=\sum_{k=1}^{K}R_k^{\mathrm{D}}$, and the uplink throughput as the sum-rate $R^{\mathrm{U}}=\sum_{j=1}^{J}R_j^{\mathrm{U}}$. The EE of the system is expressed as:

$$\eta=\frac{\text{Total Throughput}}{\text{Total Consumed Energy}}=\frac{R^{\mathrm{D}}+R^{\mathrm{U}}}{P_{\mathrm{DC}}+P^{\mathrm{D}}+Q^{\mathrm{D}}}, \tag{4.3}$$

where P_{DC} is the constant power consumption of the UAV, and where $P^{\mathrm{D}}=\beta P=\sum_{j=1}^{J}P_j^{\mathrm{D}}$ and $Q^{\mathrm{D}}=(1-\beta)P=\sum_{k=1}^{K}Q_k^{\mathrm{D}}$ are the powers dedicated to the ERs and the IRs, respectively, i.e., $P=P^{\mathrm{D}}+Q^{\mathrm{D}}$.

4.2.2 Problem Formulation

Aiming at maximizing EE, the optimization problem is formulated as follows:

$$\begin{aligned}\mathrm{OP}: \quad &\max_{Q^{\mathrm{D}},P^{\mathrm{D}},\alpha,\beta} \quad \eta\\ &\text{subject to:} \quad P\leq P_{\max},\end{aligned}$$

$$
\begin{aligned}
& P_j^{\mathrm{U}} \leq P_{j,\max}^{\mathrm{U}}, \quad \forall j, \\
& \alpha < 1, \\
& 0 \leq \beta \leq 1, \\
& h_{\mathrm{u,min}} \leq d_j \cos\theta_j, \quad \forall j, \\
& h_{\mathrm{u,min}} \leq d_k \cos\theta_k, \quad \forall k, \\
& R_j^{\mathrm{U}} \geq R_{j,\min}^{\mathrm{U}}, \quad \forall j, \\
& R_k^{\mathrm{D}} \geq R_{k,\min}^{\mathrm{D}}, \quad \forall k, \\
& P_{\mathrm{thr}}^{\mathrm{U}} \leq P_j^{\mathrm{U}} z_j - \sum_{l=j+1}^{J} P_l^{\mathrm{U}} z_l, \quad \forall j, \\
& Q_{\mathrm{thr}}^{\mathrm{D}} \leq \left(Q_k^{\mathrm{D}} - \sum_{m=1}^{k-1} Q_m^{\mathrm{D}} \right) h_K, \quad \forall k,
\end{aligned}
\tag{4.4}
$$

where $h_{\mathrm{u,min}}$ is the minimum allowed height for the UAV, $R_{j,\min}^{\mathrm{U}}$ and $R_{k,\min}^{\mathrm{D}}$ denote the minimum required rates of ER_j and IR_k, respectively, and where $P_{\mathrm{thr}}^{\mathrm{U}}$ and $Q_{\mathrm{thr}}^{\mathrm{D}}$ are the SIC detection thresholds of the uplink and downlink.

The first constraint guarantees that the transmit power of the UAV will not exceed its maximum power budget. Also, the power of ER_j has to be equal or less its maximum power, as stated in the second constraint. The third constraint insures that the percentage of the charging time is always less than one, this allows the second phase to take place and guarantees that the throughputs will not vanish. The percentage of the power budget for ERs illustrated in the forth constraint, if it is zero then the whole power will be dedicated to the IRs. On the other hand, if it is one, the UAV power will be dedicated to the ERs. When it is between zero and one, then the UAV power will be distributed among ERs and IRs according to the value of β. The fifth and sixth constraints are related to the position of the UAV, both guarantee that the UAV will not hover lower that the minimum allowable hight taking into accounts

the positions of the scheduled ERs and IRs. The QoS constraints are stated in the seventh and eighth constraints, where the acceptable throughput for each ER and each IR will not be less than a required threshold. The last two constraints treat the SIC thresholds for both uplink and dwonlink NOMA transmissions, where both thresholds depend on the parameters related to the scheduled ERs and IRs.

With these above constraints and highly coupled variables; the optimization problem is a non-convex problem; therefore, there is no way to solve it directly with the traditional methods. Accordingly, We split the optimization problem into two sub-problems. In the first one (OP_1), we aim to find the optimum position of the UAV, i.e., the optimal distances and elevation angles w.r.t. the IRs and ERs according to their demands. After getting the optimum position of the UAV which gives better links to the scheduled ERs and IRs, in the second problem (OP_2) we determine the optimal transmit power to each ER and IR, along with the optimal charging time.

4.2.3 UAV Position Optimization

In OP_1, we focus on θ_j and d_j which are given in (2.2), for all nodes at the same time. This can be achieved by associating the path losses for A2G channels related to each ER and IR by the parameters pertaining to the their demands. So, OP_1 will be as follows:

$$\begin{aligned} \mathrm{OP}_1 \qquad & \min_{d_j, d_k, \theta_j, \theta_k} \quad \sum_j \varpi_j^U \; L^{\mathrm{D}}_{\mathrm{ER_j}} + \sum_k \varpi_k^D \; L^{\mathrm{D}}_{\mathrm{IR}_k} \\ & \text{subject to:} \quad h_{\mathrm{u,min}} \leq d_j \cos\theta_j, \quad \forall j, \\ & \qquad\qquad\quad h_{\mathrm{u,min}} \leq d_k \cos\theta_k, \quad \forall k. \end{aligned} \tag{4.5}$$

The second derivative of the objective function in OP_1 reveals the convexity of the problem with respect to the distance and the elevation angle for each ER and IR. Accordingly, this optimization problem can be solved by introducing the Lagrangian multipliers $\boldsymbol{\eth_{IR}} \geq 0$ and $\boldsymbol{\eth_{ER}} \geq 0$, where $\boldsymbol{\eth_{IR}} = [\eth_{IR_1}, \eth_{IR_2}, ..., \eth_{IR_K}]$ and $\boldsymbol{\eth_{ER}} = [\eth_{ER_1}, \eth_{ER_2}, ..., \eth_{ER_J}]$. The objective function then becomes

$$\begin{aligned}
&\mathcal{L}_1(\boldsymbol{\eth_{ER}}, \boldsymbol{\eth_{IR}}, \boldsymbol{d_{ER}}, \boldsymbol{d_{IR}}, \boldsymbol{\theta_{ER}}, \boldsymbol{\theta_{IR}}) \\
&= \sum_{j=1}^{J} \varpi_j^U \ L_{\mathrm{ER_j}}^{\mathrm{D}} + \sum_{k=1}^{K} \varpi_k^D \ L_{\mathrm{IR}_k}^{\mathrm{D}} - \sum_{j=1}^{J} \eth_{ER_j}(h_{\mathrm{u,min}} - d_j \cos\theta_j - \sum_{k=1}^{K} \eth_{IR_k}(h_{\mathrm{u,min}} - d_k \cos\theta_k).
\end{aligned} \tag{4.6}$$

Exploiting the KKT conditions, one can get the optimal position of the UAV by solving the first derivatives of $\mathcal{L}_1$ w.r.t. d_{ER_j}, d_{IR_k}, θ_{ER_j} and θ_{IR_k}, respectively, as follows:

$$\begin{aligned}
\frac{\partial \mathcal{L}_1}{\partial d_{ER_j}} &= \varpi_j^U \ \frac{\partial L_{\mathrm{ER_j}}^{\mathrm{D}}}{\partial d_{ER_j}} - \eth_{ER_j} \cos\theta_j \\
&= \frac{20\, \varpi_j^U}{d_{ER_j} \ln(10)} - \eth_{ER_j} \cos\theta_j = 0,
\end{aligned} \tag{4.7}$$

$$\begin{aligned}
\frac{\partial \mathcal{L}_1}{\partial d_{IR_k}} &= \varpi_k^D \ \frac{\partial L_{\mathrm{IR_k}}^{\mathrm{D}}}{\partial d_{IR_k}} - \eth_{IR_k} \cos\theta_k \\
&= \frac{20\, \varpi_k^D}{d_{IR_k} \ln(10)} - \eth_{IR_k} \cos\theta_k = 0,
\end{aligned} \tag{4.8}$$

$$\frac{\partial \mathcal{L}_1}{\partial \theta_{ER_j}} = \varpi_j^U \frac{\partial L_{\mathrm{ER_j}}^{\mathrm{D}}}{\partial d_{ER_j}} + \eth_{ER_j} d_{ER_j} \cos\theta_j$$
$$= \frac{\varpi_j^U ab \frac{180}{\pi} (\xi_{LoS} - \xi_{NLoS}) \exp\left(-b\left(\frac{180}{\pi}\theta_{ER_j} - a\right)\right)}{\left(1 + a\exp\left(-b\left(\frac{180}{\pi}\theta_{ER_j} - a\right)\right)\right)^2} + \eth_{ER_j} d_{ER_j} \cos\theta_j = 0, \tag{4.9}$$

$$\frac{\partial \mathcal{L}_1}{\partial \theta_{IR_k}} = \varpi_k^D \frac{\partial L_{\mathrm{IR_k}}^{\mathrm{D}}}{\partial d_{IR_k}} + \eth_{IR_k} d_{IR_k} \cos\theta_k$$
$$= \frac{\varpi_k^D ab \frac{180}{\pi} (\xi_{LoS} - \xi_{NLoS}) \exp\left(-b\left(\frac{180}{\pi}\theta_{IR_k} - a\right)\right)}{\left(1 + a\exp\left(-b\left(\frac{180}{\pi}\theta_{IR_k} - a\right)\right)\right)^2} + \eth_{IR_k} d_{IR_k} \cos\theta_k = 0. \tag{4.10}$$

The new values of $\eth_{ER_j}$, and $\eth_{IR_k}$ can be simply calculated using the gradient-decent method as follows:

$$\eth_{ER_j}(i+1) = [\eth_{ER_j}(i) - \Delta_{\eth_{ER_j}}(h_{\mathrm{u,min}} - d_{ER_j}\cos\theta_j)]^+, \tag{4.11}$$

$$\eth_{IR_k}(i+1) = [\eth_{IR_j}(i) - \Delta_{\eth_{IR_k}}(h_{\mathrm{u,min}} - d_{IR_k}\cos\theta_k)]^+, \tag{4.12}$$

where $\eth_{ER_j}(i)$ and $\eth_{IR_k}(i)$ are respectively the values of $\eth_{IR_k}$ and $\eth_{ER_j}$ at the i^{th} iteration, $\Delta_{\eth_{ER_j}}$ and $\Delta_{\eth_{IR_k}}$ are the iteration steps, and $[x]^+ = \max(0, x)$. As an initialization point, we set $\eth_{ER_j} = 0$ and $\eth_{IR_k} = 0$ as shown in Algorithm 4.1, and then update them in each iteration. The output of the optimization will be the optimum position of the UAV. Algorithm 4.1 summarizes the procedure for finding the optimal UAV positioning. The results will be used in the second optimization problem.

Algorithm 4.1. UAV Position Optimization (X^*_{UAV},Y^*_{UAV},h^*_{UAV})

Input: $(x_{\mathrm{ER_j}}, y_{\mathrm{ER_j}}, h_{\mathrm{ER_j}})$, $(x_{\mathrm{IR_k}}, y_{\mathrm{IR_k}}, h_{\mathrm{IR_k}})$, ϖ_j^U,ϖ_k^D, ξ_{LoS}, ξ_{NLoS} a, b, $h_{\mathrm{u,min}}$, f; $\forall k$, $\forall j$
Output: $[x^*_{\mathrm{u}}$,y^*_{u},$h^*_{\mathrm{u}}]$

Initialization: $[x_{\mathrm{u0}}$,y_{u0},$h_{\mathrm{u0}}]$, $\eth_{ER_j} = 0$, $\eth_{IR_k} = 0$, $\forall j$, $\forall k$.

1: Update $\eth_{ER_j}$ and $\eth_{IR_k}$ according to (4.11) and (4.12).
2: Solve (4.7) for d_{ER_j}, $\forall j$.
3: Solve (4.8) for d_{IR_k}, $\forall k$.
4: Solve (4.9) for θ_{ER_j}, $\forall j$.
5: Solve (4.10) for θ_{IR_k}, $\forall k$.
6: Compute the optimal $[x^*_{\mathrm{u}}$,y^*_{u},$h^*_{\mathrm{u}}]$ by solving (4.5).

4.2.4 Energy-Efficient Resource Allocation

As the solution of OP_1 guarantees the optimal position of the UAV, which is also mean the optimal links between the UAV and the users. In OP_2, we eliminate the fifth and sixth constraints in (4.4), which are already covered by OP_1. With the remaining constraints, the optimization problem is formulated as follows:

$$
\begin{aligned}
\mathrm{OP}_2: \quad \max_{Q^{\mathrm{D}},P^{\mathrm{D}},\alpha,\beta} \quad & \frac{R^{\mathrm{D}}+R^{\mathrm{U}}}{P_{\mathrm{DC}}+P^{\mathrm{D}}+Q^{\mathrm{D}}} \\
\text{subject to:} \quad & P \le P_{\max}, \\
& P_j^{\mathrm{U}} \le P_{j,\max}^{\mathrm{U}}, \quad \forall j, \\
& \alpha < 1, \\
& 0 \le \beta \le 1, \\
& R_j^{\mathrm{U}} \ge R_{j,\min}^{\mathrm{U}}, \quad \forall j, \\
& R_k^{\mathrm{D}} \ge R_{k,\min}^{\mathrm{D}}, \quad \forall k, \\
& P_{\mathrm{thr}}^{\mathrm{U}} \le P_j^{\mathrm{U}} z_j - \sum_{l=j+1}^{J} P_l^{\mathrm{U}} z_l, \quad \forall j, \\
& Q_{\mathrm{thr}}^{\mathrm{D}} \le \left(Q_k^{\mathrm{D}} - \sum_{m=1}^{k-1} Q_m^{\mathrm{D}} \right) h_K, \quad \forall k.
\end{aligned}
\tag{4.13}
$$

It is obvious that the objective function in OP_2 is a fractional function. This fractional function with its related constraints is classified as a nonlinear fractional optimization problem with the variables P^{D}, Q^{D}, α, and β, and it is a non-convex problem. Exploiting the idea in [78], the fractional programming problem can be transformed into a convex problem by introducing the variable χ^* as the optimal EE when we have the optimal transmit power towards each ER and IR, and the optimal WPT fraction of time, α. Accordingly, the objective function can be written in a subtractive form, $\sum_{k=1}^{K} R_k^{\mathrm{D}} + \sum_{j=1}^{J} R_j^{\mathrm{U}} - \chi^*(P_{DC} + P_D + Q_D)$, which is equivalent to its original fractional form, this means that the optimal solution of the subtractive form is also the optimal solution of the fractional form [87].

By introducing $\vartheta \geq 0$, $\boldsymbol{\varsigma} \geq 0$, $\varepsilon \geq 0$, $\varrho \geq 0$, $\boldsymbol{\varphi} \geq 0$, $\boldsymbol{\lambda} \geq 0$, $\boldsymbol{\mu} \geq 0$, and $\boldsymbol{\phi} \geq 0$, as the Lagrange multipliers associated with the constraints in OP_2, where $\boldsymbol{\varsigma} = [\varsigma_1, \varsigma_2, ..., \varsigma_J]$, $\boldsymbol{\varphi} = [\varphi_1, \varphi_2, ..., \varphi_J]$, $\boldsymbol{\lambda} = [\lambda_1, \lambda_2, ..., \lambda_K]$, $\boldsymbol{\mu} = [\mu_1, \mu_2, ..., \mu_J]$, and $\boldsymbol{\phi} = [\phi_1, \phi_2, ..., \phi_K]$, the Lagrangian function of OP_2 can be formulated as:

$$
\begin{aligned}
\mathcal{L}_2(\vartheta, \boldsymbol{\varsigma}, \varepsilon, \varrho, \boldsymbol{\varphi}, \boldsymbol{\lambda}, \boldsymbol{\mu}, \boldsymbol{\phi}, Q_k^{\mathrm{D}}, P_j^{\mathrm{D}}, \alpha) = & \sum_{k=1}^{K} R_k^{\mathrm{D}} + \sum_{j=1}^{J} R_j^{\mathrm{U}} - \chi^*(P_{\mathrm{DC}} + \beta P + (1-\beta)P) \\
& - \vartheta(P - P_{\max}) - \sum_{j=1}^{J} \varsigma_j (P_j^{\mathrm{U}} - P_{j,\max}^{\mathrm{U}}) \\
& - \varepsilon(\alpha - 1) - \varrho(\beta - 1) \\
& - \sum_{j=1}^{J} \varphi_j (R_{j,\min}^{\mathrm{U}} - R_j^{\mathrm{U}}) - \sum_{k=1}^{K} \lambda_k (R_{k,\min}^{\mathrm{D}} - R_k^{\mathrm{D}}) \\
& - \sum_{j=1}^{J} \mu_j \left[P_{\mathrm{thr}}^{\mathrm{U}} - P_j^{\mathrm{U}} z_j + \sum_{l=j+1}^{J} P_l^{\mathrm{U}} z_l \right] \\
& - \sum_{k=1}^{K} \phi_k \left[Q_{\mathrm{thr}}^{\mathrm{D}} - \left(Q_k^{\mathrm{D}} - \sum_{m=1}^{k-1} Q_m^{\mathrm{D}} \right) h_K \right].
\end{aligned} \tag{4.14}
$$

We assume that the UAV uses its maximum power, such that $\beta P_{\max} = P^{\mathrm{D}}$ and

$(1-\beta)P_{\max} = Q^{\mathrm{D}}$. Our aim is to find the optimized Q_k^{D}, P_j^{D}, β, and α. This can be done through the derivation of the Lagrangian function (4.14) w.r.t. Q_k^{D}, P_j^{D}, β and α, and setting them to zero, i.e.,

$$\frac{\partial \mathcal{L}_2}{\partial Q_k^{\mathrm{D}}} = 0, \quad \frac{\partial \mathcal{L}_2}{\partial P_j^{\mathrm{D}}} = 0, \quad \frac{\partial \mathcal{L}_2}{\partial \beta} = 0, \quad \frac{\partial \mathcal{L}_2}{\partial \alpha} = 0, \tag{4.15}$$

The updating of the Lagrangian variables ϑ, $\boldsymbol{\varsigma}$, ε, ϱ, $\boldsymbol{\varphi}$, $\boldsymbol{\lambda}$, $\boldsymbol{\mu}$, and $\boldsymbol{\phi}$, can be done using the gradient method similar to what has been done in [80]. Here, we present the derivation and the closed form of Q_k^{D}. We start by folding all part of the Lagrangian equation and then we do the derivation, with some simplifications, we obtain

$$\begin{aligned}
&\frac{\mathcal{L}_2(\vartheta, \boldsymbol{\varsigma}, \varepsilon, \varrho, \boldsymbol{\varphi}, \boldsymbol{\lambda}, \boldsymbol{\mu}, \boldsymbol{\phi}, Q_k^{\mathrm{D}}, P_j^{\mathrm{D}}, \alpha)}{\partial Q_k^D} \\
&= (1+\lambda_k)\frac{\partial R_k^D}{\partial Q_k^D} + \phi_k h_K \\
&= \frac{\partial \left((1-\alpha)(1+\lambda_k) W \log_2(1 + \frac{\frac{Q_k^{\mathrm{D}} \|\mathbf{h}_k{}'\|^2}{L_{\mathrm{IR}_k}^{\mathrm{D}}(1-\alpha)}}{((1-\beta)P - Q_k^{\mathrm{D}}) \sum_{i=1, i\neq k}^{K-1} \frac{\|\mathbf{h}_k{}'\|^2}{L_{\mathrm{IR}_i}^{\mathrm{D}}(1-\alpha)} + 1}) \right)}{\partial Q_k^D} + \phi_k h_K \\
&= 0.
\end{aligned} \tag{4.16}$$

After some algebraic manipulations, we get the closed form expression of the optimized download power destined to the IR_k as shown in (4.17), where $F_k = \sum_{i=1, i\neq k}^{K-1} \frac{\|\mathbf{h}_k{}'\|^2}{L_{\mathrm{IR}_i}^{\mathrm{D}}}$.

$$\begin{aligned}
Q_k^D = &\frac{\left(\left((4F_k h_k \lambda_k - 4Fh) L_{\mathrm{IR}_i}^{\mathrm{D}} - 4F_k h_k \lambda_k + 4F_k h_k\right) h_K \phi_k W + h_k h_K {\phi_k}^2\right)(1-\alpha)^2}{\left(2F_k L_{\mathrm{IR}_i}^{\mathrm{D}} - 2F_k h_k\right)^2 h_K {\phi_k}^2} \\
&+ \frac{\left(\left(((4-4\beta)F_k h_k \lambda_k + (4\beta-4)F_k h_k) L_{\mathrm{IR}_i}^{\mathrm{D}} + (4\beta-4)F_k h_k \lambda_k + (4-4\beta)F_k h_k\right) h_K P \phi_k W + (2-2\beta)F_k h_k h_K P {\phi_k}^2\right)(1-\alpha)}{\left(2F_k L_{\mathrm{IR}_i}^{\mathrm{D}} - 2F_k h_k\right) h_K {\phi_k}^2}
\end{aligned}$$

$$+\frac{\frac{\left(\beta^2-2\beta+1\right)F_k h_k h_K P^2 {\phi_k}^2}{\left(2F_k L_{\mathrm{IR}_i}^{\mathrm{D}}-2F_k h_k\right)h_K {\phi_k}^2}+\left(2F_k L_{\mathrm{IR}_i}^{\mathrm{D}}-h_k\right)h_K\phi_k(1-\alpha)+\left((2-2\beta)F_k L_{\mathrm{IR}_i}^{\mathrm{D}}+(\beta-1)F_k h_k\right)h_K P\phi_k}{\left(2F_k L_{\mathrm{IR}_i}^{\mathrm{D}}-2F_k h_k\right)h_K\phi_k}. \tag{4.17}$$

We were also able to get the optimized download power destined to each ER, starting with the derivation as follows:

$$\begin{aligned}
&\frac{\mathcal{L}_2(\vartheta,\boldsymbol{\varsigma},\varepsilon,\varrho,\boldsymbol{\varphi},\boldsymbol{\lambda},\boldsymbol{\mu},\boldsymbol{\phi},Q_k^{\mathrm{D}},P_j^{\mathrm{D}},\alpha)}{\partial P_j^U}\\
&=(1+\varphi_j)\frac{\partial R_j^U}{\partial P_j^D}-(\varsigma_j+\mu_j)\frac{\partial P_j^U}{\partial P_j^D}\\
&=\frac{\partial\left((1-\alpha)(1+\varphi_j)W\log_2(1+\frac{\frac{\varsigma P_j^{\mathrm{D}}\|\mathbf{g}_j'\|^2\|\mathbf{z}_j'\|^2\alpha}{L_{\mathrm{ER}_j}^{\mathrm{U}}L_{\mathrm{ER}_j}^{\mathrm{D}}(1-\alpha)}}{(\beta P-P_j^{\mathrm{D}})\sum_{l=j+1}^{J}\frac{\varsigma\|\mathbf{g}_l'\|^2\|\mathbf{z}_l'\|^2\alpha}{L_{\mathrm{ER}_l}^{\mathrm{U}}L_{\mathrm{ER}_l}^{\mathrm{D}}(1-\alpha)}+1})\right)}{\partial P_j^D}-\frac{\partial\left((\varsigma_j+\mu_j)\varsigma\alpha\frac{\|\mathbf{g}_j'\|^2}{L_{\mathrm{ER}_j}^{\mathrm{D}}(1-\alpha)}P_j^D\right)}{\partial P_j^D}=0.
\end{aligned} \tag{4.18}$$

The closed form of P_j^D is derived as shown in (4.19), where $F_j=\frac{\|\mathbf{g}_j'\|^2}{L_{\mathrm{ER}_j}^{\mathrm{D}}}$, $O_j=\frac{\varsigma\|\mathbf{g}_j'\|^2\|\mathbf{z}_j'\|^2}{L_{\mathrm{ER}_j}^{\mathrm{U}}L_{\mathrm{ER}_j}^{\mathrm{D}}}$, and $O_j^*=\sum_{l=j+1}^{J}\frac{\varsigma\|\mathbf{g}_l'\|^2\|\mathbf{z}_l'\|^2}{L_{\mathrm{ER}_l}^{\mathrm{U}}L_{\mathrm{ER}_l}^{\mathrm{D}}}$.

$$\begin{aligned}
P_j^{\mathrm{D}}=&\frac{\left(\left(4\alpha(\frac{(\varsigma_j+\mu_j)\varsigma\alpha F_j}{(1-\alpha)})O_jO_j^*-4\alpha(\frac{(\varsigma_j+\mu_j)\varsigma\alpha F_j}{(1-\alpha)})O_jO_j^*\right)(1-\alpha)^2+\left(4\alpha^2\beta(\frac{(\varsigma_j+\mu_j)\varsigma\alpha F_j}{(1-\alpha)})O_jO_j^*-4\alpha^2\beta(\frac{(\varsigma_j+\mu_j)\varsigma\alpha F_j}{(1-\alpha)})O_jO_j^*\right)P(1-\alpha)\right)W(\varphi_j+1)}{(2\alpha(\frac{(\varsigma_j+\mu_j)\varsigma\alpha F_j}{(1-\alpha)})O_j^*-2\alpha(\frac{(\varsigma_j+\mu_j)\varsigma\alpha F_j}{(1-\alpha)})O_jO_j^*)^2}\\
&+\frac{(\frac{(\varsigma_j+\mu_j)\varsigma\alpha F_j}{(1-\alpha)})^2O_j(1-\alpha)^2+2\alpha\beta(\frac{(\varsigma_j+\mu_j)\varsigma\alpha F_j}{(1-\alpha)})^2O_jO_j^*P(1-\alpha)+\alpha^2\beta^2(\frac{(\varsigma_j+\mu_j)\varsigma\alpha F_j}{(1-\alpha)})^2O_jO_j^*P^2}{(2\alpha(\frac{(\varsigma_j+\mu_j)\varsigma\alpha F_j}{(1-\alpha)})O_j^*-2\alpha(\frac{(\varsigma_j+\mu_j)\varsigma\alpha F_j}{(1-\alpha)})O_jO_j^*)^2}\\
&+\frac{\left(2(\frac{(\varsigma_j+\mu_j)\varsigma\alpha F_j}{(1-\alpha)})O_j^*-(\frac{(\varsigma_j+\mu_j)\varsigma\alpha F_j}{(1-\alpha)})O_j\right)(1-\alpha)+\left(2\alpha\beta(\frac{(\varsigma_j+\mu_j)\varsigma\alpha F_j}{(1-\alpha)})O_j^*-\alpha\beta(\frac{(\varsigma_j+\mu_j)\varsigma\alpha F_j}{(1-\alpha)})O_jO_j^*\right)P}{2\alpha(\frac{(\varsigma_j+\mu_j)\varsigma\alpha F_j}{(1-\alpha)})O_j^*-2\alpha(\frac{(\varsigma_j+\mu_j)\varsigma\alpha F_j}{(1-\alpha)})O_jO_j^*}.
\end{aligned} \tag{4.19}$$

The solution of OP_2 is summarized in Algorithm 4.2.

Algorithm 4.2. Energy-Efficient Resource Allocation

Input: $(x_{\mathrm{u}},y_{\mathrm{u}},h_{\mathrm{u}})$; $(x_{\mathrm{ER}_j},y_{\mathrm{ER}_j},h_{\mathrm{ER}_j})$, $j=[1:J]$; $(x_{\mathrm{IR}_k},y_{\mathrm{IR}_k},h_{\mathrm{IR}_k})$, $k=[1:K]$, a, b, ξ_{LoS}, ξ_{NLoS}, f, η, σ, $R_{\min}^{\mathrm{U}}$, $R_{\min}^{\mathrm{D}}$, and χ^*.

Output: $[\beta,\ Q_k^{\mathrm{D}},\ P_j^{\mathrm{D}},\ \alpha]$.

Initialization: $[\beta_0,\ Q_{k_0}^{\mathrm{D}},\ P_{j_0}^{\mathrm{D}},\ \alpha_0]$, $\vartheta=0$, $\boldsymbol{\varsigma}=\mathbf{0}$, $\varepsilon=0$, $\varrho=0$ $\boldsymbol{\varphi}=\mathbf{0}$, $\boldsymbol{\lambda}=\mathbf{0}$, $\boldsymbol{\mu}=\mathbf{0}$, $\boldsymbol{\phi}=\mathbf{0}$.

1: Update the Lagrangian variables, ϑ, $\boldsymbol{\varsigma}$, ε, ϱ, $\boldsymbol{\varphi}$, $\boldsymbol{\lambda}$, $\boldsymbol{\mu}$, and $\boldsymbol{\phi}$.

2: Solve (4.15) to obtain β, Q_k^{D},P_j^{D} and α.

3: Compute $[\beta,\ Q_k^{\mathrm{D}*}$,$P_j^{\mathrm{D}*}$,$\alpha^*]$ by solving (4.13).

4.2.5 Complexity Analysis

The main optimization problem under consideration is a highly coupled non-convex problem, thus it is hard to be solved. However, with the suggested sub-optimal solution, we decomposed the problem into two sub-problems and were able to solve them efficiently through two algorithms. Both algorithms depend on the gradient descent method, for which the worst complexity is $\mathcal{O}(n \times \frac{1}{\epsilon})$ [79], where n is the number of optimization variables, and ϵ is the solution accuracy. Thus, for Algorithm 4.1, the complexity depends on the 3D plane size that the UAV considers for moving, i.e., $(x \times y \times (h_{\max} - h_{\min}))$, where the $(h_{\max} - h_{\min})$ is the allowable altitude range for moving. This could be eliminated to $(x \times y)$ only as the UAV will mostly hover at the minimum allowable height to provide better links to the ERs and IRs. For Algorithm 4.2, the complexity depends on the number of ERs (J) and IRs (K). Accordingly, the total complexity for both algorithms is $\mathcal{O}(x \times y \times (h_{\max} - h_{\min}) \times \frac{1}{\epsilon}) + \mathcal{O}((J+K) \times \frac{1}{\epsilon})$. However, if we consider that the UAV will hover at the minimum allowable height, the complexity can be reduced to $\mathcal{O}(x \times y \times \frac{1}{\epsilon}) + \mathcal{O}((J+K) \times \frac{1}{\epsilon})$. Hence, the complexity of the proposed solution depends on the ROI and the number of scheduled ERs and IRs.

4.3 System Operation With OMA and Hybrid Access Schemes

Besides NOMA, we consider system operation with three access schemes: the conventional OMA access scheme, OMA, with two hybrid schemes. The proposed hybrid schemes are the combination between NOMA and OMA in the uplink and downlink. In the hybrid downlink OMA uplink NOMA (HDOUN) scheme, we implement OMA

in the downlink along with NOMA in the uplink. In the hybrid downlink NOMA uplink OMA (HDNUO) scheme, we consider system operation with NOMA in the downlink and OMA in the uplink.

4.3.1 OMA Scheme

In the OMA protocol, the UAV sends the information separately by splitting the transmission phase, $(1-\alpha)$, equally among all IRs in the downlink, where for the uplink the same time allocation is scheduled for each ER. In this case, the throughput for IR_k and ER_j can be formulated as follows:

$$R_k^{\mathrm{D}}(\mathrm{OMA}) = \frac{(1-\alpha)}{K} W \log_2 \left(1 + \frac{K Q^{\mathrm{D}} \|\mathbf{h}_k'\|^2}{L_{\mathrm{IR}_k}^{\mathrm{D}}(1-\alpha)}\right), \tag{4.20}$$

$$R_j^{\mathrm{U}}(\mathrm{OMA}) = \frac{(1-\alpha)}{J} W \log_2 \left(1 + \frac{J\zeta P^{\mathrm{D}} \|\mathbf{g}_j'\|^2 \|\mathbf{z}_j'\|^2 \alpha}{L_{\mathrm{ER}_j}^{\mathrm{U}} L_{\mathrm{ER}_j}^{\mathrm{D}}(1-\alpha)}\right). \tag{4.21}$$

4.3.2 HDOUN Scheme

In this scheme, the downlink information transmissions are carried out through the OMA scheme, while the uplink information transmissions are done via NOMA. Accordingly, the EE can be formulated as follows:

$$\eta(\mathrm{HDOUN}) = \frac{\sum_{k=1}^{K} R_k^{\mathrm{D}}(\mathrm{OMA}) + \sum_{j=1}^{\mathrm{J}} \mathrm{R_j^U}}{P_{\mathrm{DC}} + P^{\mathrm{D}} + Q^{\mathrm{D}}}, \tag{4.22}$$

4.3.3 HDNUO Scheme

Here, the system operation with this scheme is the opposite of the one above, i.e., NOMA is implemented in the downlink and OMA is used in the uplink. Here, the

EE can be formulated as:

$$\eta(\text{HDNUO}) = \frac{\sum_{k=1}^{K} R_k^{\text{D}} + \sum_{j=1}^{J} R_j^{\text{U}}(\text{OMA})}{P_{\text{DC}} + P^{\text{D}} + Q^{\text{D}}}, \tag{4.23}$$

4.4 Simulation Results

In this section, we show the results of applying the proposed algorithms on the different access schemes for linear and circular scenarios. In the simulations, we set $a = 9.6$, $b = 0.28$, $\xi_{\text{LoS}} = 1$ dB, $\xi_{\text{NLoS}} = 20$ dB, $f = 2$ GHz, $W = 200$ kHz, $\eta = 0.8$, $\sigma^2 = 1$, and $N_E = N_I = 2$. We set $Q_{\text{thr}}^{\text{D}} = P_{\text{thr}}^{\text{U}} = 0.05$ Watt, $P_{\text{DC}} = 5$ Watt, $P_{\max} = 3$ Watt, and $R_{\min}^{\text{U}} = R_{\min}^{\text{D}} = 6$ Kbps, unless stated otherwise.

4.4.1 Linear Scenario

Let us consider the scheduling of four ground users at a time, i.e., four ERs and four IRs. The positions of ER_1, ER_2, and ER_3 are fixed at (1,0,0), (2,0,0), and (3,0,0), respectively, and we vary the horizontal coordinate of ER_4 (x,0,0). Also, the position of IR_1, IR_2, IR_3 are set to (-1,0,0), (-2,0,0), and (-3,0,0), respectively, and we vary the horizontal coordinate of IR_4 (-x,0,0). In the case of scheduling two ERs with two IRs or three ERs with three IRs, the setup remains the same while the varying of the horizontal coordinate becomes for the weakest users in each setup, i.e., ER_2 with IR_2, and ER_3 with IR_3, respectively. We assume that all ERs and IRs have the same demands. Accordingly, the UAV will hover over the center between the ERs and IRs with the minimum allowable height, i.e., (0,0,20).

Energy Efficiency in the Linear Scenario

We consider three different access schemes, OMA, NOMA, and hybrid. We also consider three scheduling scenarios, in the first case we schedule two ERs and two IRs. Secondly, we assume three ERs along with three IRs. Finally, we have four ERs with four IRs.

Scenario with Two ERs and Two IRs Figure 4.4 compares the effect of different access schemes, i.e., OMA, NOMA and hybrid, on the EE of the system. The results are plotted as a function of the distance of ER_2 from the UAV taking into account that the downlink throughput of IR_2 is constructed from the same distance of the uplink throughput of ER_2. The EE with the OMA scheme is better than that with NOMA for the short distances between ER_2 and the UAV. This is mainly due to the short distance between ER_1 and ER_2, and the short distance between IR_1 and IR_2, which increase the interferences and thus decrease the throughputs.

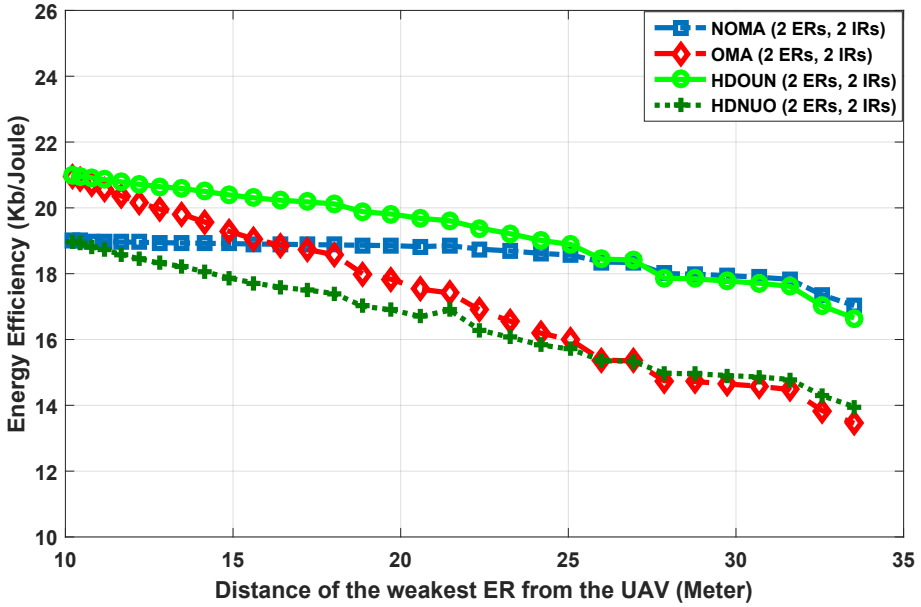

Figure 4.4: System energy efficiency versus the distance of ER_2 from the UAV.

At some point, when ER_2 becomes farther from the UAV and, hence, the distances between ERs and IRs increase, NOMA starts to outperform OMA considerably, and the difference increases as the distance of ER_2 from the UAV increases. However, the hybrid scheme which includes OMA in the downlink for the IRs and NOMA in the uplink for the ERs, outperforms both as it combines the advantages of the two schemes for different stages of the process. This scheme overcomes the shortages of NOMA in the short distances and the shortages of OMA for the long distances of the users from the UAV.

Scenario with three ERs and Three IRs Figure 4.5 shows the effect of different OMA, NOMA and hybrid schemes, on the EE of the system when three ERs along with three IRs are scheduled at a time. The results are plotted as a function of the distance of ER_3 from the UAV taking into account that the downlink throughput of IR_3 is constructed from the same distance of the uplink throughput of ER_3. As observed from the figure, the EE with the OMA scheme is better than that with the NOMA scheme for all cases, which is mainly due to the short distances within the three ERs, and within the three IRs, which increase the interferences and thus decrease the throughputs. At some point, when ER_3 becomes farther from the UAV and, hence, the distances between ERs and IRs increase, the hybrid scheme starts to outperform OMA and the difference gets increased as the distance of ER_2 from the UAV increases.

Scenario with Four ERs and Four IRs Figure 4.6 illustrates the performance of the three access schemes on the EE of the system. The results are plotted as a function of the distance of ER_4 from the UAV taking into account that the downlink throughput of IR_4 is constructed from the same distance of the uplink throughput of

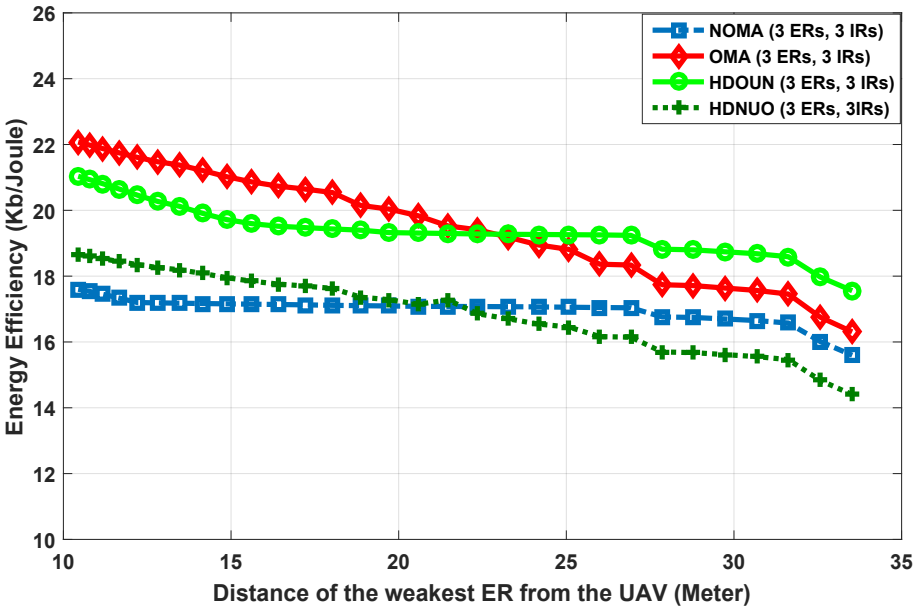

Figure 4.5: System energy efficiency versus the distance of ER_3 from the UAV.

ER_4. The EE with the OMA scheme is better than that with NOMA and the hybrid schemes for all cases, due to the short distances within the four ERs, and within the four IRs, which increase the interferences and thus decrease the throughputs.

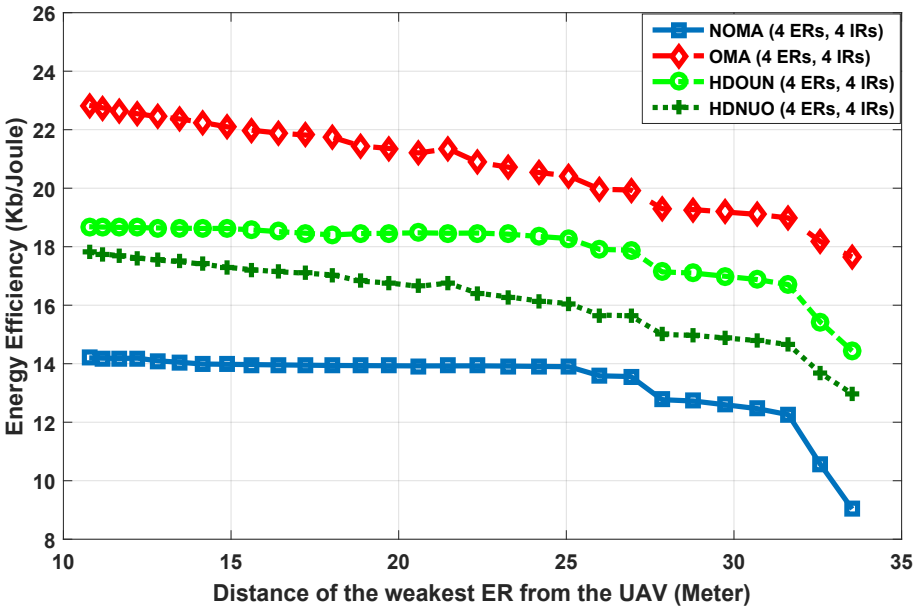

Figure 4.6: System energy efficiency versus the distance of ER_4 from the UAV.

Comparing the three scheduling setups, we can deduce that the increase of the number of scheduled users will considerably reduce the efficiency of NOMA and consequently the efficiency of the hybrid scheme as NOMA is also part of it. As the power budget of the UAV is the same for all scenarios, the degradation of the EE is the result of the degradation of the throughputs as a consequence of the increased interferences of the setups with a higher number of users.

Impact of the UAV's Power Budget

Let us now look at the effect of a change in the power budget of the UAV on the system EE. Here, we consider the scenario with two ERs and two IRs as an example; the other scenarios almost have almost the same trend. Figure 4.7 compares the effect of the UAV's power budget on the system EE (cf. the influence of the power budget on the nominator and denominator of the EE formula). By increasing the power budget, EE also increases as the amount of power destined to the ground users increase, which enhances their throughputs. However, the consumed energy of the UAV will also increase. Consequently, at some point (almost after 3 W in this case), EE will decrease as the increase on the power consumption becomes less beneficial compared to the gain in the throughputs. Note that with all power budgets, the constraints should be satisfied. One can notice that with a low power budget, for large distances of the weakest users from the UAV, EE is very low, due to the small amount of power destined to those users with huge path losses.

Harvesting Time

Now, we investigate the normalized harvesting time, α^*. For the system with two ERs and tow IRs, Figure 4.8 shows the optimal normalized harvesting time, α^*, for different positions of ER_2, while the position of ER_1 remains fixed. The figure compares the

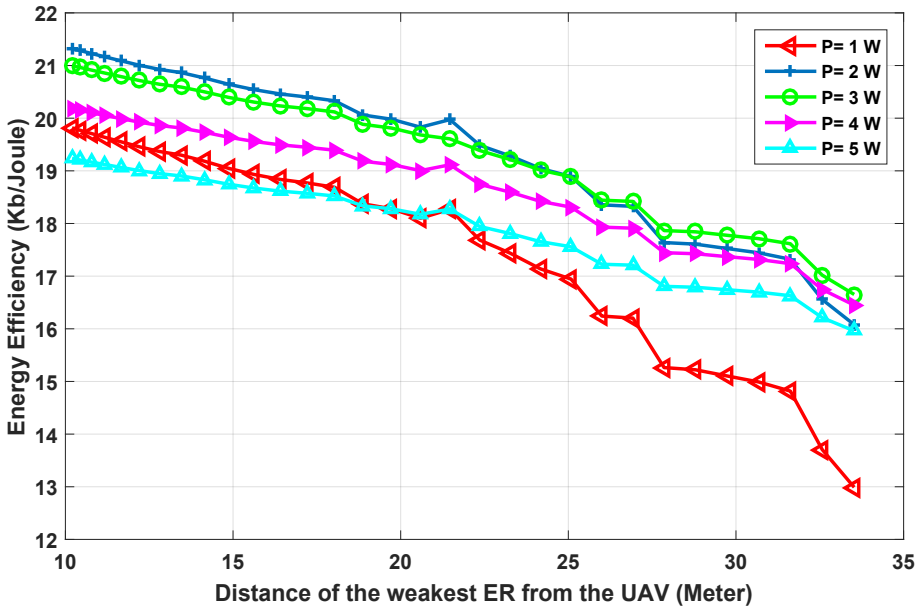

Figure 4.7: System energy efficiency with HDOUN access scheme versus the distance of ER_2 from the UAV for different power budgets.

fraction of time slot needed for the WPT to ERs to enable their uplink transmissions using different schemes. As observed, in all cases, the WPT time in the NOMA case is higher compared to the other cases. It is worth mentioning that this parameter is very important for maximizing the objective function, however, as the UAV will be hovering for the whole period T to handle the uplink and downlink transmissions, there is no gain in reducing the time to do other missions. Hence, for other scenarios with more users, the trend is the same, but with higher values as the time for charging three or four ERs will be more than that for the case with two ERs.

4.4.2 Circular Scenario

We consider three different cases of user scheduling: two ERs with two IRs at a time, three ERs with three IRs at a time, and four ERs with four IRs at a time. The positions of the ERs are set on the circumference of a zero origin circle (0,0,0), where the first ER is set at (x,0,10) and the positions of the other ERs are set uniformly on

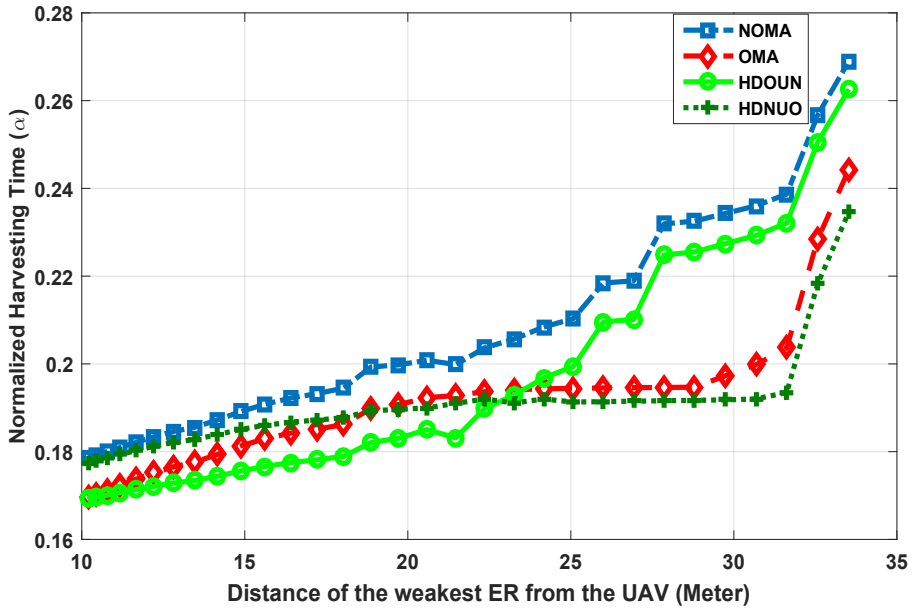

Figure 4.8: Normalized harvesting time in the linear scenario.

this circle. The positions of the IRs are fixed and set uniformly on the circumference of the big circle with the same origin of the small circle, (0,0,0), where the IR_1 is set at (25,0,0). Hence, there will always be two different heights for the ERs and IRs. Different from the linear scenario, in the circular scenario the distances from the UAV to all ERs are the same, which is also valid for the distances from the UAV to the IRs. Besides, as the rate requirements of the IRs are the same, and regardless of the ERs demands, the UAV will hover over the common center of the two circles with the minimum allowable height, i.e., (0,0,20).

Energy Efficiency in the Circular Scenario

In this scenario, we consider the OMA and NOMA schemes. Figure 4.9 shows the effect of these schemes on the system EE. It is clear that OMA outperforms NOMA in all cases. The EE with OMA increases as the number of users increases, while for NOMA, the EE decreases when the number of users gets higher. In this scenario, NOMA would not be that efficient as there is almost no distinctions between the

users. Also, as the number of users increases, the interferences also increase.

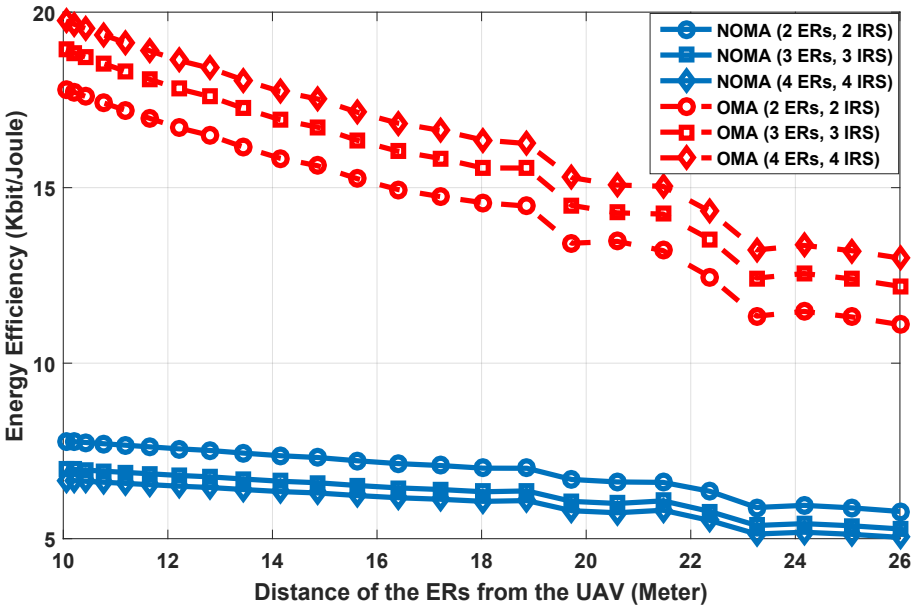

Figure 4.9: System energy efficiency versus the distance of ERs from the UAV in the circular scenario.

Impact of the UAV's Power Budget

Figure 4.10 shows the effect of changing the power budget on the system EE with NOMA, where we consider two ERs and two IRs as an example, noting that the other scenarios have almost the same trend. It is obvious that by increasing the power budget of the UAV, EE also increases. This is a result of destining more power to the ground nodes, which enhance their throughputs, this is noticed between the values of 1 W and 2 W. However, EE starts to decrease at some point and keeps decreasing as the energy consumption of the UAV increases. Hence, the trend is almost the same like in the linear scenario, as the increase in the power budget becomes less beneficial to the throughputs and more severe on the power consumption of the UAV.

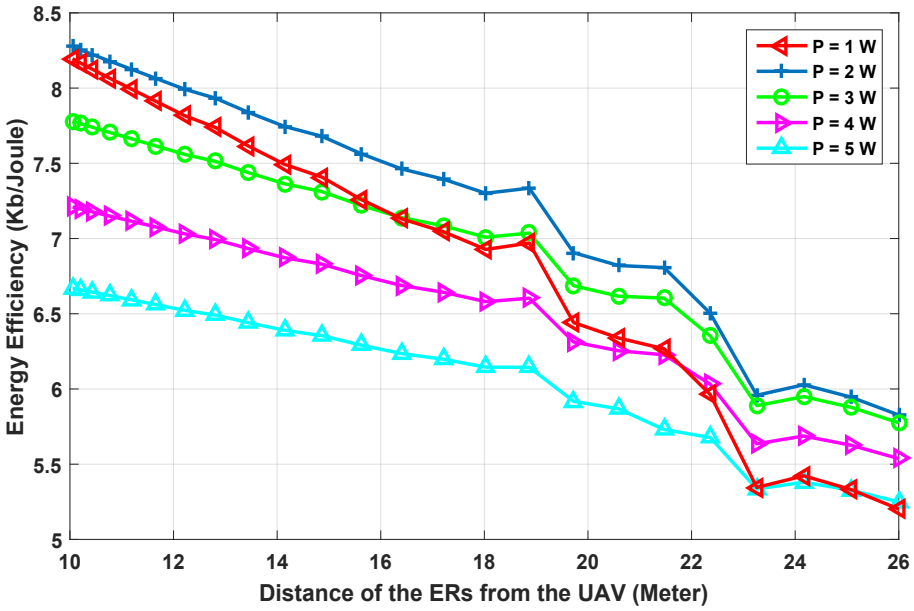

Figure 4.10: System energy efficiency with NOMA versus the distance of ERs from the UAV for different power budgets.

Harvesting Time

We also explored the normalized harvesting time, α^*, for both NOMA and OMA. For the different combinations of ERs and IRs, Figure 4.8 shows the optimal normalized harvesting time, α^*, for different positions of the ERs, while the position of the IRs remains fixed.

The figure compares the fraction of time slot needed for the WPT to ERs to enable their uplink transmissions using NOMA and OMA schemes. It is clear that, in all cases, the WPT time in the NOMA case is higher compared to the one with OMA. In addition, one can notice that the time for charging three or four ERs will be more than that for the case with two ERs, however, this difference is not that considerable in the case of NOMA. The mission of the UAV will last for the whole period of T, to handle the transmissions of ERs and IRs.

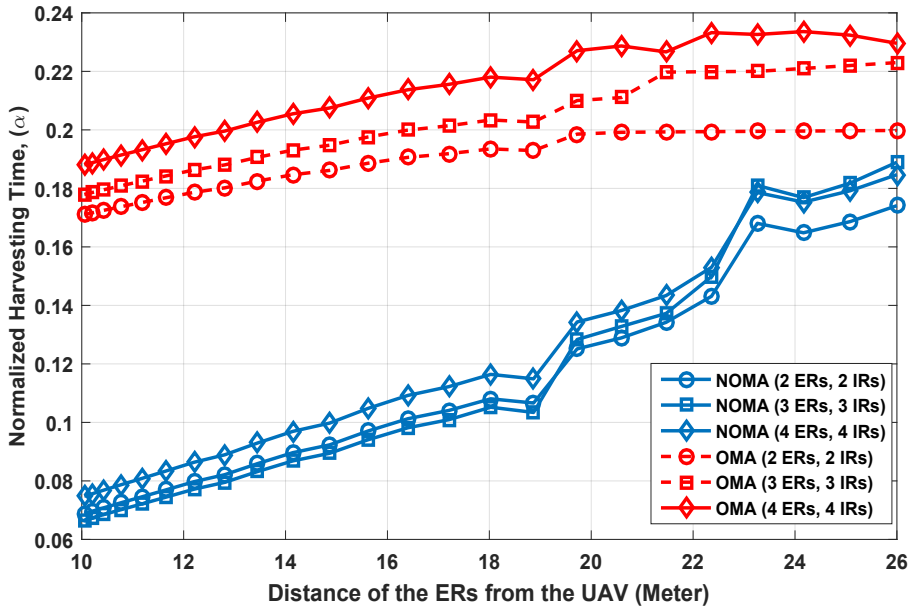

Figure 4.11: Normalized harvesting time in the circular scenario.

4.5 Summary

In this chapter, we investigated the resource allocation in a multiple-antenna UAV deployed for transmitting data to IRs, as well as wireless energy to ERs to assist their uplink communications through different accessing protocols. The optimization problem was solved by minimizing the channels path loss according to the GNs' demands and then optimizing the transmit powers to maximize the system's EE. The results showed, for the linear scenario, an enhancement in the EE for system operation of HDOUN with a small number of ground nodes, while as the number of ground nodes increases, OMA starts to perform better. On the other hand, OMA consistently outperforms NOMA for all cases for the circular scenario, the difference increasing when the number of GNs increases. In all previous three chapters, we have tackled the scenarios where a single UAV is used, however, in cases where the ROI is huge and cannot be covered by a single UAV, multiple UAVs are needed. Thus, in the coming chapter, we will start investigating EE optimization in multi-UAV aided networks.

Chapter 5

Multiple UAV Wireless Powered Communication Networks

In this chapter, we tackle the energy efficiency optimization in wireless communication networks, where multiple UAVs deploy power transfer towards several ERs to enable their uplink data transmissions through NOMA. We present the details of the MUAV-WPCN systems and the different related constraints. We propose a set of collision avoidance constraints to avoid collisions between UAVs as they move to enhance the charging efficiency for the ERs. Also, we consider the optimal switching between energy and information transmissions by enabling a time allocation scheme. Besides, we take into account several constraints related to the guaranteeing of a SIC threshold in the uplink, and also consider the required QoS of the ERs.

5.1 MUAV-WPCN System and Channel Models

In this work, a network of ERs that are enabled by multiple UAVs is taken into account. We consider M multi-antennas UAVs serving several single-antenna ERs that are distributed in a region of interest (ROI) (Figure 5.1). We assume that the

area can be divided into several different clusters that can be determined to provide the required coverage for a given ROI, where each cluster will be served by only one UAV. Hence, the UAV does not have the perfect ULI of ERs in its cluster. The number of antennas at the UAV is N, and it is assumed to be the same for all UAVs. The time slot T is divided into two phases. In the first phase, $\alpha_m T$ $(0 < \alpha_m < 1)$, each UAV transmits energy signals to the scheduled ERs on its cluster. In the second phase, $(1 - \alpha_m)T$, the ERs utilize the harvested energy during the first phase to transmit their data to the same UAV. The data transmissions on the uplink (U) are carried out based on the NOMA scheme. Without loss of generality, we set the time slot duration T to be unity. The position of the UAV$_m$ is denoted (x_m, y_m, h_m)

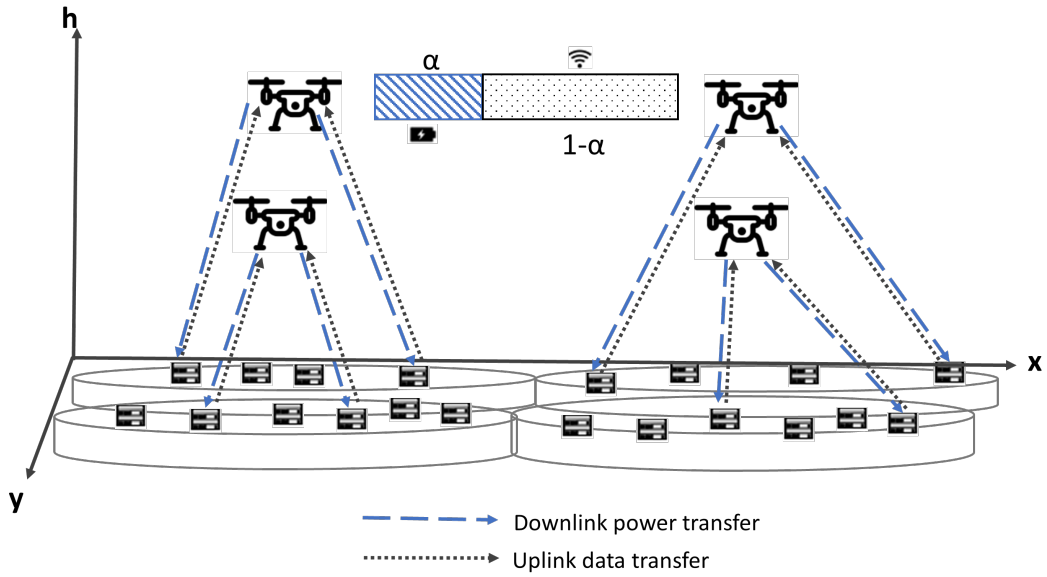

Figure 5.1: MUAV-WPCN system model.

5.1.1 Users Distribution

We consider the partial ULI approach of the ERs [88], where initially, the UAV will not have perfect information about the ERs locations. The UAV will be sent to a

specific cluster in the ROI; the partial ULI known by the UAV is the ERs distribution within the cluster [89]. In this work, we consider a uniform distribution for circles and segments within the cluster to increase the number of possible locations of ERs, which will be the intersection between any circle and segment (Figure 5.2). At the beginning, the UAV will be hovering at the minimum allowable height over the cluster center. The users that need to be charged will send side information about their identity, which will be related to their segment and circle (e.g., an ID for ER that is located in the intersection between circle no. j and segment no. k is j,k ($\mathrm{ER}_{j,k}$) along with their rate demands. According to this received information and the predetermined number of the scheduled users, the UAV will choose the users who will start the process and accordingly position itself to send the power and receive the data. To indicate the required rate in the uplink for the ER, a quantized level of this rate is sent from each ER to its associated UAV. Based on this side information, the UAV specifies the relative demand of each ER, denoted $\varpi^{\mathrm{U}}_{j,k}$, such that $\sum_{j,k} \varpi^{\mathrm{U}}_{j,k} = 1$. Here, a larger value of ϖ means a higher rate demand. The location of $\mathrm{ER}_{j,k}$ is $(x_{\mathrm{ER}_j}, y_{\mathrm{ER}_j}, h_{\mathrm{ER}_j})$. By a slight abuse of notation, we replace the ID of ER, j,k, to be j in the rest of the formulation.

A binary variable of user association with specific UAV_m is denoted $\chi_{m,j}$. If UAV_m serves $\mathrm{ER}_{m,j}$, $\chi_{m,j} = 1$, otherwise it is zero. Note that UAV_m can serve multiple ERs; however, $\mathrm{ER}_{m,j}$ can only be served by a single UAV. These can be formulated as follows:

$$\sum_{m=1}^{M} \chi_{m,j} = 1, \quad \forall j \tag{5.1}$$

$$\chi_{m,j} \in \{0,1\} \quad \forall m, \forall j \tag{5.2}$$

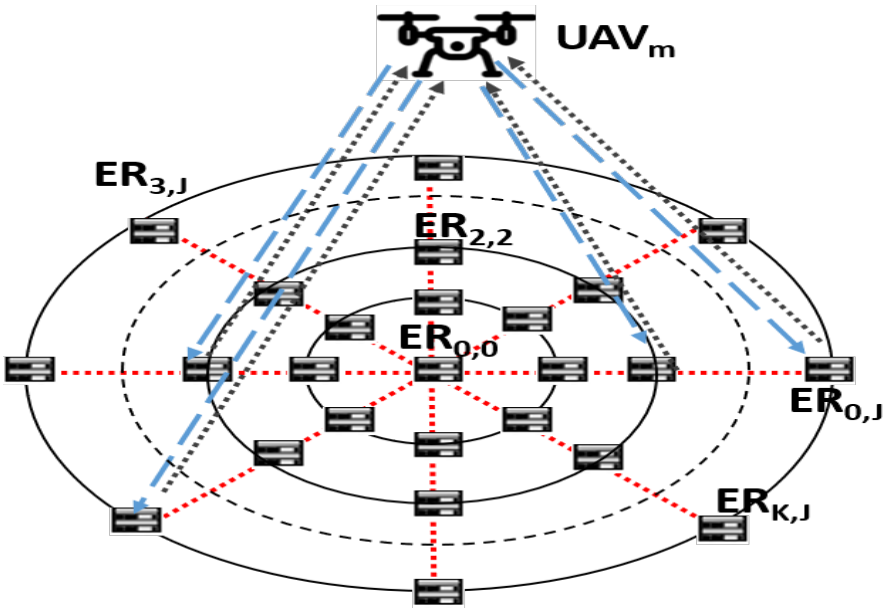

Figure 5.2: Distribution of ERs in cluster m for MUAV-WPCN.

5.1.2 Channel Models

For the channel models, we adopted the models used in [90] to handle the considered system model with multiple UAVs scenario. The channels between the UAVs (e.g., UAV$_m$) and ERs (e.g., ER$_{m,j}$), are of two types: air-to-ground (A2G) from the UAV to ERs, and ground-to-air (G2A) from ERs to the UAV. For ER$_{m,j}$, $j = 1, \cdots, J$, in each cluster and UAV$_m$, $m = 1, \cdots, M$, the complex channel vector of the A2G link is denoted $\mathbf{g}_{m,j} \in \mathbb{C}^{1\times N}$, and the one of the G2A is $\mathbf{z}_{j,m} \in \mathbb{C}^{N\times 1}$. First, we have $\mathbf{g}_{m,j} = \mathbf{g}'_{m,j}/\sqrt{L^{\mathrm{D}}_{m,j}}$, where $L^{\mathrm{D}}_{m,j}$ is the average path-loss, and $\mathbf{g}'_{m,j} = [g'_{m,j_1}, g'_{m,j_2}, \ldots, g'_{m.j_N}]$ is the normalized channel fading vector. For Rician fading, $\mathbf{g}'_{m,j}$ can be written as [80]:

$$\mathbf{g_{m,j}}' = \sqrt{\frac{\mathcal{K}}{\mathcal{K}+1}}\mathbf{1}_{1\times N} + \sqrt{\frac{1}{\mathcal{K}+1}}\tilde{\mathbf{g}}_{m,j}, \tag{5.3}$$

where $\mathcal{K}$ is the Rice factor, $\mathbf{1}_{1\times N}$ is a unity row vector, and the non-line of sight (NLoS) fading component $\tilde{\mathbf{g}}_{m,j}$ is a row vector whose elements are independent and

identically distributed (i.i.d.) complex Gaussian random variables with zero mean and unit variance, i.e., $\mathcal{CN}(0,1)$. The average A2G free-space distance-dependent path loss of $\mathrm{ER}_{m,j}$, $L^{\mathrm{D}}_{m,j}$ in dB, is given by:

$$L^{\mathrm{D}}_{m,j} = p_{\mathrm{LoS}_{m,j}}\, L_{\mathrm{LoS}_{m,j}} + (1 - p_{\mathrm{LoS}_{m,j}})\, L_{\mathrm{NLoS}_{m,j}}, \tag{5.4}$$

where the LoS and NLoS path losses are, respectively, given by:

$$L_{\mathrm{LoS}_{m,j}} = 20\log_{10}\left(\frac{4\pi f d_{m,j}}{c}\right) + \xi_{\mathrm{LoS}_{m,j}}, \tag{5.5}$$

$$L_{\mathrm{NLoS}_{m,j}} = 20\log_{10}\left(\frac{4\pi f d_{m,j}}{c}\right) + \xi_{\mathrm{NLoS}_{m,j}}, \tag{5.6}$$

where f is the carrier frequency, c is the speed of light, and $\xi_{\mathrm{LoS}_{m,j}}$ and $\xi_{\mathrm{NLoS}_{m,j}}$ are the average environment-dependent excessive path losses in dB [72]. In (5.4), $p_{\mathrm{LoS}_{m,j}}$ denotes the probability that the UAV has LoS with $\mathrm{ER}_{m,j}$ [72], given by:

$$p_{\mathrm{LoS}_{m,j}} = \frac{1}{1 + a\exp\left(-b\,(\frac{180}{\pi}\theta_{m,j} - a)\right)}, \tag{5.7}$$

where a and b are constant values related to the environment, and $\theta_{m,j} = \arccos(H_{\mathrm{UAV_m}}/d_{m,j})$ is the elevation angle in radian between UAV_m and $\mathrm{ER}_{m,j}$, where $d_{m,j}$ is the Euclidean distance:

$$d_{m,j} = \sqrt{(x_m - x_{\mathrm{ER}_{m,j}})^2 + (y_m - y_{\mathrm{ER}_{m,j}})^2 + (h_m - h_{\mathrm{ER}_{m,j}})^2} \tag{5.8}$$

For the channel between $\mathrm{ER}_{m,j}$ and UAV_m, $\mathbf{z}_{j,m}$, we also consider a Rician model as for $\mathbf{g}_{m,j}$, with $\mathbf{z}_{m,j} = \mathbf{z}'_{m,j}/\sqrt{L^{\mathrm{U}}_{m,j}}$ and $L^{\mathrm{U}}_{m,j}$ being the average G2A distance-dependent path-loss.

5.2 Energy Transmission

The UAV$_m$ transmits an energy signal $\mathbf{x} \in \mathbb{C}^{N\times 1}$, which consists of J energy beams, one for each ER, i.e.,

$$\mathbf{x} = \sum_{j=1}^{J} \sqrt{P_{m,j}^{\mathrm{D}}}\, \mathbf{w}_{m,j} s_{m,j}^{\mathrm{ER}}, \tag{5.9}$$

where $P_{m,j}^{\mathrm{D}}$ is the transmit power destined for ER$_{m,j}$, $s_{m,j}^{\mathrm{ER}} \in \mathcal{CN}(0,1)$ denotes the energy-carrying signal, and $\mathbf{w}_{m,j} \in \mathbb{C}^{N\times 1}$ is the corresponding energy beamforming vector. For the j^{th} ER, the received signal is given by:

$$y_{m,j}^{\mathrm{ER}} = \mathbf{g}_{m,j} \sum_{i=1}^{J} \sqrt{P_{m,i}^{\mathrm{D}}}\, \mathbf{w}_{m,j} s_{m,j}^{\mathrm{ER}} + \sum_{l=1, l\neq m}^{M} \mathbf{g}_{l,j} \sum_{i=1}^{J} \sqrt{P_{l,i}}\, \mathbf{w}_{l,i}\, s_{l,i}^{\mathrm{ER}} + n_{m,j}^{\mathrm{ER}}, \tag{5.10}$$

where $n_{m,j}^{\mathrm{ER}} \sim \mathcal{CN}(0, \sigma^2)$ is the additive white gaussian noise (AWGN). Also, equal noise powers for all ERs are assumed, i.e., σ^2. The second term represents the effect on ER$_{m,j}$ from the simultaneous power transmissions from other UAVs to the ERs in their clusters. It is assumed that the harvested energy only results from the energy signal in each cluster, excluding any noise. The availability of a perfect CSI is assumed, thus, the optimal weight vector $\mathbf{w}_{m,j}^{\star}$ is $\mathbf{g}_{m,j}^{\dagger}/\|\mathbf{g}_{m,j}\|$. Hence, the harvested energy by ER$_{m,j}$ during the first phase is given by:

$$E_{m,j} = \zeta_j \alpha_m |\mathbf{g}_{m,j} \mathbf{w}_{m,j}^{\star}|^2 \sum_{i=1}^{J} P_{m,i}^{\mathrm{D}} \; = \zeta_j \alpha_m \frac{\|\mathbf{g}'_{m,j}\|^2}{L_{m,j}^{\mathrm{D}}} P_m^{\mathrm{D}}, \tag{5.11}$$

where $0 < \zeta_j \leq 1$ is the energy-harvesting circuit efficiency, assumed to be the same for all ERs, and P_m^{D} is the total transmission power of UAV$_m$.

5.3 Uplink Information Transmission

In the second phase, ERs use the harvested energy for their uplink communication with the same UAV. The transmit power from the j^{th} ER is $P^{\text{U}}_{m,j} = \frac{E_{m,j}}{1-\alpha_m}$. The UAV receives the superposed message signal of J ERs, and applies SIC to decode each device's message. The received signal at the m^{th} UAV, is given by:

$$\mathbf{y}_{\text{UAV}_m} = \sum_{j=1}^{J} \sqrt{P^{\text{U}}_{m,j}}\, \mathbf{z}_{j,m} s_{m,j} + \mathbf{n}, \tag{5.12}$$

where $s_{m,j} \in \mathcal{CN}(0,1)$ is the normalized data symbol of $\text{ER}_{m,j}$ towards UAV_m, and $\mathbf{n}$ is the AWGN with zero mean and covariance matrix $\mathbb{E}\{\mathbf{n}\mathbf{n}^{\dagger}\} = \sigma^2 \mathbf{I}_{N_E}$, where $\mathbf{I}$ is the identity matrix.

5.4 Energy Efficiency Maximization

5.4.1 Energy Efficiency Formulation

To be able to formulate the system's EE, we have to start by constructing the information throughput for the uplink phase. Based on (5.11) and (5.12), the rate related to a given ER can be expressed as [83]:

$$R^{\text{U}}_{m,j} = (1-\alpha_m) W \log_2 \left(1 + \frac{\frac{\zeta P^{\text{D}}_{m,j} \|\mathbf{g'_{m,j}}\|^2 \|\mathbf{z'_{m,j}}\|^2 \alpha_m}{L^{\text{U}}_{m,j} L^{\text{D}}_{m,j} (1-\alpha_m)}}{\sum\limits_{l=j+1}^{J} \frac{\zeta P^{\text{D}}_{m,l} \|\mathbf{g'_{m,l}}\|^2 \|\mathbf{z'_{m,l}}\|^2 \alpha_m}{L^{\text{U}}_{m,l} L^{\text{D}}_{m,l} (1-\alpha_m)} + 1} \right). \tag{5.13}$$

The signal of the highest channel gain user, is decoded first at the UAV. As a result, this ER encounters interference from all other ERs. Then, the signal for the second highest channel gain user is decoded until the last scheduled one, $\text{ER}_{m,J}$, [85]. The

uplink throughput for specific UAV_m can be defined as the sum-rate $R_m^{\text{U}} = \sum_{j=1}^{J} R_{m,j}^{\text{U}}$. The EE of the system is expressed as:

$$\eta = \frac{\sum\limits_{m=1}^{M} \left(\text{Total Throughput}\right)_m}{\sum\limits_{m=1}^{M} \left(\text{Total Consumed Energy}\right)_m} = \frac{\sum\limits_{m=1}^{M} R_m^{\text{U}}}{\sum\limits_{m=1}^{M} \left(P_{\text{DC}_m} + P_m^{\text{D}}\right)}, \tag{5.14}$$

where P_{DC_m} is the constant power consumption of UAV_m.

5.4.2 Problem Formulation

The target is to maximize the system's EE; accordingly, we can formulate the optimization problem as follows:

$$\begin{aligned}
\text{OP}: \max_{P_{m,j}^{\text{D}}, d_{m,j}, \theta_{m,j}} \quad & \eta \\
\text{subject to: } & P_m^{\text{D}} \leq P_{m,\max}^{\text{D}}, \quad \forall m, \\
& P_{m,j}^{\text{U}} \leq P_{m,j,\max}^{\text{U}}, \quad \forall j, \forall m, \\
& \alpha_m < 1, \quad \forall m, \\
& h_{m,\min} \leq d_{m,j} \cos(\theta_{m,j}), \quad \forall j, \forall m \\
& d_{m,\max} \leq r_m - r_{\text{UAV}_m}, \quad \forall m \\
& \sum_{m=1}^{M} \chi_{m,j} = 1, \quad \forall j \\
& \chi_{m,j} \in \{0,1\} \quad \forall m, \forall j \\
& R_{m,j}^{\text{U}} \geq R_{m,j,\min}^{\text{U}}, \quad \forall j, \forall m, \\
& P_{\text{thr}}^{\text{U}} \leq P_{m,j}^{\text{U}} z_{m,j} - \sum_{l=j+1}^{J} P_{m,l}^{\text{U}} z_{m,l}, \forall j, \forall m
\end{aligned} \tag{5.15}$$

where $P_{m,\max}^{\text{D}}$ and $P_{m,j,\max}^{\text{U}}$ are the maximum transmit power for UAV_m and ER_j, respectively, $d_{m,\max}$ is the maximum allowable distance that UAV_m can travel during

T, r_m is the cluster radius, r_{UAV_m} is the UAV_m radius, $R^{\mathrm{U}}_{m,j,\min}$ denotes the minimum required rates of ER_j, $P^{\mathrm{U}}_{\mathrm{thr}}$ is the SIC detection thresholds of the uplink transmission, and $z_{m,j}$ ($\|\mathbf{z}'_{m,l}\|^2/L^{\mathrm{U}}_{\mathrm{ER}_{m,j}}$) is the channel gain between $\mathrm{ER}_{m,k}$ and UAV_m. The optimization problem is a non-convex problem with highly coupled variables; therefore, it is hard to be solved directly by existing convex optimization methods. Accordingly, we decompose the optimization problem into two sub-problems. In the first one (OP_1), we focus on finding the optimal distances and elevation angles w.r.t. the ERs according to their demands and their associations to the UAVs; this will conclude the optimum positions of the UAVs. After getting the UAVs' optimum position, in the second problem (OP_2), we aim to optimize the optimal power of each ER.

5.4.3 UAV Positioning and User Association

In OP_1, the aim is to get the optimal $\theta_{m,j}$ and $d_{m,j}$, which are given in (5.4), for all nodes that are associated with a specific UAV in a specific cluster. This can be obtained by linking the path losses for A2G channels related to each node by the parameters associating with the nodes' demands. Therefore, OP_1 can be given as follows:

$$
\begin{aligned}
\mathrm{OP}_1 \qquad \min_{d_{m,j},\theta_{m,j}} \quad & \sum_j \varpi_j^U \; L^{\mathrm{D}}_{m,j} \\
\text{subject to:} \quad & h_{m,\min} \le d_{m,j}\cos\theta_{m,j}, \quad \forall j, \forall m, \\
& d_{m,\max} \le r_m - r_{\mathrm{UAV_m}}, \quad \forall m, \\
& \sum_{m=1}^{M} \chi_{m,j} = 1, \quad \forall j, \\
& \chi_{m,j} \in \{0,1\} \quad \forall m, \forall j
\end{aligned}
\tag{5.16}
$$

Given that each UAV, at the beginning of the process, will be hovering at the minimum allowable height over the center of its cluster, each ER that needs to be served will send its ID along with its demand to the UAV in its cluster. Accordingly, $\chi_{m,j}$ for each ER that asks to be served in each cluster can be determined. Therefore, this sub-problem can be solved by introducing the Lagrangian multipliers $\boldsymbol{\eth} \geq 0$ for each cluster, where $\boldsymbol{\eth} = [\eth_1, \eth_2, ..., \eth_J]$. The objective function then becomes

$$\begin{aligned} \mathcal{L}_1(\boldsymbol{\eth}, \boldsymbol{d_{\mathbf{ER}}}, \boldsymbol{\theta_{\mathbf{ER}}}) = & \sum_{j=1}^{J} \varpi_j^{\mathrm{U}} \; L_{m,j}^{\mathrm{D}} \\ & - \sum_{j=1}^{J} \eth_j (h_{m,\min} - d_{m,j} \cos\theta_{m,j}). \end{aligned} \tag{5.17}$$

Depending on the KKT conditions [76], the optimal position of the UAV for each cluster can be obtained by solving the first derivatives of $\mathcal{L}_1$ w.r.t. $d_{m,j}$, and $\theta_{m,j}$, respectively, as follows:

$$\begin{aligned} \frac{\partial \mathcal{L}_1}{\partial d_{m,j}} &= \varpi_j^{\mathrm{U}} \; \frac{\partial L_{m,j}^{\mathrm{D}}}{\partial d_{m,j}} - \eth_j \cos\theta_{m,j} \\ &= \frac{20\, \varpi_j^{\mathrm{U}}}{d_{m,j} \ln(10)} - \eth_j \cos\theta_{m,j} = 0, \end{aligned} \tag{5.18}$$

$$\begin{aligned} \frac{\partial \mathcal{L}_1}{\partial \theta_{m,j}} &= \varpi_j^{\mathrm{U}} \; \frac{\partial L_{m,j}^{\mathrm{D}}}{\partial \theta_{m,j}} + \eth_j d_{m,j} \cos\theta_{m,j} \\ &= \frac{\varpi_j^{\mathrm{U}} ab \frac{180}{\pi} (\xi_{\mathrm{LoS}} - \xi_{\mathrm{NLoS}}) \exp\left(-b\,(\frac{180}{\pi}\theta_{m,j} - a)\right)}{\left(1 + a \exp\left(-b\,(\frac{180}{\pi}\theta_{m,j} - a)\right)\right)^2} \\ &+ \eth_j d_{m,j} \cos\theta_{m,j} = 0. \end{aligned} \tag{5.19}$$

The new value of $\eth_j$ can be calculated using the gradient-decent method as follows:

$$\eth_j(i+1) = [\eth_j(i) - \Delta_{\eth_{m,j}}(h_{m,\min} - d_{m,j}\cos\theta_{m,j})]^+, \tag{5.20}$$

where $\eth_j(i)$ is the value $\eth_j$ at the i^{th} iteration, $\triangle_{\eth_j}$ is the iteration step, and $[x]^+ = \max(0, x)$. The procedure for finding the optimal positions of the UAVs is summarized in Algorithm 5.1, where the results of this algorithm will be used in OP_2.

Algorithm 5.1. 3D UAV Location Optimization

Input: ϖ_j^{U}, ξ_{LoS}, ξ_{NLoS} a, b, $h_{m,\min}$, f, r_m, r_{UAV}, and ERs' I.D; $\forall j$, $\forall m$.
Output: $(x_m,y_m,h_m)^*$, $\forall m$.
Initialization: $(x_m,y_m,h_m)^0$, $\eth_j = 0$, $\forall j$, $\forall m$.
1: Determine $\chi_{m,j}$, as per (5.1) and (5.2), $\forall j$, $\forall m$.
2: Update $\eth_j$ according to (5.20), $\forall j$, $\forall m$.
3: Solve (5.18) for $d_{m,j}$, $\forall j$, $\forall m$.
4: Solve (5.19) for $\theta_{m,j}$, $\forall j$, $\forall m$.
5: Compute the optimal $(x_m,y_m,h_m)^*$, $\forall m$, by solving (5.16).

5.4.4 Energy-Efficient Resource Allocation

Based on the constraints that have been treated in OP_1, and the results of Algorithm 5.1, we formulate OP_2 as follows:

$$\begin{aligned}
\text{OP}_2: \quad & \max_{P_{m,j}^{\text{D}}} \quad \eta \\
\text{subject to: } & P_m^D \le P_{m,\max}^{\text{D}}, \quad \forall m, \\
& P_{m,j}^{\text{U}} \le P_{m,j,\max}^{\text{U}}, \quad \forall j, \forall m, \\
& \alpha_m < 1, \quad \forall m, \\
& R_{m,j}^{\text{U}} \ge R_{m,j,\min}^{\text{U}}, \quad \forall j, \forall m, \\
& P_{\text{thr}}^{\text{U}} \le P_{m,j}^{\text{U}} z_{m,j} - \sum_{l=j+1}^{J} P_{m,l}^{\text{U}} z_{m,l}, \forall j, \forall m
\end{aligned} \tag{5.21}$$

OP_2 is a fractional programming problem that can be converted into a convex problem by introducing the variable F^* as the optimal EE when we have the optimal power for each UAV [87]. This concludes that the optimization of the converted problem is also the optimization of the original one [87]. Moreover, we introduce $\boldsymbol{\varsigma} \geq 0$, $\boldsymbol{\varphi_m} \geq 0$, $\boldsymbol{\lambda} \geq 0$, $\boldsymbol{\mu_m} \geq 0$, and $\boldsymbol{\phi_m} \geq 0$, as the Lagrange multipliers associated with the constraints in OP_2, where $\boldsymbol{\varsigma} = [\varsigma_1, \varsigma_2, ..., \varsigma_M]$, $\boldsymbol{\varphi_m} = [\varphi_{m,1}, \varphi_{m,2}, ..., \varphi_{m,J}]$, $\boldsymbol{\lambda} = [\lambda_1, \lambda_2, ..., \lambda_M]$, $\boldsymbol{\mu_m} = [\mu_{m,1}, \mu_{m,2}, ..., \mu_{m,J}]$, and $\boldsymbol{\phi_m} = [\phi_{m,1}, \phi_{m,2}, ..., \phi_{m,J}]$.

The Lagrangian function of OP_2 can be formulated as:

$$
\begin{aligned}
&\mathcal{L}_2(\boldsymbol{\varsigma}, \boldsymbol{\varphi_m}, \boldsymbol{\lambda}, \boldsymbol{\mu_m}, \boldsymbol{\phi_m}, P^{\mathrm{D}}_{m,j}) \\
&= \sum_{m=1}^{M} R^{\mathrm{U}}_m - F^*(\sum_{m=1}^{M} P_{\mathrm{DC}_m} + \sum_{m=1}^{M} P^{\mathrm{D}}_m) \\
&- \sum_{m=1}^{M} \varsigma_m (P^{\mathrm{D}}_m - P^{\mathrm{D}}_{m,\max}) - \sum_{m=1}^{M} \sum_{j=1}^{J} \varphi_{m,j} (P^{\mathrm{U}}_{m,j} - P^{\mathrm{U}}_{m,j,\max}) \\
&- \sum_{m=1}^{M} \lambda_m (\alpha_m - 1) - \sum_{m=1}^{M} \sum_{j=1}^{J} \mu_{m,j} (R^{\mathrm{U}}_{m,j,\min} - R^{\mathrm{U}}_{m,j}) \\
&- \sum_{m=1}^{M} \sum_{j=1}^{J} \phi_{m,j} \left[P^{\mathrm{U}}_{\mathrm{thr}} - P^{\mathrm{U}}_{m,j} z_{m,j} + \sum_{l=j+1}^{J} P^{\mathrm{U}}_{m,l} z_{m,l} \right].
\end{aligned}
\tag{5.22}
$$

To get the optimized transmit power towards each ER in each cluster, we derive the Lagrangian function (5.22) w.r.t. $P^{\mathrm{D}}_{m,j}$ and set the derivative to zero:

$$
\frac{\partial \mathcal{L}_2(\boldsymbol{\varsigma}, \boldsymbol{\varphi_m}, \boldsymbol{\lambda}, \boldsymbol{\mu_m}, \boldsymbol{\phi_m}, P^{\mathrm{D}}_{m,j})}{\partial P^{\mathrm{D}}_{m,j}} = 0 \tag{5.23}
$$

The updating of the Lagrangian variables $\boldsymbol{\varsigma}$, $\boldsymbol{\varphi_m}$, $\boldsymbol{\lambda}$, $\boldsymbol{\mu_m}$, and $\boldsymbol{\phi_m}$ can be done using the gradient method similar to what has been done in the previous subsection for $\boldsymbol{\eth}$ in (5.20). Algorithm 5.2 summarizes the solution for OP_2.

Algorithm 5.2. Energy-Efficient Resource Allocation

Input: $(x_m,y_m,h_m)^*$, ξ_{LoS}, ξ_{NLoS} a, b, $h_{m,\min}$, ERs' I.D, f, η, σ, and $R^{\text{U}}_{\min}$, $\forall j$, $\forall m$.
Output: $(P^{\text{D}}_{m,j})^*$, $\forall j$, $\forall m$.
Initialization: $(P^{\text{D}}_{m,j})^0$, $\boldsymbol{\varsigma} = \mathbf{0}$, $\boldsymbol{\varphi}_m = \mathbf{0}$, $\boldsymbol{\lambda} = \mathbf{0}$, $\boldsymbol{\mu}_m = \mathbf{0}$, $\boldsymbol{\phi}_m = \mathbf{0}$.
1: Update the Lagrangian variables, $\boldsymbol{\varsigma}$, $\boldsymbol{\varphi_m}$, $\boldsymbol{\lambda}$, $\boldsymbol{\mu_m}$, and $\boldsymbol{\phi_m}$.
2: Solve (5.23) to obtain $P^{\text{D}}_{m,j}$.
3: Compute $(P^{\text{D}}_{m,j})^*$, $\forall j$, $\forall m$ by solving (5.21).

5.4.5 Complexity Analysis

Both algorithms that we use to solve the optimization problem are based on the gradient-descent method, where the worst complexity is $\mathcal{O}(n \times \frac{1}{\epsilon})$ [79], with n being the number of optimization variables and ϵ the solution accuracy. Thus, for Algorithm 5.1, the complexity depends on the 3D plane size that the UAVs consider for moving, i.e., $x \times y \times (h_{m,\max} - h_{m,\min})$, where $(h_{m,\max} - h_{m,\min})$ is the allowable altitude range for moving. For Algorithm 5.2, the complexity depends on the numbers of UAVs (M) and ERs (J). Accordingly, the total complexity for both algorithms is $\mathcal{O}(x \times y \times (h_{m,\max} - h_{m,\min}) \times \frac{1}{\epsilon}) + \mathcal{O}(M \times J \times \frac{1}{\epsilon})$.

5.5 Simulation Results

In this section, we perform simulations to evaluate the effectiveness of the proposed algorithms for different cases and access schemes. In the simulation, we consider 100×100 m^2 as the ROI, with $M = 4$ UAVs to provide the coverage for that area. Also, $H_{\text{UAV,min}} = 10$ m, and $r_{\text{UAV}_m} = 0.5$ m for all UAVs, and $r_C = 25$ m for all clusters. In addition, we set $a = 9.6$, $b = 0.28$, $\xi_{\text{LoS}} = 1$ dB, $\xi_{\text{NLoS}} = 20$ dB, $f = 2$ GHz, $W = 200$ kHz, $\eta = 0.8$ and $\sigma^2 = 1$. We also set $P^{\text{U}}_{\text{thr}} = 0.05$ Watt, $P_{\text{DC}} = 5$ Watt, $P_{\max} = 3$ Watt, and $R^{\text{U}}_{\min}$= 12 Kbps. We consider that eight ERs ask to be served, two in each cluster at the same time. These ERs are $\text{ER}_{0,0}$, $\text{ER}_{3,0}$ in the first cluster,

$ER_{1,2}$, $ER_{3,2}$ in the second cluster, $ER_{5,0}$, $ER_{5,2}$ in the third cluster, and $ER_{4,2}$, $ER_{2,5}$ in the fourth cluster. We consider three different cases:

- **Case 1** "No consideration for the service demands of the ERs": Each UAV will hover at the minimum allowable height over the center of its cluster.
- **Case 2** "Same service demands for both ERs in the cluster" (e.g., in the first cluster, $\varpi^{U}_{0,0} = \varpi^{U}_{3,0} = 0.5$): At the beginning of the process, each UAV will hover at the minimum allowable height over the center of its cluster, then move to the optimal position according to the same ERs' service demands.
- **Case 3** "Different service demands for each ER in the cluster" (e.g., in the first cluster, $\varpi^{U}_{0,0} = 0.75$ and $\varpi^{U}_{3,0} = 0.25$): At the beginning of the process, each UAV will hover at the minimum allowable height over the center of its cluster, then move to the optimal position according to different ER service demands.

5.5.1 3D Positions of the UAVs

The UAVs in Case 1 will be hovering at the minimum allowable height over the centers of their clusters. Note that these positions will be fixed during the whole process. Accordingly, the positions for UAV_1, UAV_2, UAV_3 and UAV_4 are, respectively, (25,25,10), (75,25,10), (75,75,10) and (25,75,10) as shown in Figure 5.3. For Case 2, the UAVs will move from the initial positions to the optimal points according to Algorithm 5.1 depending on the same service demands for both ERs in each cluster. Accordingly, the optimal positions of UAV_1, UAV_2, UAV_3, and UAV_4 will be (32.5,25,10), (75,37.5,10), (87.5,87.5,10), and (18.628,77.5,10), respectively, as shown in Figure 5.4.

The optimal positions of the UAVs for Case 3, which handles different ER service demands, are shown in Figure 5.5.

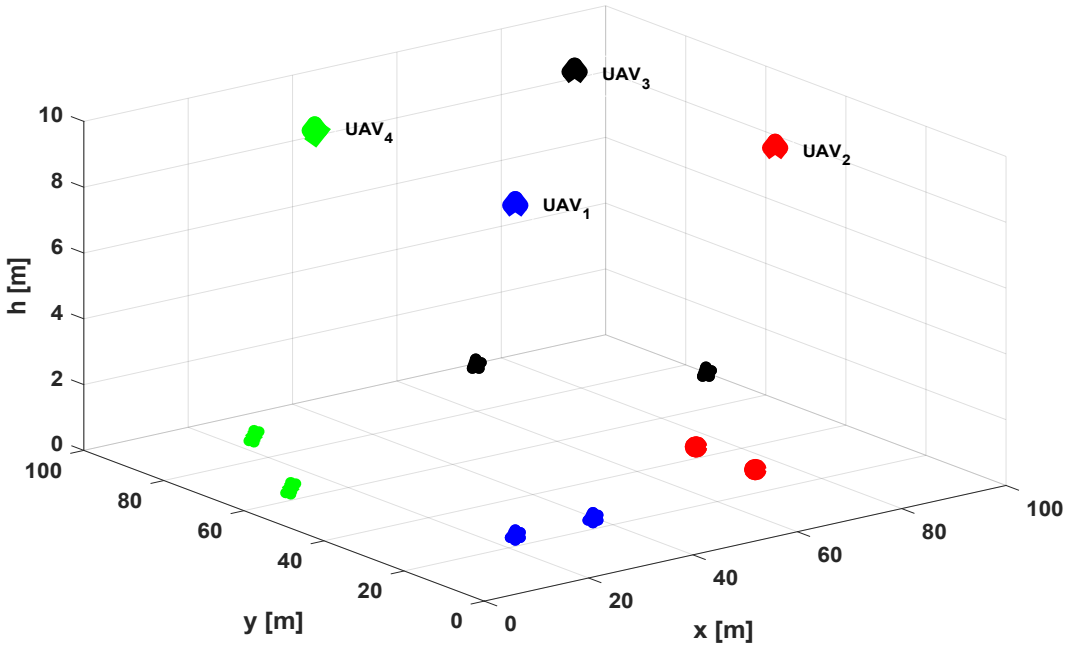

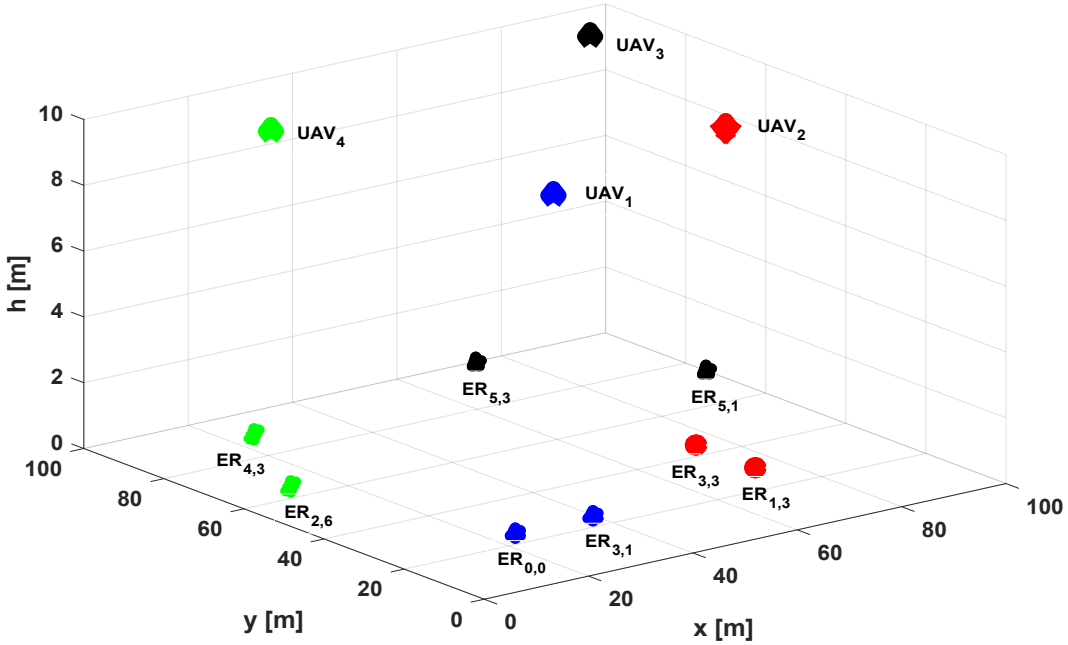

Figure 5.4: Optimal locations of the UAVs for Case 2 (MUAV-WPCN).

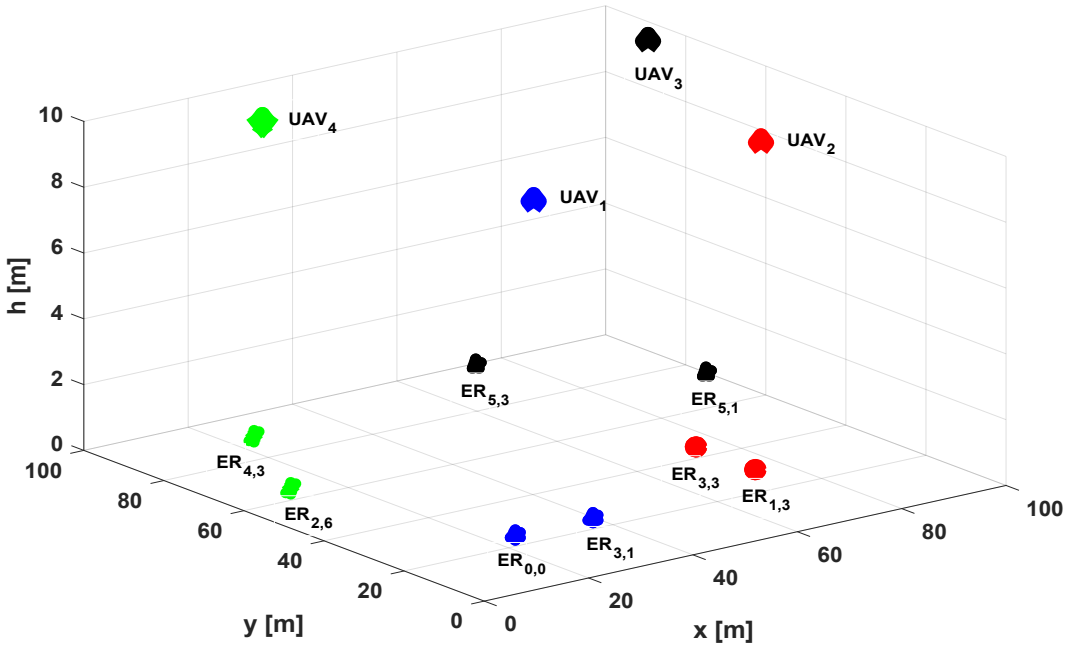

Figure 5.5: Optimal locations of the UAVs for Case 3 (MUAV-WPCN).

5.5.2 Energy Efficiency Optimization for All Cases

We compare the performance of applying the algorithms on the three cases for NOMA and OMA schemes, as shown in Figure 5.6, which exhibits EE with respect to the normalized charging time (α_m) that is set to be the same for all UAVs. One can notice that in all cases, NOMA outperforms OMA. However, the differences are varying from one case to another. In the first case, there is a feasible distinction between the links of the two scheduled ERs in each cluster from their associated UAV, and this is where the superiority of NOMA becomes clear. According to our proposed method, which suggested that the moving of the UAVs depending on the ERs' service demands, Cases 2 and 3 outperform Case 1 for NOMA and OMA. However, NOMA's superiority over OMA almost disappears in Case 2, as each UAV will hover almost over the middle distance between both ERs in its cluster as they have similar service demands. In Case 3, where different node service demands are considered, the EE performance is

the best among all cases, and the NOMA scheme is better than OMA.

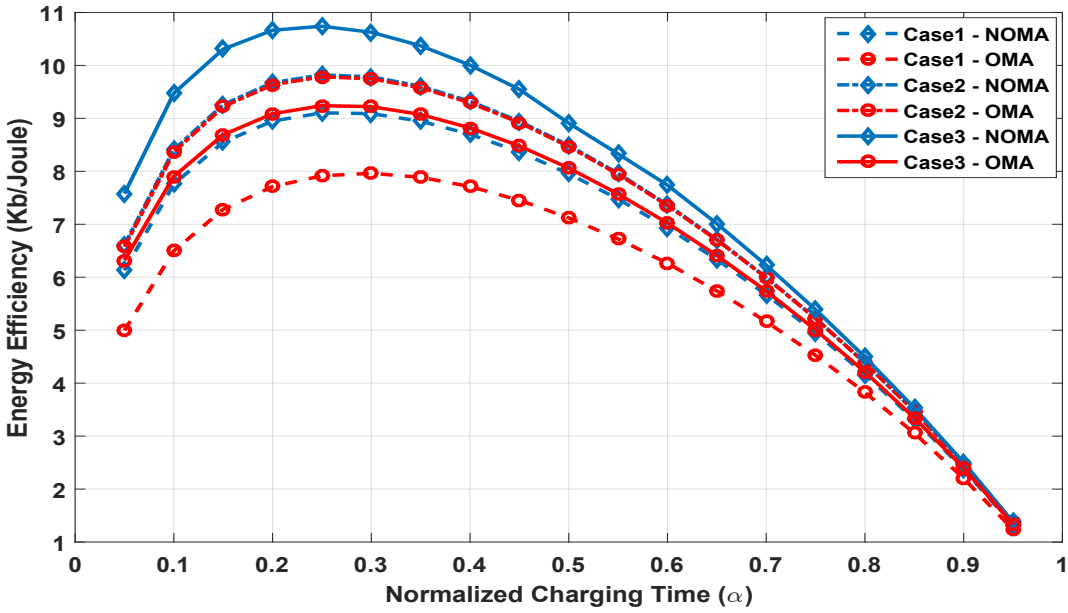

Figure 5.6: System energy efficiency versus normalized charging time for MUAV-WPCN

5.6 Summary

In this chapter, we investigated the resource allocation for multiple UAV networks that are deployed for sending wireless energy to several ERs to enable their uplink communications. The optimization problem was decomposed into two sub-problems. In the first one, and to enhance the communication links between the UAVs and ERs, the UAVs move to the optimal positions depending on the service demands from ERs in their clusters. Secondly, the maximization of the network's EE was solved by optimizing the transmit powers towards the ERs in all clusters. The results showed that the proposed allocation scheme could achieve significant EE. In particular, for most cases, the EE of the NOMA-based system outperforms that of OMA w.r.t. the normalized charging time.

This chapter tackled the optimization problem with M UAVs and J ERs, which is

comprehensive and general. However, this scenario is limited to the using of multiple UAVs to charge ERs, where as we mentioned before, in many cases, UAVs are called to not only charge devices, but also to send and/or collect information to/from them. Therefore, in the next chapter, we will discuss the integration of the proposed scheme in the context of multi-UAV within SWIPT networks.

Chapter 6

Multiple UAV Simultaneous Wireless Information and Power Transfer

In this chapter, we investigate the EE optimization in a wireless communication network that consists of multiple UAVs, ERs and IRs. We consider several cases depending on different combinations of the devices' rate requirements. We present the details of the most general scenario, i.e., MUA-SWIPT, where partial ULI is considered. The optimization problem to maximize the overall EE is formulated and solved using Lagrangian optimization and gradient-descent methods. The optimization process is decomposed into two sub-problems that handle the optimization of the 3D positions of the UAVs at first, and then, allocate the available resources to maximize the system EE.

6.1 MUAV-SWIPT System and Channel Models

A network of multiple devices that are enabled by multiple UAVs is considered. There are two types of devices; IRs and ERs. We consider M multi-antenna UAVs serving several single-antenna devices that are distributed in a ROI (Figure 6.1). We assume

that the area can be divided into a number of clusters that can be determined to be able to provide the required coverage for a given ROI, where each cluster will be served by only one UAV. Hence, the UAV does not have perfect ULI of the GNs in its cluster. The total number of antennas at the UAV is $N = N_E + N_I$, with N_E used for the ERs, and N_I dedicated to the IRs; this is the same for all UAVs. The time slot T is divided into two phases. In the first phase, $\alpha_m T$ $(0 < \alpha_m < 1)$, each UAV transmits energy signals to the scheduled ERs in its cluster. In the second phase, $(1 - \alpha_m)T$, the ERs make use of the harvested energy to transmit their always-available data to the associated UAV. Simultaneously, the UAV transmits information to the IRs. The data transmissions on the uplink (U) and downlink (D) are performed according to the NOMA protocol. Without loss of generality, the time slot duration T is set to unity. The position of UAV_m is denoted by $(x_{\text{UAV}_m}, y_{\text{UAV}_m}, h_{\text{UAV}_m})$.

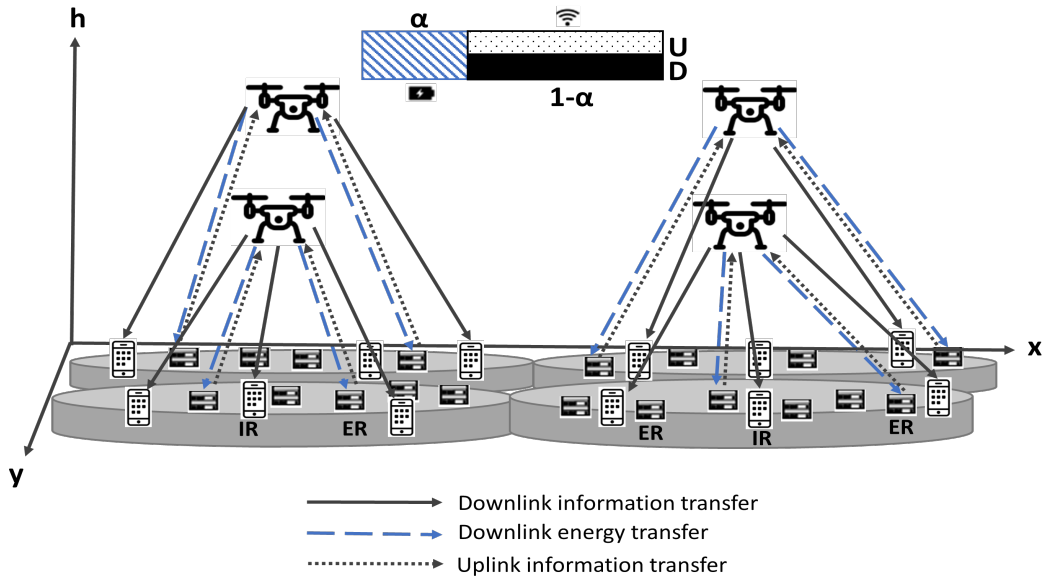

Figure 6.1: MUAV-SWIPT system model

6.1.1 Distribution of Devices

Similar to Chapter 5, we consider the partial ULI approach where, initially, the UAV will not have perfect information about the locations of the GNs (ERs and IRs). Each UAV will be sent to a specific cluster in the ROI. The partial information related to the GNs that is known by the UAV is their distribution within the cluster. In this work, we consider the uniform distribution for circles and segments within the cluster to increase the number of GNs' possible locations, which will be the intersection between any circle and segment (Figure 6.2). At the beginning, the UAV will be hovering at the minimum allowable height over the center of the cluster, then the devices that need to be served will send side information about their identities to the UAV with the best link to each of them, which usually has the shortest distance to each of them. This information is related to their segment and circle (e.g., ID of GN that is located in the intersection between segment no. ψ and circle no. ϕ is ψ,ϕ ($\mathrm{GN}_{\psi,\phi}$)) along with their rate demands. Based on this received information and the predetermined number of the scheduled GNs, the UAV chooses the devices that will be served, and positions itself accordingly to start sending power and sending/receiving data.

For simplicity in the rest of the formulation, we replace the notation $\mathrm{GN}_{\psi,\phi}$ depending on its type. For ER, it becomes $\mathrm{ER}_{m,j}$, and for IR, it becomes $\mathrm{IR}_{m,k}$. In each cluster, there are K IRs and J ERs. The location of $\mathrm{ER}_{m,j}$ is denoted $(x_{\mathrm{ER}_j}, y_{\mathrm{ER}_j}, h_{\mathrm{ER}_j})$, and the one of $\mathrm{IR}_{m,k}$ is denoted $(x_{\mathrm{IR}_k}, y_{\mathrm{IR}_k}, h_{\mathrm{IR}_k})$. A quantized level of the uplink rate requirement is sent from each ER to its associated UAV to indicate its power demand. Based on this side information, and knowledge of the rate requirements of the IRs, each UAV determines the relative demand of each ER and IR, denoted Υ_j^{U} and Υ_k^{D}, respectively, such that $\sum_{j,k} \Upsilon_j^{\mathrm{U}} + \Upsilon_k^{\mathrm{D}} = 1$. Here, a larger

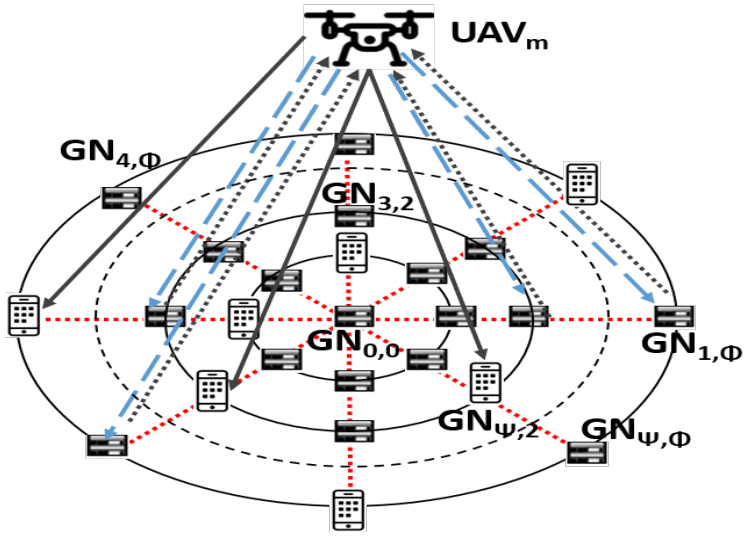

Figure 6.2: Distribution of devices in cluster m for MUAV-SWIPT.

value of Υ means a higher rate demand. A binary variable of ER association with a specific UAV$_m$ is denoted $\chi_{m,j}$, and the one for IR is denoted $\chi_{m,k}$. If ER$_{m,j}$ is served by UAV$_m$, then $\chi_{m,j} = 1$, otherwise it is zero. Note that UAV$_m$ can serve multiple ERs; however, ER$_{m,j}$ can only be served by one UAV, and this is also applicable for IR$_{m,k}$ with UAV$_m$. These can be formulated as follows:

$$\sum_{m=1}^{M} \chi_{m,j} = 1, \quad \forall j. \tag{6.1}$$

$$\sum_{m=1}^{M} \chi_{m,k} = 1, \quad \forall k. \tag{6.2}$$

$$\chi_{m,j} \in \{0,1\} \quad \forall m, \forall j. \tag{6.3}$$

$$\chi_{m,k} \in \{0,1\} \quad \forall m, \forall k. \tag{6.4}$$

6.1.2 Channel Models

There are three types of channels in the network: air-to-ground (A2G) from the UAVs to IRs and ERs, ground-to-air (G2A) from the ERs to the UAVs, and ground-to-ground (G2G) between the ERs and IRs. The complex channel vector of link UAV_m-$\text{IR}_{m,k}$ is denoted $\mathbf{h}_{m,k} \in \mathbb{C}^{1\times N_I}$, $m = 1, \cdots, M$, and $k = 1, \cdots, K$. For $\text{ER}_{m,j}$, $j = 1, \cdots, J$, the complex channel vector of the A2G link is denoted $\mathbf{g}_{m,j} \in \mathbb{C}^{1\times N_E}$. The G2A channel related to $\text{ER}_{m,j}$ is $\mathbf{z}_{j,m} \in \mathbb{C}^{N_E\times 1}$. First, we have $\mathbf{g}_{m,j} = \mathbf{g}'_{m,j}/\sqrt{L^{\text{D}}_{\text{ER}_{m,j}}}$, where $L^{\text{D}}_{\text{ER}_{m,j}}$ is the average path-loss, and $\mathbf{g}'_{m,j} = [g'_{m,j_1}, g'_{m,j_2}, \ldots, g'_{m.j_{N_E}}]$ is the normalized channel fading vector. For Rician fading, $\mathbf{g}'_{m,j}$ can be written as in (5.3). The average A2G free-space distance-dependent path loss of $\text{ER}_{m,j}$, $L^{\text{D}}_{\text{ER}_{m,j}}$ in dB, is given as in (5.4). The probability that UAV_m has LoS with $\text{ER}_{m,j}$ is given as in (5.7), and the Euclidean distance, $d_{m,j}$, is given as in (5.8). Accordingly, we can obtain the average A2G free-space distance-dependent path loss of $\text{ER}_{m,j}$, $L^{\text{D}}_{\text{ER}_{m,j}}$ in dB, as follows:

$$L^{\text{D}}_{\text{ER}_{m,j}} = \frac{\xi_{\text{LoS}_{m,j}} - \xi_{\text{NLoS}_{m,j}}}{1 + a\exp\left(-b\ \left(\frac{180}{\pi}\theta_{m,j} - a\right)\right)} + 20\log\left(\frac{4\pi f d_{m,j}}{c}\right) + \xi_{\text{NLoS}_{m,j}}, \tag{6.5}$$

The A2G channel model described above w.r.t. ERs ($\mathbf{g}$) applies to the IRs ($\mathbf{h}$) by replacing k with j, and IR with ER in (5.3)-(5.8) and (6.5). For the channel between $\text{ER}_{m,j}$ and UAV_m, $\mathbf{z}_{m,j}$, we also consider a Rician model as for $\mathbf{g}_{m,j}$, with $\mathbf{z}_{m,j} = \mathbf{z}'_{m,j}/\sqrt{L^{\text{U}}_{\text{ER}_{m,j}}}$, and $L^{\text{U}}_{\text{ER}_{m,j}}$ being the G2A distance-dependent path-loss. For the G2G channel, the complex channel of link $\text{ER}_{m,j}$-$\text{IR}_{m,k}$ is denoted $\mathbf{e}_{j,k}$, $j = 1, \cdots, J$, and $k = 1, \cdots, K$, which includes the Rayleigh fading from the j^{th} ER to the the k^{th} IR along with the path loss as adopted in [91].

6.2 Energy Transmission

For cluster m, UAV_m transmits energy signal $\mathbf{x}_{m,1} \in \mathbb{C}^{N_E \times 1}$, which consists of J energy beams, one for each ER, i.e.,

$$\mathbf{x}_{m,1} = \sqrt{\beta_m P_m} \sum_{j=1}^{J} \mathbf{w}_{m,j}\, s_{m,j}^{\text{ER}}, \tag{6.6}$$

where P_m is the transmit power of UAV_m, $s_{m,j}^{\text{ER}} \in \mathcal{CN}(0,1)$ denotes the energy-carrying signal, and $\mathbf{w}_{m,j} \in \mathbb{C}^{N_E \times 1}$ is the corresponding energy beamforming vector. Here, β_m indicates the percentage of power destined to the ERs in m^{th} cluster, and $(1-\beta_m)$ indicates the percentage of power destined to the IRs. Hence, a larger value for β_m means that higher priority will be given to the WPT. For the j^{th} ER served by the UAV_m in the m^{th} cluster, its received signal is given by:

$$y_{m,j}^{\text{ER}} = \mathbf{g}_{m,j}\sqrt{\beta_m P_m}\mathbf{w}_{m,j} s_{m,j}^{\text{ER}} + \sum_{l=1, l\neq m}^{M} \mathbf{g}_{l,j}\sqrt{\beta_l P_l} \sum_{i=1}^{J} \mathbf{w}_{l,i}\, s_{l,i}^{\text{ER}} + n_{m,j}^{\text{ER}}, \tag{6.7}$$

where $n_{m,j}^{\text{ER}} \sim \mathcal{CN}(0, \sigma^2)$ is the AWGN, with equal noise powers assumed for all ERs, i.e., σ^2. The second term in (6.7) represents the effect on $\text{ER}_{m,j}$ from the simultaneous WPT from other UAVs to the ERs in their clusters. It is assumed that the harvested energy results from the energy signals in the cluster where the device is located, and that noise does not take part in it. Assuming the availability of perfect channel state information (CSI), the optimal weight vector $\mathbf{w}_{m,j}^{\star}$ is $\mathbf{g}_{m,j}^{\dagger}/\|\mathbf{g}_{m,j}\|$. Hence, the harvested energy by $\text{ER}_{m,j}$ during the first phase is given by

$$E_{m,j} = \zeta_j \alpha_m |\mathbf{g}_{m,j}\mathbf{w}_{m,j}^{\star}|^2 \sum_{i=1}^{J} P_{m,i}^{\text{D}} \; = \zeta_j \alpha_m \frac{\|\mathbf{g}'_{m,j}\|^2}{L_{m,j}^{\text{D}}} P_m^{\text{D}}, \tag{6.8}$$

where $0 < \zeta_j \leq 1$ is the energy-harvesting circuit efficiency [73], assumed the same for all ERs, and $P_m^{\mathrm{D}} = \beta_m P_m = \sum_{j=1}^{J} P_{m,j}^{\mathrm{D}}$ is the sum-power dedicated by UAV_m to its J ERs.

6.3 Information Transmission

In the second phase, ERs use the harvested energy for their uplink communication with the UAVs, simultaneously with the downlink transmission from the UAVs to the IRs.

6.3.1 Uplink Information Transmission

The transmit power from the j^{th} ER in cluster m served by UAV_m is $P_{j,m}^{\mathrm{U}} = \frac{E_{m,j}}{1-\alpha_m}$. The UAV receives the superposed message signal of J ERs, and applies SIC to decode each device's message. The received signal at UAV_m, $\mathbf{y}_{\mathrm{UAV}_m} \in \mathbb{C}^{N_{\mathrm{E}} \times J}$, is expressed as

$$\mathbf{y}_m = \sum_{j=1}^{J} \sqrt{P_{m,j}^{\mathrm{U}}} \mathbf{z}_{m,j} s_{m,j}^{\mathrm{ER}} + \mathbf{H}_{\mathrm{SI}_m} \sqrt{(1-\beta_m) P_m} \sum_{k=1}^{K} \mathbf{v}_{m,k} s_{m,k}^{\mathrm{IR}} + \mathbf{n}_m, \tag{6.9}$$

where $s_{m,j} \in \mathcal{CN}(0,1)$ is the normalized data symbol of $\mathrm{ER}_{m,j}$ towards UAV_m. Further, $\mathbf{H}_{\mathrm{SI}_m} \in \mathbb{C}^{N_I \times N_E}$ is the self-interference (SI) channel due to the simultaneous uplink and downlink processes [82], with independent entries drawn from $\mathcal{CN}(0, \sigma_{\mathrm{SI}}^2)$ where σ_{SI}^2 account for the residual SI power after suppression [92], $\mathbf{v}_{m,k} \in \mathbb{C}^{N_{\mathrm{I}} \times 1}$ is the corresponding beamforming vector, $s_{m,k}^{\mathrm{IR}} \in \mathcal{CN}(0,1)$ denotes the information-bearing signal of the k^{th} IR, and $\mathbf{n_m}$ is the AWGN vector with zero mean and covariance matrix $\mathbb{E}\{\mathbf{n_m} \mathbf{n_m}^{\dagger}\} = \sigma^2 \mathbf{I}_{N_{\mathrm{E}}}$, where $\mathbf{I}_{N_{\mathrm{E}}}$ is the identity matrix. We assume that powerful SI cancellation is in place [82], but since some SI will remain [93], we consider the effect of the residual SI.

6.3.2 Downlink Information Transmission

The data signal $\mathbf{x}_{m,2} \in \mathbb{C}^{N_I \times 1}$ sent by UAV_m to its IRs consists of K information beams, one for each IR:

$$\mathbf{x}_{m,2} = \sqrt{(1-\beta_m)P_m} \sum_{k=1}^{K} \mathbf{v}_{m,k}\, s_{m,k}^{\text{IR}}. \tag{6.10}$$

In each cluster, each IR encounters interference from the uplink signals of ERs towards the UAV, as well as interference from the UAVs' downlink beams to other IRs. hence, the received signal at $\text{IR}_{m,k}$ is given by

$$\begin{aligned} y_{m,k}^{\text{IR}} = \mathbf{h}_{m,k}\sqrt{(1-\beta_m)P_m}\sum_{i=1}^{K}\mathbf{v}_{m,i}s_{m,i}^{\text{IR}} + \sum_{m=1}^{M}\sum_{j=1}^{J}\sqrt{P_{m,j}^{\text{U}}}e_{m,j,k}s_{m,j}^{\text{ER}} \\ + \sum_{l=1,l\neq m}^{M}\mathbf{h}_{l,k}\sqrt{(1-\beta_l)P_l}\sum_{i=1}^{K}\mathbf{v}_{l,i}s_{l,i}^{\text{IR}} + n_{m,k}^{\text{IR}}, \end{aligned} \tag{6.11}$$

The third term in (6.11) represents the interference on $\text{IR}_{m,k}$ from the downlink signals to the IRs in other clusters. For any $\text{IR}_{m,k}$, since the interferences from the ERs and IRs in other clusters are small compared to the interferences from ERs and other IRs in its cluster, their effects can be neglected. Hence, the signal-to-interference-plus-noise ratio (SINR) at $\text{IR}_{m,k}$ is

$$\gamma_{m,k} = \frac{Q_{m,k}^{\text{D}}|\mathbf{h}_{m,k}\mathbf{v}_{m,k}^{\star}|^2}{(Q_m^{\text{D}} - Q_{m,k}^{\text{D}})\sum\limits_{\substack{i=1\\ i\neq k}}^{K}|\mathbf{h}_{m,k}\mathbf{v}_{m,i}^{\star}|^2 + \sum\limits_{j=1}^{J}P_{m,j}^{\text{U}}|e_{m,j,k}|^2 + 1}, \tag{6.12}$$

where $Q_{m,k}^{\text{D}}$ is the transmit power used for the data transfer from UAV_m to $\text{IR}_{m,k}$.

6.4 Energy Efficiency Maximization

6.4.1 Energy Efficiency Formulation

To formulate the EE of the system under consideration, we have to construct the throughputs of the downlink and uplink stages for all clusters. For the downlink information NOMA setup, where the channel gains of IRs are increasing when closer to the UAV (channel gain of $\mathrm{IR}_{m,1}$ is larger than $\mathrm{IR}_{m,2}$, and so on until $\mathrm{IR}_{m,K}$), the rate related to a given IR can be expressed in the unit of *bps* as [83]:

$$R^{\mathrm{D}}_{m,k}=(1-\alpha_m)W\log_2\left(1+\frac{\frac{Q^{\mathrm{D}}_{m,k}\|\mathbf{h}'_{m,k}\|^2}{L^{\mathrm{D}}_{\mathrm{IR}_{m,k}}(1-\alpha_m)}}{\left((1-\beta_m)P_m-Q^{\mathrm{D}}_{m,k}\right)\sum\limits_{i=1,i\neq k}^{K}\frac{\|\mathbf{h}'_{m,k}\|^2}{L^{\mathrm{D}}_{\mathrm{IR}_{m,i}}(1-\alpha_m)}+\sum\limits_{j=1}^{J}\frac{\zeta P^{\mathrm{D}}_{m,j}\|\mathbf{g}'_{m,j}\|^2\|\mathbf{z}'_{m,j}\|^2|e'_{m,j,k}|^2\alpha_m}{L^{\mathrm{U}}_{\mathrm{ER}_{m,j}}L^{\mathrm{D}}_{\mathrm{ER}_{m,j}}L_{\mathrm{NLoS}_{j,k}}(1-\alpha_m)}+1}\right). \tag{6.13}$$

where W is the bandwidth, assumed the same for all GNs. According to the principles of power-domain NOMA, for a given IR, the strong interfering signals are mainly due to the transmissions to devices with low channel gains. The weakest-channel device, $\mathrm{IR}_{m,K}$, which receives low interferences due to the relatively low powers of devices' messages with high channel gains, cannot cancel any interference. However, the highest channel gain device, $\mathrm{IR}_{m,1}$, which receives strong interference due to the relatively high powers of the transmissions to weak devices, can cancel all interfering signals [85]. On the other hand, for the uplink NOMA throughput, knowing that the channel gains are stronger when ERs are closer to the UAV (channel gain of $\mathrm{ER}_{m,1}$ is larger than $\mathrm{ER}_{m,2}$, and so on until $\mathrm{ER}_{m,J}$), then based on (6.8) and (6.9), the rate

related to a given ER in a given cluster can be expressed as [83]:

$$R^{\mathrm{U}}_{m,j}=(1-\alpha_m)W\log_2\left(1+\frac{\frac{\zeta P^{\mathrm{D}}_{m,j}\|\mathbf{g}'_{m,j}\|^2\|\mathbf{z}'_{m,j}\|^2\alpha_m}{L^{\mathrm{U}}_{\mathrm{ER}_{j,m}}L^{\mathrm{D}}_{\mathrm{ER}_{m,j}}{}^{(1-\alpha_m)}}}{\left(\beta_m P_m-P^{\mathrm{D}}_{m,j}\right)\sum\limits_{l=j+1}^{J}\frac{\zeta\|\mathbf{g}'_{m,l}\|^2\|\mathbf{z}'_{m,l}\|^2\alpha_m}{L^{\mathrm{U}}_{\mathrm{ER}_{m,l}}L^{\mathrm{D}}_{\mathrm{ER}_{m,l}}{}^{(1-\alpha_m)}}+(1-\beta_m)P_m\sum\limits_{k=1}^{K}\|H_{\mathrm{SI}_m}v_{m,k}\|^2+1}\right). \tag{6.14}$$

The signal of the highest channel gain device, $\mathrm{ER}_{m,1}$, is decoded first at the UAV. As a result, $\mathrm{ER}_{m,1}$ experiences interference from all other ERs. Then, the signal for the second-highest channel gain device is decoded, and so on until the last device, $\mathrm{ER}_{m,J}$, [85]. For a specific UAV_m, let us define the uplink throughput as the sum-rate of all ERs in the cluster, i.e., $R^{\mathrm{U}}_m=\sum_{j=1}^{J}R^{\mathrm{U}}_{m,j}$, and the downlink throughput as the sum-rate of all IRs, i.e., $R^{\mathrm{D}}_m=\sum_{k=1}^{K}R^{\mathrm{D}}_{m,k}$. The EE of the system is expressed as

$$\eta=\frac{\sum\limits_{m=1}^{M}\left(\text{Total Throughput}\right)_m}{\sum\limits_{m=1}^{M}\left(\text{Total Consumed Energy}\right)_m}=\frac{\sum\limits_{m=1}^{M}R^{\mathrm{U}}_m+R^{\mathrm{D}}_m}{\sum\limits_{m=1}^{M}P_{\mathrm{DC}_m}+P^{\mathrm{D}}_m+Q^{\mathrm{D}}_m(1-\alpha_m)}, \tag{6.15}$$

where P_{DC_m} is the constant power consumption of UAV_m, and where $P^{\mathrm{D}}_m=\beta_m P_m=\sum_{j=1}^{J}P^{\mathrm{D}}_{m,j}$ and $Q^{\mathrm{D}}_m=(1-\beta_m)P_m=\sum_{k=1}^{K}Q^{\mathrm{D}}_{m,k}$ are the powers dedicated to the ERs and the IRs, respectively, i.e., $P_m=P^{\mathrm{D}}_m+Q^{\mathrm{D}}_m$.

6.4.2 Problem Formulation

The optimization problem which aims to maximize EE is formulated as follows:

$$\begin{aligned}(\mathrm{OP})\quad &\max_{P^{\mathrm{D}}_{m,j},Q^{\mathrm{D}}_{m,k},d_{m,j},\theta_{m,j}}\quad \eta\\ \text{s.t.:}\quad & P_m\le P_{m,\max},\quad \forall m,\\ & P^{\mathrm{U}}_{m,j}\le P^{\mathrm{U}}_{m,j,\max},\quad \forall j,\forall m,\end{aligned}$$

$$
\begin{aligned}
&\alpha_m < 1, \quad \forall m, \\
&0 \leq \beta_m \leq 1, \quad \forall m, \\
&h_{m,\min} \leq d_{m,j} \cos\theta_{m,j}, \quad \forall j, \forall m, \\
&h_{m,\min} \leq d_{m,k} \cos\theta_{m,k}, \quad \forall k, \forall m, \\
&d_{m,\max} \leq r_m - r_{\mathrm{UAV}_m}, \quad \forall m, \\
&\sum_{m=1}^{M} \chi_{m,j} = 1, \quad \forall j \\
&\chi_{m,j} \in \{0,1\}, \quad \forall j, \forall m \\
&\sum_{m=1}^{M} \chi_{m,k} = 1, \quad \forall k \\
&\chi_{m,k} \in \{0,1\}, \quad \forall k, \forall m \\
&R^{\mathrm{U}}_{m,j} \geq R^{\mathrm{U}}_{m,j,\min}, \quad \forall j, \forall m, \\
&R^{\mathrm{D}}_{m,k} \geq R^{\mathrm{D}}_{m,k,\min}, \quad \forall k, \forall m, \\
&P^{\mathrm{U}}_{m,\mathrm{thr}} \leq P^{\mathrm{U}}_{m,j} z_{m,j} - \sum_{l=j+1}^{J} P^{\mathrm{U}}_{l,j} z_{l,j}, \quad \forall j, \forall m, \\
&Q^{\mathrm{D}}_{m,\mathrm{thr}} \leq \left(Q^{\mathrm{D}}_{m,k} - \sum_{i=1, i\neq k}^{K} Q^{\mathrm{D}}_{m,i} \right) h_{m,K}, \quad \forall k, \forall m,
\end{aligned}
\tag{6.16}
$$

where $P^{D}_{m,\max}$ and $P^{\mathrm{U}}_{m,j,\max}$ are the maximum transmit powers of UAV_m and $\mathrm{ER}_{m,j}$, respectively, $h_{\mathrm{UAV}_m,\min}$ is the minimum allowed height for UAV_m, $d_{\mathrm{UAV}_m,\max}$ is the maximum allowable distance that UAV_m can travel during T, r_m is the cluster radius, r_{UAV_m} is the UAV radius, $R^{\mathrm{U}}_{m,j,\min}$ and $R^{\mathrm{D}}_{m,k,\min}$ denote the minimum required rates of $\mathrm{ER}_{m,j}$ and $\mathrm{IR}_{m,k}$, respectively. Finally, $P^{\mathrm{U}}_{m,\mathrm{thr}}$ and $Q^{\mathrm{D}}_{m,\mathrm{thr}}$ are the SIC detection thresholds of the uplink and downlink, $z_{m,j}$ ($\|\mathbf{z}'_{m,l}\|^2 / L^{\mathrm{U}}_{\mathrm{ER}_{m,j}}$) is the channel gain between $\mathrm{ER}_{m,k}$ and UAV_m, and $h_{m,K}$ ($\|\mathbf{h}'_{m,K}\|^2 / L^{\mathrm{D}}_{\mathrm{IR}_{m,K}}$) is the channel gain between UAV_m and $\mathrm{IR}_{m,K}$.

The optimization problem is a non-convex problem with highly coupled variables; therefore, it is hard to be solved directly by existing convex optimization methods. Accordingly, we decompose the optimization problem into two sub-problems. In the first one (OP_1), we aim to find the UAVs' optimum positions, i.e., the optimal distances and elevation angles w.r.t. the ERs and IRs according to their demands and their associations to the UAVs. After getting the UAVs' optimum positions, in the second problem (OP_2), we determine the optimal powers towards each user in each cluster.

6.4.3 UAV Positioning and User Association

In OP_1, we care about $(\theta_{m,j}, d_{m,j})$ and $(\theta_{m,k}, d_{m,k})$ which are contained in (6.5), for all scheduled ERs and IRs that are associated with any specific UAV in each cluster at the same time. This can be achieved by connecting the path losses for A2G channels related to each GN by the parameters pertaining to the nodes' demands. So, OP_1 will be as follows:

$$
\begin{aligned}
(\mathrm{OP}_1) \quad & \min_{d_{m,j}, d_{m,k}, \theta_{m,j}, \theta_{m,k}} \quad \sum_{j} \Upsilon_j^{\mathrm{U}} \; L^{\mathrm{D}}_{\mathrm{ER}_{m,j}} + \sum_{k} \Upsilon_k^{\mathrm{D}} \; L^{\mathrm{D}}_{\mathrm{IR}_{m,k}} \\
\text{s.t.:} \quad & h_{m,\min} \leq d_{m,j} \cos\theta_{m,j}, \quad \forall j, \forall m, \\
& h_{m,\min} \leq d_{m,k} \cos\theta_{m,k}, \quad \forall k, \forall m, \\
& d_{m,\max} \leq r_m - r_{\mathrm{UAV}_m}, \quad \forall m, \\
& \sum_{m=1}^{M} \chi_{m,j} = 1, \quad \forall j \\
& \chi_{m,j} \in \{0,1\} \quad \forall j, \forall m \\
& \sum_{m=1}^{M} \chi_{m,k} = 1, \quad \forall k \\
& \chi_{m,k} \in \{0,1\} \quad \forall k, \forall m.
\end{aligned}
\tag{6.17}
$$

Given that each UAV, at the beginning of the process, will be hovering at the minimum allowable height over the center of its cluster, each device (ER or IR) that needs to be served will send its ID to the UAV in its cluster. Accordingly, $\chi_{m,j}$ of each ER and $\chi_{m,k}$ of each IR that ask to be served in each cluster can be determined. This optimization problem can be solved by introducing the Lagrangian multipliers $\boldsymbol{\Omega_{IR_m}} \geq 0$ and $\boldsymbol{\Omega_{ER_m}} \geq 0$, where $\boldsymbol{\Omega_{IR_m}} = [\Omega_{\mathrm{IR}_{m,1}}, \Omega_{\mathrm{IR}_{m,2}}, ..., \Omega_{\mathrm{IR}_{m,K}}]$ and $\boldsymbol{\Omega_{ER_m}} = [\Omega_{\mathrm{ER}_{m,1}}, \Omega_{\mathrm{ER}_{m,2}}, ..., \Omega_{\mathrm{ER}_{m,J}}]$. The objective function then becomes

$$\begin{aligned}
&\mathcal{L}_1(\boldsymbol{\Omega_{ER_m}}, \boldsymbol{\Omega_{IR_m}}, \boldsymbol{d_{m,j}}, \boldsymbol{d_{m,k}}, \boldsymbol{\theta_{m,j}}, \boldsymbol{\theta_{m,k}}) \\
&= \sum_{j=1}^{J} \Upsilon_j^{\mathrm{U}} \; L_{\mathrm{ER_{m,j}}}^{\mathrm{D}} + \sum_{k=1}^{K} \Upsilon_k^{\mathrm{D}} \; L_{\mathrm{IR}_{m,k}}^{\mathrm{D}} \\
&- \sum_{j=1}^{J} \Omega_{\mathrm{ER}_{m,j}} (h_{m,\min} - d_{m,j} \cos\theta_{m,j}) \\
&- \sum_{k=1}^{K} \Omega_{\mathrm{IR}_{m,k}} (h_{m,\min} - d_{m,k} \cos\theta_{m,k}).
\end{aligned} \tag{6.18}$$

Exploiting the Karush–Kuhn–Tucker (KKT) conditions, one can obtain the optimal position of the UAV by solving the first derivatives of $\mathcal{L}_1$ w.r.t. $d_{m,j}$, $d_{m,k}$, $\theta_{m,j}$ and $\theta_{m,k}$, respectively, as follows:

$$\begin{aligned}
\frac{\partial \mathcal{L}_1}{\partial d_{m,j}} &= \Upsilon_j^{\mathrm{U}} \; \frac{\partial L_{\mathrm{ER}_{m,j}}^{\mathrm{D}}}{\partial d_{m,j}} - \Omega_{\mathrm{ER}_{m,j}} \cos\theta_{m,j} \\
&= \frac{20\,\Upsilon_j^{\mathrm{U}}}{d_{m,j} \ln(10)} - \Omega_{\mathrm{ER}_{m,j}} \cos\theta_{m,j} = 0,
\end{aligned} \tag{6.19}$$

$$\begin{aligned}
\frac{\partial \mathcal{L}_1}{\partial d_{m,k}} &= \Upsilon_k^{\mathrm{D}} \; \frac{\partial L_{\mathrm{IR}_{m,k}}^{\mathrm{D}}}{\partial d_{m,k}} - \Omega_{\mathrm{IR}_{m,k}} \cos\theta_{m,k} \\
&= \frac{20\,\Upsilon_k^{\mathrm{D}}}{d_{m,k} \ln(10)} - \Omega_{\mathrm{IR}_{m,k}} \cos\theta_{m,k} = 0,
\end{aligned} \tag{6.20}$$

$$\frac{\partial \mathcal{L}_1}{\partial \theta_{m,j}} = \Upsilon_j^{\mathrm{U}} \; \frac{\partial L_{\mathrm{ER}_{m,j}}^{\mathrm{D}}}{\partial d_{m,j}} + \Omega_{\mathrm{ER}_{m,j}} d_{m,j} \cos\theta_{m,j}$$

$$= \frac{\Upsilon_j^{\mathrm{U}} ab \frac{180}{\pi} (\xi_{\mathrm{LoS}} - \xi_{\mathrm{NLoS}}) \exp\left(-b\left(\frac{180}{\pi}\theta_{m,j} - a\right)\right)}{\left(1 + a\exp\left(-b\left(\frac{180}{\pi}\theta_{m,j} - a\right)\right)\right)^2} + \Omega_{\mathrm{ER}_{m,j}} d_{m,j} \cos\theta_{m,j} = 0, \tag{6.21}$$

$$\frac{\partial \mathcal{L}_1}{\partial \theta_{m,k}} = \Upsilon_k^{\mathrm{D}} \frac{\partial L_{\mathrm{IR}_{m,k}}^{\mathrm{D}}}{\partial d_{m,k}} + \Omega_{\mathrm{IR}_{m,k}} d_{m,k} \cos\theta_{m,k}$$
$$= \frac{\Upsilon_k^{\mathrm{D}} ab \frac{180}{\pi} (\xi_{\mathrm{LoS}} - \xi_{\mathrm{NLoS}}) \exp\left(-b\left(\frac{180}{\pi}\theta_{m,k} - a\right)\right)}{\left(1 + a\exp\left(-b\left(\frac{180}{\pi}\theta_{m,k} - a\right)\right)\right)^2} + \Omega_{\mathrm{IR}_{m,k}} d_{m,k} \cos\theta_{m,k} = 0. \tag{6.22}$$

The new values of $\Omega_{\mathrm{ER}_{m,j}}$ and $\Omega_{\mathrm{IR}_{m,k}}$ can be calculated using the gradient-descent method [76]:

$$\Omega_{\mathrm{ER}_{m,j}}(i+1) = [\Omega_{\mathrm{ER}_{m,j}}(i) - \Delta_{\Omega_{\mathrm{ER}_{m,j}}}(h_{m,\min} - d_{m,j}\cos\theta_{m,j})]^+,$$

$$\Omega_{\mathrm{IR}_{m,k}}(i+1) = [\Omega_{\mathrm{IR}_{m,k}}(i) - \Delta_{\Omega_{\mathrm{IR}_{m,k}}}(h_{m,\min} - d_{m,k}\cos\theta_{m,j})]^+,$$

where $\Omega_{\mathrm{ER}_{m,j}}(i)$ and $\Omega_{\mathrm{IR}_{m,k}}(i)$ are respectively the values of $\Omega_{\mathrm{IR}_{m,k}}$ and $\Omega_{\mathrm{ER}_{m,j}}$ at the i^{th} iteration, $\triangle_{\Omega_{\mathrm{ER}_{m,j}}}$ and $\triangle_{\Omega_{\mathrm{IR}_{m,k}}}$ are the iteration steps, and $[x]^+ = \max(0, x)$. The output of the optimization will be the optimum positions of the UAVs. Algorithm 6.1 summarizes the procedure. The results will be used in the second optimization problem.

Algorithm 6.1. 3D UAV Location Optimization

Input: Υ_j^{U},Υ_k^{D}, ξ_{LoS}, ξ_{NLoS} a, b, $h_{m,\min}$, f, r_m, $r_{\mathrm{UAV_m}}$, and GNs' ID, $\forall j$, $\forall k$, $\forall m$.
Output: $(x_m, y_m, h_m)^*$, $\forall m$.
Initialization: $(x_m, y_m, h_m)^0$, $\Omega_{\mathrm{ER}_{m,j}} = 0$, $\Omega_{\mathrm{IR}_{m,k}} = 0$, $\forall j$, $\forall k$, $\forall m$.
1: Determine $\chi_{m,j}$, as per (6.1) and (6.3), $\forall j$, $\forall m$.
2: Determine $\chi_{m,k}$, as per (6.2) and (6.4), $\forall k$, $\forall m$.
3: Update $\Omega_{\mathrm{ER}_{m,j}}$ and $\Omega_{\mathrm{IR}_{m,k}}$ according to (6.23) and (6.23).
4: Solve (6.19) for $d_{m,j}$, $\forall j$, $\forall m$.
5: Solve (6.20) for $d_{m,k}$, $\forall k$, $\forall m$.
6: Solve (6.21) for $\theta_{m,j}$, $\forall j$, $\forall m$.
7: Solve (6.22) for $\theta_{m,k}$, $\forall k$, $\forall m$.
8: Compute the optimal $(x_m, y_m, h_m)^*$, $\forall m$, by solving (6.17).

6.4.4 Energy-Efficient Resource Allocation

Based on the constraints that have been treated in OP_1, and the results of Algorithm 6.1, we formulate OP_2 as follows:

$$
\begin{aligned}
(\mathrm{OP}_2) \quad & \max_{P_{m,j}^{\mathrm{D}}, Q_{m,k}^{\mathrm{D}}} \quad \eta \\
\text{s.t.:} \quad & P_m \le P_{m,\max}, \quad \forall m, \\
& P_{m,j}^{\mathrm{U}} \le P_{m,j,\max}^{\mathrm{U}}, \quad \forall j, \forall m, \\
& \alpha_m < 1, \quad \forall m, \\
& 0 \le \beta_m \le 1, \quad \forall m, \\
& R_{m,j}^{\mathrm{U}} \ge R_{m,j,\min}^{\mathrm{U}}, \quad \forall j, \forall m, \\
& R_{m,k}^{\mathrm{D}} \ge R_{m,k,\min}^{\mathrm{D}}, \quad \forall k, \forall m, \\
& P_{m,\mathrm{thr}}^{\mathrm{U}} \le P_{m,j}^{\mathrm{U}} z_{m,j} - \sum_{l=j+1}^{J} P_{m,l}^{\mathrm{U}} z_{m,l}, \quad \forall j, \forall m, \\
& Q_{m,\mathrm{thr}}^{\mathrm{D}} \le \left(Q_{m,k}^{\mathrm{D}} - \sum_{i=1, i\neq k}^{K} Q_{m,i}^{\mathrm{D}} \right) h_{m,K}, \ \forall k, \forall m.
\end{aligned}
\tag{6.23}
$$

It is obvious that OP_2 is a fractional optimization problem with the variables $P^{\mathrm{D}}_{m,j}$ and $Q^{\mathrm{D}}_{m,k}$, and is non-convex. Exploiting the idea in [78], the fractional programming problem can be transformed into a convex problem by introducing the variable F^* as the optimal EE when we have the optimal power for each ER and IR. Accordingly, the objective function becomes $\sum_{m=1}^{M} R^{\mathrm{U}}_m + R^{\mathrm{D}}_m - F^* \sum_{m=1}^{M} (P_{\mathrm{DC}_m} + P^{\mathrm{D}}_m + Q^{\mathrm{D}}_m(1-\alpha_m))$. By introducing $\boldsymbol{\vartheta} \geq 0$, $\boldsymbol{\varsigma_m} \geq 0$, $\boldsymbol{\varepsilon} \geq 0$, $\boldsymbol{\varrho} \geq 0$, $\boldsymbol{\varphi_m} \geq 0$, $\boldsymbol{\lambda_m} \geq 0$, $\boldsymbol{\mu_m} \geq 0$, and $\boldsymbol{\rho_m} \geq 0$, as the Lagrange multipliers associated with the constraints in OP_2, where $\boldsymbol{\vartheta} = [\vartheta_1, \vartheta_2, ..., \vartheta_M]$, $\boldsymbol{\varsigma_m} = [\varsigma_{m,1}, \varsigma_{m,2}, ..., \varsigma_{m,J}]$, $\boldsymbol{\varepsilon} = [\varepsilon_1, \varepsilon_2, ..., \varepsilon_M]$, $\boldsymbol{\varrho} = [\varrho_1, \varrho_2, ..., \varrho_M]$, $\boldsymbol{\varphi_m} = [\varphi_{m,1}, \varphi_{m,2}, ..., \varphi_{m,J}]$, $\boldsymbol{\lambda_m} = [\lambda_{m,1}, \lambda_{m,2}, ..., \lambda_{m,K}]$, $\boldsymbol{\mu_m} = [\mu_{m,1}, \mu_{m,1}, ..., \mu_{m,J}]$, and $\boldsymbol{\rho_m} = [\rho_{m,1}, \rho_{m,1}, ..., \rho_{m,K}]$, then the Lagrangian function of OP_2 can be formulated as:

$$
\begin{aligned}
&\mathcal{L}_2(\boldsymbol{\vartheta}, \boldsymbol{\varsigma_m}, \boldsymbol{\varepsilon}, \boldsymbol{\varrho}, \boldsymbol{\varphi_m}, \boldsymbol{\lambda_m}, \boldsymbol{\mu_m}, \boldsymbol{\rho_m}, Q^{\mathrm{D}}_{m,k}, P^{\mathrm{D}}_{m,j}) \\
&= \sum_{m=1}^{M} R^{\mathrm{U}}_m + R^{\mathrm{D}}_m - F^* \sum_{m=1}^{M} (P_{\mathrm{DC}_m} + P^{\mathrm{D}}_m + Q^{\mathrm{D}}_m(1-\alpha_m)) \\
&- \sum_{m=1}^{M} \vartheta_m (P_m - P_{m,\max}) - \sum_{m=1}^{M} \sum_{j=1}^{J} \varsigma_{m,j} (P^{\mathrm{U}}_{m,j} - P^{\mathrm{U}}_{m,j,\max}) \\
&- \sum_{m=1}^{M} \varepsilon_m (\alpha_m - 1) - \sum_{m=1}^{M} \sum_{j=1}^{J} \varphi_{m,j} (R^{\mathrm{U}}_{m,j,\min} - R^{\mathrm{U}}_{m,j}) \\
&- \sum_{m=1}^{M} \varrho_m (\beta_m - 1) - \sum_{m=1}^{M} \sum_{k=1}^{K} \lambda_{m,k} (R^{\mathrm{D}}_{m,k,\min} - R^{\mathrm{D}}_{m,k}) \\
&- \sum_{m=1}^{M} \sum_{j=1}^{J} \mu_{m,j} \left[P^{\mathrm{U}}_{m,\mathrm{thr}} - P^{\mathrm{U}}_{m,j} z_{m,j} - \sum_{l=j+1}^{J} P^{\mathrm{U}}_{m,l} z_{m,l} \right] \\
&- \sum_{m=1}^{M} \sum_{k=1}^{K} \rho_{m,k} \left[Q^{\mathrm{D}}_{m,\mathrm{thr}} - \left(Q^{\mathrm{D}}_{m,k} - \sum_{i=1, i\neq k}^{K} Q^{\mathrm{D}}_{m,i} \right) h_{m,K} \right].
\end{aligned} \tag{6.24}
$$

Our goal is to find the optimized $Q^{\mathrm{D}}_{m,k}$, $P^{\mathrm{D}}_{m,j}$. We assume that UAV_m uses its maximum power, such that $\beta_m P_{m,\max} = P^{\mathrm{D}}_m$ and $(1-\beta_m) P_{m,\max} = Q^{\mathrm{D}}_m$. Taking into account that OP_2 is a nonlinear programming problem, this can be done through

derivation of the Lagrangian function (6.24) w.r.t. $Q^{\mathrm{D}}_{m,k}$ and $P^{\mathrm{D}}_{m,j}$, and then setting them to zero, i.e.,

$$\frac{\partial \mathcal{L}_2(\boldsymbol{\vartheta}, \boldsymbol{\varsigma_m}, \boldsymbol{\varepsilon}, \boldsymbol{\varrho}, \boldsymbol{\varphi_m}, \boldsymbol{\lambda_m}, \boldsymbol{\mu_m}, \boldsymbol{\rho_m}, Q^{\mathrm{D}}_{m,k}, P^{\mathrm{D}}_{m,j})}{\partial Q^{\mathrm{D}}_{m,k}} = 0, \tag{6.25}$$

$$\frac{\partial \mathcal{L}_2(\boldsymbol{\vartheta}, \boldsymbol{\varsigma_m}, \boldsymbol{\varepsilon}, \boldsymbol{\varrho}, \boldsymbol{\varphi_m}, \boldsymbol{\lambda_m}, \boldsymbol{\mu_m}, \boldsymbol{\rho_m}, Q^{\mathrm{D}}_{m,k}, P^{\mathrm{D}}_{m,j})}{\partial P^{\mathrm{D}}_{m,j}} = 0. \tag{6.26}$$

The updating of the Lagrangian variables ($\boldsymbol{\vartheta}$, $\boldsymbol{\varsigma_m}$, $\boldsymbol{\varepsilon}$, $\boldsymbol{\varrho}$, $\boldsymbol{\varphi_m}$, $\boldsymbol{\lambda_m}$, $\boldsymbol{\mu_m}$, and $\boldsymbol{\rho_m}$) can be done using the gradient-descent method:

$$\vartheta_m(i+1) = [\vartheta_m(i) - \triangle_{\vartheta_m}(P_{m,\max} - P_m)]^+, \tag{6.27}$$

$$\varsigma_{m,j}(i+1) = [\varsigma_{m,j}(i) - \triangle_{\varsigma_{m,j}}(P^{\mathrm{U}}_{m,j,\max} - P^{\mathrm{U}}_{m,j})]^+, \tag{6.28}$$

$$\varepsilon_m(i+1) = [\varepsilon_m(i) - \triangle_{\varepsilon_m}(1 - \alpha_m)]^+, \tag{6.29}$$

$$\varrho_m(i+1) = [\varrho_m(i) - \triangle_{\varrho_m}(1 - \beta_m)]^+, \tag{6.30}$$

$$\varphi_{m,j}(i+1) = [\varphi_{m,j}(i) - \triangle_{\varphi_{m,j}}(R^{\mathrm{U}}_{m,j,\min} - R^{\mathrm{U}}_{m,j})]^+, \tag{6.31}$$

$$\lambda_{m,k}(i+1) = [\lambda_{m,k}(i) - \triangle_{\lambda_{m,k}}(R^{\mathrm{D}}_{m,k,\min} - R^{\mathrm{D}}_{m,k})]^+, \tag{6.32}$$

$$\mu_{m,j}(i+1) = [\mu_{m,j}(i) - \triangle_{\mu_{m,j}}(P^{\mathrm{U}}_{m,\mathrm{thr}} - P^{\mathrm{U}}_{m,j} z_{m,j} - \sum_{l=j+1}^{J} P^{\mathrm{U}}_{m,l} z_{m,l})]^+, \tag{6.33}$$

$$\phi_{m,k}(i+1) = [\phi_{m,k}(i) - \triangle_{\phi_{m,k}}(Q^{\mathrm{D}}_{m,\mathrm{thr}} - (Q^{\mathrm{D}}_{m,k} - \sum_{i=1, i\neq k}^{K} Q^{\mathrm{D}}_{m,i}) h_{m,K})]^+, \tag{6.34}$$

where i is the iteration index, and the $\triangle$'s are the iteration steps.

The solution of OP_2 is summarized in Algorithm 6.2.

Algorithm 6.2. Energy-Efficient Resource Allocation

Input: $(x_m,y_m,h_m)^*$, ξ_{LoS}, ξ_{NLoS}, a, b, $h_{m,\min}$, GNs' ID, f, η, σ, $R^{\text{D}}_{\min}$ and $R^{\text{U}}_{\min}$, $\forall j$, $\forall k$, $\forall m$.

Output: $(Q^{\text{D}}_{m,k}, P^{\text{D}}_{m,j})^*$.

Initialization: $(Q^{\text{D}}_{m,k}, P^{\text{D}}_{m,j})^0$, $\boldsymbol{\vartheta} = \mathbf{0}$, $\boldsymbol{\varsigma}_m = \mathbf{0}$, $\boldsymbol{\varepsilon} = \mathbf{0}$, $\boldsymbol{\varrho} = \mathbf{0}$ $\boldsymbol{\varphi}_m = \mathbf{0}$, $\boldsymbol{\lambda}_m = \mathbf{0}$, $\boldsymbol{\mu}_m = \mathbf{0}$, $\boldsymbol{\rho}_m = \mathbf{0}$.

1: Update the Lagrangian variables, $\boldsymbol{\vartheta}$, $\boldsymbol{\varepsilon}$, $\boldsymbol{\varrho}$, $\boldsymbol{\lambda_m}$, and $\boldsymbol{\rho_m}$ based on (6.27), (6.29), (6.30), (6.32), and (6.34), respectively.
2: Solve (6.25) for $Q^{\text{D}}_{m,k}$.
3: Update the Lagrangian variables, $\boldsymbol{\vartheta}$, $\boldsymbol{\varsigma_m}$, $\boldsymbol{\varepsilon}$, $\boldsymbol{\varrho}$, $\boldsymbol{\varphi_m}$, and $\boldsymbol{\mu_m}$ based on (6.27), (6.28), (6.29), (6.30), (6.31), and (6.33), respectively.
4: Solve (6.26) for $P^{\text{D}}_{m,j}$.
5: Compute $(Q^{\text{D}}_{m,k}, P^{\text{D}}_{m,j})^*$, $\forall m$, $\forall k$, $\forall j$, by solving (6.23).

6.4.5 Complexity Analysis

In the previous sections, we explained that the optimization problem under consideration is a highly coupled non-convex problem, thus it is extremely difficult to be solved. However, with the suggested sub-optimal solution, we decomposed the problem into two sub-problems and were able to solve them efficiently by proposing two algorithms. Both algorithms are based on the gradient-descent method, where the worst complexity of such method is $\mathcal{O}(n \times \frac{1}{\epsilon})$ [79], with n being the number of optimization variables and ϵ the solution accuracy. Thus, for Algorithm 6.1, the complexity depends on the 3D plane size that the UAVs consider for moving, i.e., i.e., $x \times y \times (h_{m,\max} - h_{m,\min})$, where $(h_{m,\max} - h_{m,\min})$ is the allowable altitude range for moving. For Algorithm 6.2, the complexity depends on the numbers of UAVs (M), ERs (J), and IRs (K). As such, the total complexity for both algorithms is $\mathcal{O}(x \times y \times (h_{m,\max} - h_{m,\min}) \times \frac{1}{\epsilon}) + \mathcal{O}(M \times (J + K) \times \frac{1}{\epsilon})$.

6.5 Simulation Results

In this section, we perform several simulations to evaluate the proposed algorithms' effectiveness for multiple-UAV scenario. We adopt the UAV parameters to meet the specifications of existing small UAVs that can handle this kind of UAV-based processes [94]. Also, we assume the propagation parameters to correspond to an urban environment [72]. Accordingly, in the simulations, we set $a = 9.6$, $b = 0.28$, $\xi_{\text{LoS}} = 1$ dB, $\xi_{\text{NLoS}} = 20$ dB, $f = 2$ GHz, $W = 200$ kHz, $\eta = 0.8$, and $N_E = N_I = 2$. We set $Q_{\text{thr}}^{\text{D}} = P_{\text{thr}}^{\text{U}} = 0.05$ Watt, $P_{\text{DC}} = 5$ Watt, $P_{\max} = 3$ Watt, and $R_{\min}^{\text{U}} = R_{\min}^{\text{D}}$= 12 Kbps, unless stated otherwise. In this multiple-UAV scenario, we consider that there are 4 UAVs (M=4) to cover the ROI of 100x100 m^2, which also means that we have four identical clusters with a radius of 25 m, the centers of clusters 1, 2, 3 and 4 are (25,25), (75,25), (75,75) and (25,75), respectively. For the GNs' distribution, we consider that the circles are uniformly formulated by increasing 1 m for the radius from the center of each cluster, with the segments formed by increasing the angle of a segment by $\pi/2$ from the positive horizontal plane in each cluster, i.e., $\phi = 1, \cdots, 25$, $\psi = 1, \cdots, 4$, in each cluster. For the simulations, we consider that 16 GNs ask to be served at the same time, 4 in each cluster. In cluster 1, $\text{GN}_{1,5}$ and $\text{GN}_{1,15}$ are ERs, and $\text{GN}_{3,5}$ and $\text{GN}_{3,15}$ are IRs. In cluster 2, $\text{GN}_{2,5}$ and $\text{GN}_{2,10}$ are ERs, and $\text{GN}_{2,15}$ and $\text{GN}_{2,20}$ are IRs. In cluster 3, $\text{GN}_{1,25}$ and $\text{GN}_{2,25}$ are ERs, and $\text{GN}_{3,25}$ and $\text{GN}_{4,25}$ are IRs. In cluster 4, $\text{GN}_{1,5}$ and $\text{GN}_{1,15}$ are ERs, and $\text{GN}_{2,5}$ and $\text{GN}_{2,15}$ are IRs. In this multiple-UAV scenario, we consider four different cases according to different combinations of the GNs' demands:

- Case-1 "No consideration for the GNs' service demands": Each UAV will hover at the minimum allowable height over the center of its cluster.

- Case-2 “Same service demands for all GNs in the cluster" (e.g., in any cluster, $\Upsilon_1^{\mathrm{U}} = \Upsilon_2^{\mathrm{U}} = \Upsilon_1^{\mathrm{D}} = \Upsilon_2^{\mathrm{D}} = 0.25$): At the beginning of the process, each UAV hovers at the minimum allowable height over the center of its cluster, and then moves to the optimal position according to the same GNs' service demands.

- Case-3 “Different service demands for each GN in the cluster, $\Upsilon^{\mathrm{U}} > \Upsilon^{\mathrm{D}}$": The service demands for ERs are higher than those of IRs (e.g., in any cluster, $\Upsilon_1^{\mathrm{U}} + \Upsilon_2^{\mathrm{U}} = 0.75$, and $\Upsilon_1^{\mathrm{D}} + \Upsilon_2^{\mathrm{D}} = 0.25$): Each UAV hovers at the minimum allowable height over the center of its cluster, at the beginning of the process, then moves to the optimal position according to these different GNs' service demands.

- Case-4 “Different service demands for each GN in the cluster, $\Upsilon^{\mathrm{D}} > \Upsilon^{\mathrm{U}}$": The service demands of IRs are higher than the ones of ERs (e.g., in any cluster, $\Upsilon_1^{\mathrm{U}} + \Upsilon_2^{\mathrm{U}} = 0.25$, and $\Upsilon_1^{\mathrm{D}} + \Upsilon_2^{\mathrm{D}} = 0.75$): Each UAV initially hovers at the minimum allowable height over the center of its cluster, and then moves to the optimal position according to the GNs' service demands.

6.5.1 3D Positions of the UAVs

As the GNs' service demands will not be taken into account in Case-1, the four UAVs will be hovering at the minimum allowable height over the centers of their clusters. These positions will be fixed during the whole process. The positions are (25,25,10) for UAV_1, (75,25,10) for UAV_2, (75,75,10) for UAV_3, and (25,75,10) for UAV_4, as shown in Figure 6.3. For the remaining cases 2, 3, and 4, the UAVs will move from the initial positions to the optimal points according to Algorithm 6.1. In Case-2, this will be depending on the same service demands of all GNs in each cluster; hence, the optimal positions of UAV_1, UAV_2, UAV_3 and UAV_4 will be (25,25,10), (75,37.5,10), (75,75,10) and (35,85,10), respectively, as shown in Figure 6.4.

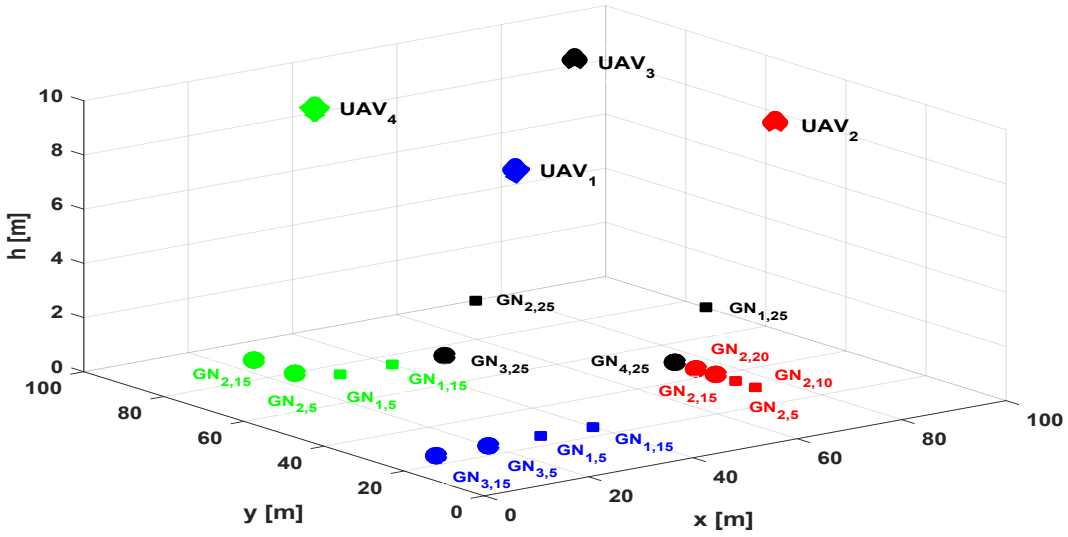

Figure 6.3: The locations of the UAVs for Case-1 (MUAV-SWIPT).

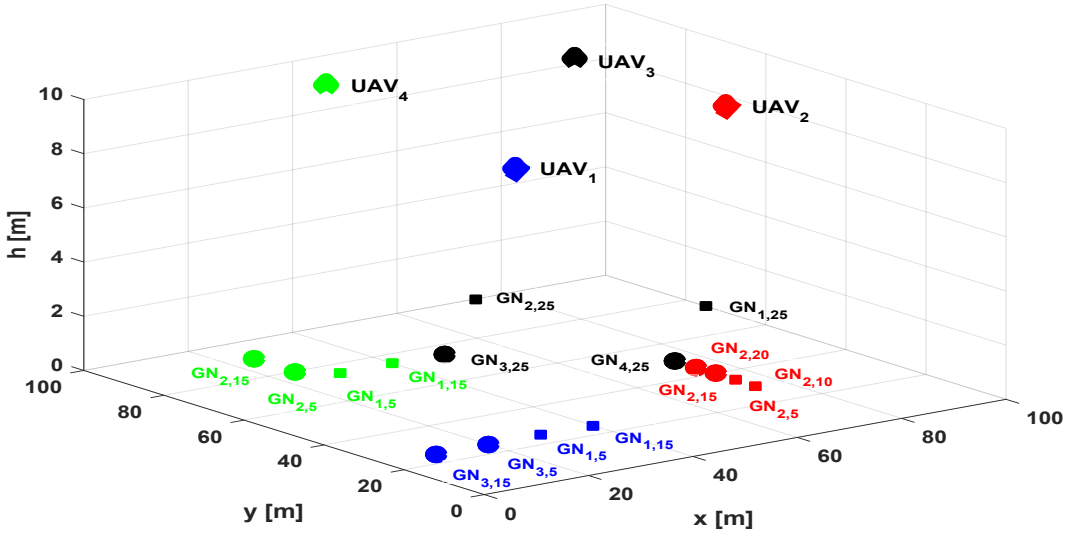

Figure 6.4: The optimal locations of the UAVs for Case-2 (MUAV-SWIPT).

We note that each UAV will relocate its position to be somewhere between all scheduled GNs in its cluster, as the demands are the same for all of them. In Case-3, where the demands of ERs are higher than the ones of IRs, we notice that each UAV will take the optimal position to be near the ERs to be able to meet their demands. Thus, the optimal positions of UAV_1, UAV_2, UAV_3, and UAV_4 will be (35,25,10), (75,32.5,10), (87.5,87.5,10) and (35,75,10), respectively, as shown in Figure 6.5.

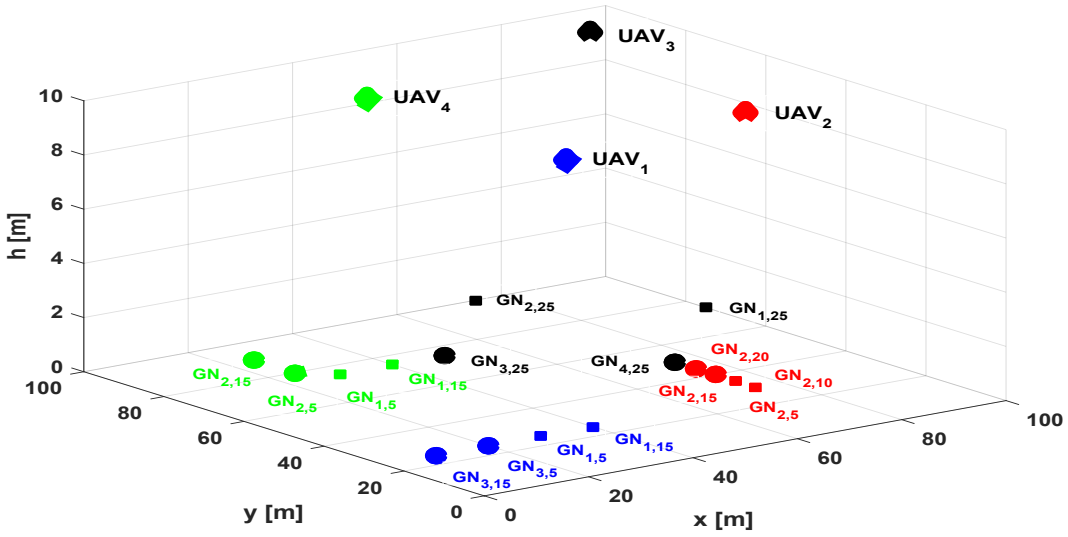

Figure 6.5: The optimal locations of the UAVs for Case-3 (MUAV-SWIPT).

When the service demands of IRs are greater as compared to the ones of the ERs as defined in Case-4, the UAV in each cluster moves towards the IRs to satisfy their demands. Figure 6.6 shows the optimal positions of the UAVs in the ROI. The positions are (15,25,10) for UAV_1, (75,42.5,10) for UAV_2, (62.5,62.5,10) for UAV_3, and (25.85.10) for UAV_4.

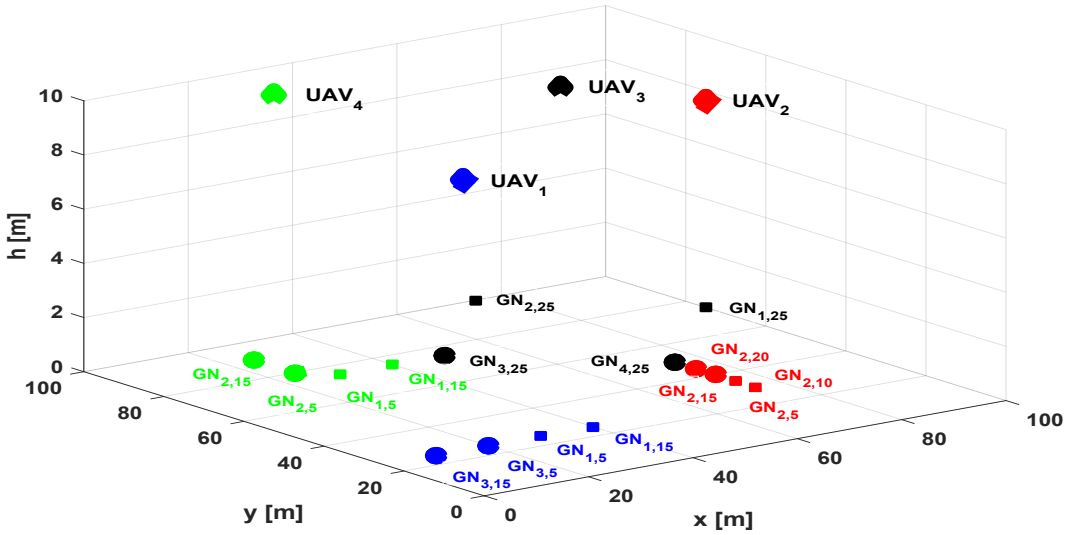

Figure 6.6: The optimal locations of the UAVs for Case-4 (MUAV-SWIPT).

Figure 6.7 shows the 2D optimal positions of the UAVs for the four cases. This explains the changes of the positions of the UAVs from one case to another. Note that the height is fixed for all UAVs in all cases.

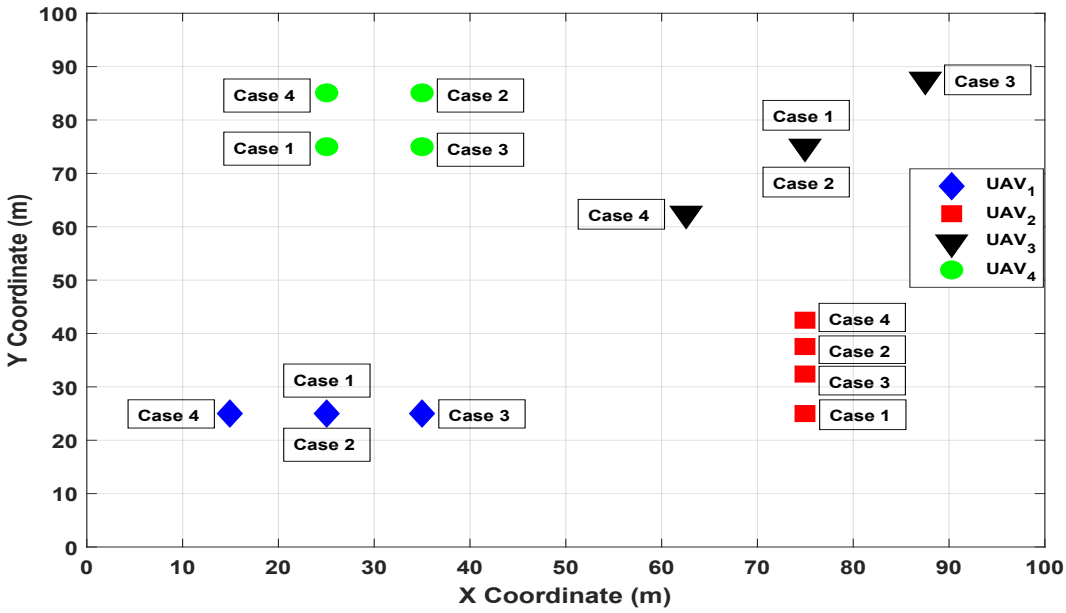

Figure 6.7: The 2D optimal locations of the UAVs for all cases of MUAV-SWIPT network.

6.5.2 Energy Efficiency Optimization

We compare the performance resulting from applying the algorithms to the four cases for NOMA and OMA schemes as shown in Figure 6.8, which illustrates the EE w.r.t. the normalized charging time (α) which is set the same for all UAVs. One can notice that in all cases, NOMA outperforms OMA. However, the differences vary from case to case. It is clear that the EE for Case-2, which considers equal service demands for all GNs, is the best compared to the other cases for NOMA and OMA schemes. Compared to Case-1, which does not consider the GNs' service demands at all, we notice that the UAVs' positioning in Case-2 enhances the system EE, as all UAVs provide better links for all GNs in their clusters. However, the EE in Case-1 outperforms those in cases

3 and 4, where the GNs' demands are also considered, and this also shows the effect of the distribution of the scheduled nodes on the overall performance. For Case-3, where the demands of ERs are more significant than the ones of IRs, the UAVs move closer to the ERs, providing them with much stronger links compared to the IRs. This degrades the total downlink throughput for IRs, which is reflected in the system EE. For Case-4, where the demands of IRs are more extensive than the ones of ERs, the UAVs travel towards the IRs to meet their needs. This severely degrades the total uplink throughputs of ERs, as they depend on the links for receiving the power on the downlink and then use it on the uplink, so the both links are affected and this is

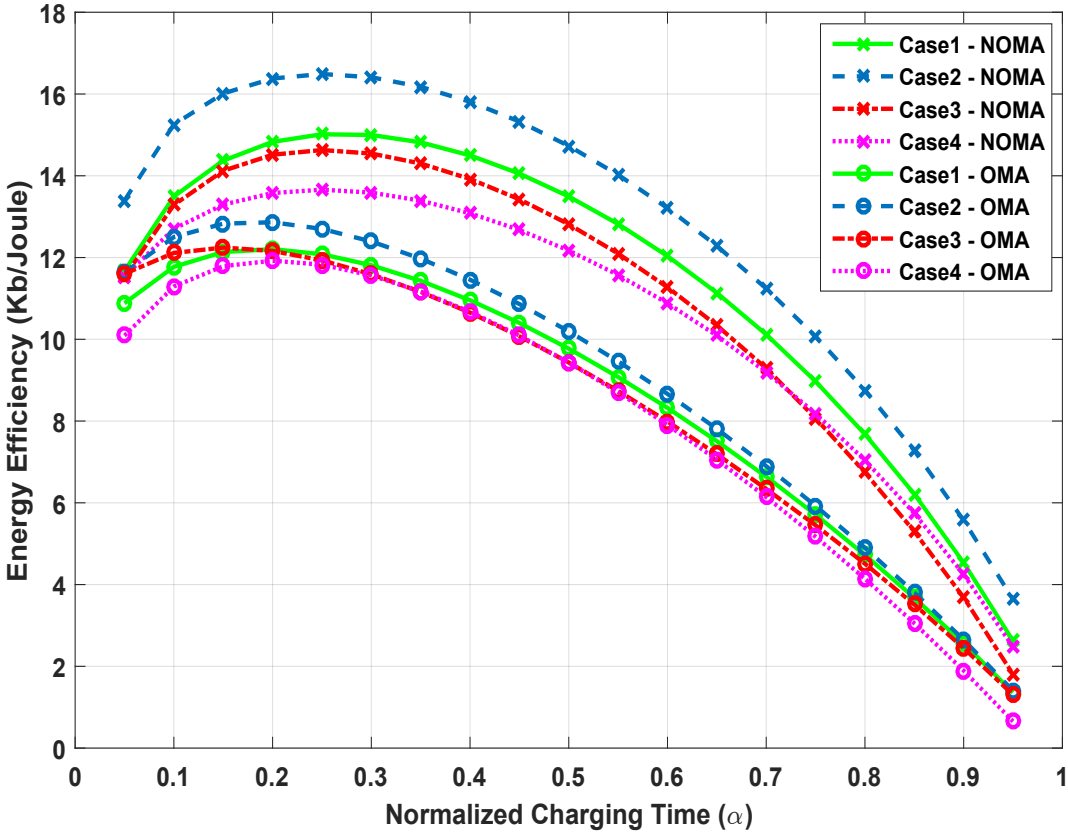

Figure 6.8: System energy efficiency versus normalized charging time for MUAV-SWIPT network

6.6 Summary

This chapter investigated resource allocation in a network deploying multiple multi-antenna UAVs for transmitting data to IRs and wireless energy to ERs to enable their uplink data communication through the NOMA protocol. A general highly coupled non-convex optimization problem was formulated to maximize the network's EE while satisfying many constraints related to the user association, UAV positions, power budgets, collision avoidance, acceptable QoS, and SIC thresholds. The problem was solved after decomposing it into two sub-problems by minimizing the path losses of the A2G channels according to the devices' demands and optimizing the transmit powers towards maximizing the EE. The results showed the superiority of NOMA over OMA, where the case with equal rate requirement has the best performance. This scenario, i.e., MUAV-SWIPT, is the most general scenario that handles the information and power transmissions for a general number of UAVs, ERs, and IRs and takes into account the positioning of the UAVs for different cases according to the devices' demands.

Chapter 7

Conclusions and Future Work

7.1 Conclusions

Unmanned aerial vehicles (UAVs) are becoming more reachable and available to be used in numerous applications. UAVs are considered an appealing and efficient solution for many challenges with their cost-effectiveness, flexibility, 3D mobility, and freestyle solutions. One of UAVs' crucial applications is in the area of wireless communications, where reliable and cost-effective services can be provided through a network of single or multiple UAVs. For example, UAVs can be deployed to enable power and information transfer in Internet of Things (IoT) networks for both energy receivers (ER) or/and information receivers (IR), where the ground nodes (GNs) are energy-constrained, their lifetimes are limited by the battery capacity, and may not communicate over long ranges. Although the application and effectiveness of the UAV wireless powered communication networks (UAV-WPCN) are promising, this comes with many challenges related to the limited power budget, the UAV placement, the quality of service (QoS), and many other complexities. Intuitively, many other challenges are added in terms of using multiple UAVs, which is becoming essential in many

cases to enhance the network's coverage. For instance, the UAVs' placement and user association have become more complicated.

Towards addressing these challenges, in this thesis, we proposed a novel methodology to optimize the performance of the UAV-WPCN with its different topologies and applications. We provided the required steps to be followed for most applicable networks, where specific considerations have to be accounted for in each case. The optimization problem's solution has two main steps; firstly, the path loss of the air-to-ground channels is minimized by optimizing the UAV position depending on the GNs' service demands. Secondly, using the optimized positioning and a closed-form expression for the energy efficiency (EE), a resource allocation aiming to maximize EE is developed using Lagrangian optimization and gradient-descent methods.

We applied the proposed methodology for five suggested system models, which reflect different practical cases and setups. In the first contribution of this thesis, we proposed a UAV-WPCN system model, where a multiple-antenna UAV charges GNs through wireless power transfer (WPT) to assist their uplink data communication with a terrestrial base station (BS) through an orthogonal multiple access (OMA) scheme. In the second contribution, we presented a system model, namely UAV-WIPT, where a fixed position single UAV deploys information and power transfer towards co-located IRs and ERs to enable downlink and uplink data transmission through a non-orthogonal multiple access (NOMA) scheme. We extended this in our third contribution to handle the UAV-based simultaneous information and power transfer (UAV-SWIPT) systems for an arbitrary number of ERs and IRs. We also proposed two hybrid access schemes depending on the NOMA and OMA schemes: hybrid downlink OMA uplink NOMA (HDOUN) and hybrid downlink NOMA uplink OMA (HDNUO) and derived closed-form formulas for the optimal transmit power

towards each ER and IR. Finally, we considered multiple UAV scenarios in the context of WPCN and SWIPT systems. In MUAV-WPCN systems, we considered the partial user location information (ULI) approach, where multiple UAVs deploy WPT towards several ERs to enable their uplink data transmissions through the NOMA scheme. For the MUAV-SWIPT networks, we address the optimization of the EE of a wireless network, where M multiple-antenna UAVs serve as simultaneous power and information transmitters towards J ERs and K IRs, which also considered the partial ULI approach. We also proposed collision avoidance constraints to avoid UAVs' collisions as they move to enhance the links for the ERs and IRs.

In summary, with the five different setups, the proposed methodology provides a comprehensive understanding for the management of the available resources for the UAV-WPCN systems. It is clear that the consideration of the system's EE as the key point is essential and logical as UAV's power significantly impacts the system performance. Hence, the power budget of the UAV has to be able to handle the minimum rate requirements of all users. Moreover, the distance of the users from the UAV has multiple consequences. Generally, an increase in distances increases the path loss and the charging time, and decreases the EE. It is worth mentioning that although NOMA shows its superiority in many cases, however, the topology and distribution of the ground nodes, ERs and IRs, plays a vital role in figuring out the suitable access scheme to be used.

7.2 Future Work

The advancements in the UAV-based communication networks enable various applications and provide free-style solutions for many practical scenarios. For instance, in the context of IoT devices, UAVs can provide energy supply for those low-power

and hard-to-reach devices by sending RF signals to charge them simultaneously. In this thesis, we proposed a general methodology to optimize the performance for several topologies of the UAV-enabled WPT networks based on the EE maximization framework. Based on this proposed methodology and experimental results, some enhancements can be explored. We briefly discuss these suggestions to motivate future research directions.

- In our system specifications, we assumed the availability of the channel state information (CSI), which has been widely followed in the literature. Therefore, we did not go through the details of obtaining the CSI in the networks. However, for a more practical system model, the details of obtaining the CSI and its consequences on the overall system performance could be considered. This will further enrich the proposed framework and make it more realistic.

- The proposed methodology in this thesis mainly considers the decomposition of the main optimization problem in most cases. This is a very efficient and standard procedure when dealing with the non-convex optimization problem. However, this leads to a sub-optimal solution with some limitations when dealing with online optimization, such as the placement and trajectory design, where the channel propagation environments vary due to the presence of obstacles between UAVs and GNs. Machine learning techniques could be a good candidate in this regard, which will lead to an online solution that will enhance the links between the UAVs and their related GNs.

- We considered a linear energy harvesting model at the ERs for converting the received RF signal into usable energy, which is commonly adopted in the literature. However, in practice, this may not be precisely the case where a non-linear

behavior is expected. As this non-linear model is not well studied in the literature in the context of UAV-enabled WPT networks, a comprehensive study in this regard is very important. It is expected that this non-linear modeling will make the handling of the position optimization of the UAVs more challenging. For instance, hovering closely above the ERs could not be the best solution due to the energy saturation at high RF power with a non-linear model.

- In the context of multiple UAV networks, there are two main approaches to be followed, cluster-based or network-based. In the cluster-based, which we considered in this thesis, multiple clusters for each group of the GNs can be formulated. Usually, a single UAV is dedicated for serving this set of GNs. On the other hand, for the network-based scheme, the UAVs will serve the GNs in the network without any clustering consideration, and multiple UAVs may serve a single GN or multiple GNs simultaneously. The cluster-based approach is more manageable and practical. However, considering the network-based approach for UAV-WPT networks is a valuable research to be done.

- With the availability of the dominant line of sight (LoS) air-to-ground links in UAV-based communication networks, new security threats at the physical layer are expected. UAV-based networks are hence more susceptible to the jamming/eavesdropping attacks by malicious ground nodes than terrestrial communications over fading channels. The security of UAV-enabled WPT networks is outside the scope of this thesis; however, efficient security techniques for such networks are essential to be investigated.

- For more realistic and practical understanding of the optimization for the UAV-WPT networks, it is worth to conduct field experiments and apply the proposed

methodology and algorithms therein. This will give an engineering aspect to the work and will take into consideration more constraints that could have been ignored in the simulations. This is also important in order to ensure the validity, scalability, and practicality of the general proposed scenarios.

Bibliography

[1] A. Merwaday and I. Guvenc. UAV assisted heterogeneous networks for public safety communications. In *IEEE Wireless Communications and Networking Conference Workshops*, pages 329–334, 2015.

[2] C. F. Liew, D. DeLatte, N. Takeishi, and T. Yairi. Recent developments in aerial robotics: A survey and prototypes overview. *CoRR*, abs/1711.10085, 2017.

[3] M. Mozaffari, W. Saad, M. Bennis, Y. Nam, and M. Debbah. A tutorial on UAVs for wireless networks: Applications, challenges, and open problems. *IEEE Communications Surveys Tutorials*, 21(3):2334–2360, 2019.

[4] A. Al-Hourani, S. Kandeepan, and A. Jamalipour. Modeling air-to-ground path loss for low altitude platforms in urban environments. In *IEEE Global Communications Conference*, pages 2898–2904, 2014.

[5] M. Mozaffari, W. Saad, M. Bennis, and M. Debbah. Efficient deployment of multiple unmanned aerial vehicles for optimal wireless coverage. *IEEE Communications Letters*, 20(8):1647–1650, 2016.

[6] C. A. Wargo, G. C. Church, J. Glaneueski, and M. Strout. Unmanned aircraft systems (UAS) research and future analysis. In *IEEE Aerospace Conference*, pages 1–16, 2014.

[7] Y. Zeng, R. Zhang, and T. J. Lim. Wireless communications with unmanned aerial vehicles: opportunities and challenges. *IEEE Communications Magazine*, 54(5):36–42, 2016.

[8] J. G. Andrews, S. Buzzi, W. Choi, S. V. Hanly, A. Lozano, A. C. K. Soong, and J. C. Zhang. What will 5G be? *IEEE Journal on Selected Areas in Communications*, 32(6):1065–1082, 2014.

[9] I. Bor-Yaliniz and H. Yanikomeroglu. The new frontier in ran heterogeneity: Multi-tier drone-cells. *IEEE Communications Magazine*, 54(11):48–55, 2016.

[10] S. Rohde and C. Wietfeld. Interference aware positioning of aerial relays for cell overload and outage compensation. In *IEEE Vehicular Technology Conference*, pages 1–5, 2012.

[11] V. Sharma, M. Bennis, and R. Kumar. UAV-assisted heterogeneous networks for capacity enhancement. *IEEE Communications Letters*, 20(6):1207–1210, 2016.

[12] S. Rahman, G. Kim, Y. Cho, and A. Khan. Positioning of UAVs for throughput maximization in software-defined disaster area UAV communication networks. *Journal of Communications and Networks*, 20(5):452–463, 2018.

[13] Z. Xue, J. Wang, G. Ding, and Q. Wu. Joint 3D location and power optimization for UAV-enabled relaying systems. *IEEE Access*, 6:43113–43124, 2018.

[14] X. Zhou, R. Zhang, and C. K. Ho. Wireless information and power transfer: Architecture design and rate-energy tradeoff. In *IEEE Global Communications Conference*, pages 3982–3987, 2012.

[15] S. Bi, C. K. Ho, and R. Zhang. Wireless powered communication: opportunities and challenges. *IEEE Communications Magazine*, 53(4):117–125, 2015.

[16] E. Vinogradov, H. Sallouha, S. Bast, M. Azari, and S. Pollin. Tutorial on UAVs: A blue sky view on wireless communication. *Journal of Mobile Multimedia*, 14(4):395–468, 2018.

[17] Y. Zeng, J. Lyu, and R. Zhang. Cellular-connected UAV: Potential, challenges, and promising technologies. *IEEE Wireless Communications*, 26(1):120–127, 2019.

[18] Y. Li, Z. Yuan, and C. Peng. A control-plane perspective on reducing data access latency in LTE networks. In *ACM Annual International Conference on Mobile Computing and Networking*, pages 56–69, 2017.

[19] M. Mozaffari, W. Saad, M. Bennis, and M. Debbah. Unmanned aerial vehicle with underlaid device-to-device communications: Performance and tradeoffs. *IEEE Transactions on Wireless Communications*, 15(6):3949–3963, 2016.

[20] X. Li, W. Feng, J. Wang, Y. Chen, N. Ge, and C. Wang. Enabling 5G on the ocean: A hybrid satellite-UAV-terrestrial network solution. *IEEE Wireless Communications*, 27(6):116–121, 2020.

[21] J. Mcclintock, D. Buchmueller, V. Gopalakrishnan, F. Hensel, J. Johansson, B. Porter, and A. Roths. Systems, devices and methods delivering energy using an uncrewed autonomous vehicle, US Patent, US9778653B1, USA, 2017.

[22] M. Bacco, A.Berton, E. Ferro, C. Gennaro, A. Gotta, S. Matteoli, F. Paonessa, M. Ruggeri, G. Virone, and A. Zanella. Smart farming: Opportunities, challenges and technology enablers. In *IEEE IoT Vertical and Topical Summit on Agriculture - Tuscany*, pages 1–6, 2018.

[23] Y. Zeng, B. Clerckx, and R. Zhang. Communications and signals design for wireless power transmission. *IEEE Transactions on Communications*, 65(5):2264–2290, 2017.

[24] F. Wu, D. Yang, L. Xiao, and L. Cuthbert. Energy consumption and completion time tradeoff in rotary-wing UAV enabled WPCN. *IEEE Access*, 7:79617–79635, 2019.

[25] J. Xu, Y. Zeng, and R. Zhang. UAV-enabled wireless power transfer: Trajectory design and energy region characterization. In *IEEE Global Communications Conference Workshops*, pages 1–7, 2017.

[26] X. Sun, W. Yang, and Y. Cai. Secure communication in NOMA-assisted millimeter-wave SWIPT UAV networks. *IEEE Internet of Things Journal*, 7(3):1884–1897, 2020.

[27] G. Im and J. Lee. Outage probability for cooperative NOMA systems with imperfect SIC in cognitive radio networks. *IEEE Communications Letters*, 23(4):692–695, 2019.

[28] Z. Ding, R. Schober, and H. Poor. A general MIMO framework for NOMA downlink and uplink transmission based on signal alignment. *IEEE Transactions on Wireless Communications*, 15(6):4438–4454, 2016.

[29] M. Mozaffari, W. Saad, M. Bennis, and M. Debbah. Mobile unmanned aerial vehicles (UAVs) for energy-efficient internet of things communications. *IEEE Transactions on Wireless Communications*, 16(11):7574–7589, 2017.

[30] L. Sboui, H. Ghazzai, Z. Rezki, and M. S. Alouini. Energy-efficient power allocation for UAV cognitive radio systems. In *IEEE Vehicular Technology Conference*, pages 1–5, 2017.

[31] S. Cui, A.J. Goldsmith, and A. Bahai. Energy-efficiency of MIMO and cooperative MIMO techniques in sensor networks. *IEEE Journal on Selected Areas in Communications*, 22(6):1089–1098, 2004.

[32] C. You and R. Zhang. 3D trajectory optimization in rician fading for UAV-enabled data harvesting. *IEEE Transactions on Wireless Communications*, 18(6):3192–3207, 2019.

[33] M. Azari, F. Rosas, K. Chen, and S. Pollin. Ultra reliable UAV communication using altitude and cooperation diversity. *IEEE Transactions on Communications*, 66(1):330–344, 2018.

[34] F. Ono, H. Ochiai, and R. Miura. A wireless relay network based on unmanned aircraft system with rate optimization. *IEEE Transactions on Wireless Communications*, 15(11):7699–7708, 2016.

[35] J. Lyu, Y. Zeng, and R. Zhang. Cyclical multiple access in UAV-aided communications: A throughput-delay tradeoff. *IEEE Wireless Communications Letters*, 5(6):600–603, 2016.

[36] Q. Wu, J. Xu, and R. Zhang. Capacity characterization of UAV-enabled two-user broadcast channel. *IEEE Journal on Selected Areas in Communications*, 36(9):1955–1971, 2018.

[37] M. Azari, Y. Murillo, O. Amin, F. Rosas, M. Alouini, and S. Pollin. Coverage maximization for a poisson field of drone cells. In *IEEE International Symposium on Personal, Indoor, and Mobile Radio Communications*, pages 1–6, 2017.

[38] B. Galkin, J. Kibilda, and L. DaSilva. Coverage analysis for low-altitude UAV networks in urban environments. In *IEEE Global Communications Conference*, pages 1–6, 2017.

[39] M. Alzenad, A. El-Keyi, F. Lagum, and H. Yanikomeroglu. 3-D placement of an unmanned aerial vehicle base station (UAV-BS) for energy-efficient maximal coverage. *IEEE Wireless Communications Letters*, 6(4):434–437, 2017.

[40] L. Liu, S. Zhang, and R. Zhang. Comp in the sky: UAV placement and movement optimization for multi-user communications. *IEEE Transactions on Communications*, 67(8):5645–5658, 2019.

[41] Y. Zeng, R. Zhang, and T. J. Lim. Throughput maximization for UAV-enabled mobile relaying systems. *IEEE Transactions on Communications*, 64(12):4983–4996, 2016.

[42] X. Zhou, J. Guo, S. Durrani, and H. Yanikomeroglu. Uplink coverage performance of an underlay drone cell for temporary events. In *IEEE International Conference on Communications Workshops*, pages 1–6, 2018.

[43] F. Lagum, I. Bor-Yaliniz, and H. Yanikomeroglu. Strategic densification with UAV-BSs in cellular networks. *IEEE Wireless Communications Letters*, 7(3):384–387, 2018.

[44] H. He, S. Zhang, Y. Zeng, and R. Zhang. Joint altitude and beamwidth optimization for UAV-enabled multiuser communications. *IEEE Communications Letters*, 22(2):344–347, 2018.

[45] J. Chen and D. Gesbert. Optimal positioning of flying relays for wireless networks: A los map approach. In *IEEE International Conference on Communications*, pages 1–6, 2017.

[46] M. Mozaffari, W. Saad, M. Bennis, and M. Debbah. Drone small cells in the clouds: Design, deployment and performance analysis. In *IEEE Global Communications Conference*, pages 1–6, 2015.

[47] Jiaxun Li, Haitao Zhao, Haijun Wang, Fanglin Gu, Jibo Wei, Hao Yin, and Baoquan Ren. Joint optimization on trajectory, altitude, velocity, and link scheduling for minimum mission time in UAV-aided data collection. *IEEE Internet of Things Journal*, 7(2):1464–1475, 2020.

[48] J. Xu, Y. Zeng, and R. Zhang. UAV-enabled wireless power transfer: Trajectory design and energy optimization. *IEEE Transactions on Wireless Communications*, 17(8):5092–5106, 2018.

[49] H. Wang, J. Wang, G. Ding, L. Wang, T. A. Tsiftsis, and P. K. Sharma. Resource allocation for energy harvesting-powered D2D communication underlaying UAV-assisted networks. *IEEE Transactions on Green Communications and Networking*, 2(1):14–24, 2018.

[50] L. Xie, J. Xu, and R. Zhang. Throughput maximization for UAV-enabled wireless powered communication networks. *IEEE Internet of Things Journal*, 6(2):1690–1703, 2019.

[51] Y. Wang, W. Yang, X. Shang, and Y. Cai. Energy-efficient secure transmission for UAV-enabled wireless powered communication. In *IEEE International Conference on Wireless Communications and Signal Processing*, pages 1–5, 2018.

[52] Y. Du, K. Yang, K. Wang, G. Zhang, Y. Zhao, and D. Chen. Joint resources and workflow scheduling in UAV-enabled wirelessly-powered mec for IoT systems. *IEEE Transactions on Vehicular Technology*, 68(10):10187–10200, 2019.

[53] P. K. Sharma and D. I. Kim. UAV-enabled downlink wireless system with non-orthogonal multiple access. In *IEEE Global Communications Conference Workshops*, pages 1–6, 2017.

[54] S. Jeong, O. Simeone, and J. Kang. Mobile edge computing via a UAV-mounted cloudlet: Optimization of bit allocation and path planning. *IEEE Transactions on Vehicular Technology*, 67(3):2049–2063, 2018.

[55] M. F. Sohail, C. Y. Leow, and S. Won. Non-orthogonal multiple access for unmanned aerial vehicle assisted communication. *IEEE Access*, 6:22716–22727, 2018.

[56] W. Mei and R. Zhang. Uplink cooperative NOMA for cellular-connected UAV. *IEEE Journal of Selected Topics in Signal Processing*, 13(3):644–656, 2019.

[57] M. F. Sohail and C. Y. Leow. Maximized fairness for NOMA based drone communication system. In *IEEE Malaysia International Conference on Communications*, pages 119–123, 2017.

[58] J. Baek, S. I. Han, and Y. Han. Optimal resource allocation for non-orthogonal transmission in UAV relay systems. *IEEE Wireless Communications Letters*, 7(3):356–359, 2018.

[59] A. Nasir, H. Tuan, T. Duong, and H. Poor. UAV-enabled communication using NOMA. *CoRR*, abs/1806.03604, 2018.

[60] T. Hou, Y. Liu, Z. Song, X. Sun, and Y. Chen. Multiple antenna aided NOMA in UAV networks: A stochastic geometry approach. *IEEE Transactions on Communications*, 67(2):1031–1044, 2019.

[61] X. Hong, P. Liu, F. Zhou, S. Guo, and Z. Chu. Resource allocation for secure UAV-assisted SWIPT systems. *IEEE Access*, 7:24248–24257, 2019.

[62] F. Huang, J. Chen, H. Wang, G. Ding, Z. Xue, Y. Yang, and F. Song. UAV-assisted SWIPT in internet of things with power splitting: Trajectory design and power allocation. *IEEE Access*, 7:68260–68270, 2019.

[63] S. Yin, Y. Zhao, and L. Li. UAV-assisted cooperative communications with time-sharing SWIPT. In *IEEE International Conference on Communication*, pages 1–6, 2018.

[64] V. V. Chetlur and H. S. Dhillon. Downlink coverage analysis for a finite 3-D wireless network of unmanned aerial vehicles. *IEEE Transactions on Communications*, 65(10):4543–4558, 2017.

[65] S. Enayati, H. Saeedi, H. Pishro-Nik, and H. Yanikomeroglu. Moving aerial base station networks: A stochastic geometry analysis and design perspective. *IEEE Transactions on Wireless Communications*, 18(6):2977–2988, 2019.

[66] F. Huang, J. Chen, H. Wang, G. Ding, Y. Gong, and Y. Yang. Multiple-UAV-assisted SWIPT in internet of things: User association and power allocation. *IEEE Access*, 7:124244–124255, 2019.

[67] Q. Wu, Y. Zeng, and R. Zhang. Joint trajectory and communication design for multi-UAV enabled wireless networks. *IEEE Transactions on Wireless Communications*, 17(3):2109–2121, 2018.

[68] R. Narasimhan. Finite-SNR diversity—multiplexing tradeoff for correlated rayleigh and rician MIMO channels. *IEEE Transactions on Information Theory*, 52(9):3965–3979, 2006.

[69] A. Paulraj, R. Nabar, and D. Gore. *Introduction to space-time wireless communications*. Cambridge University Press, 2003.

[70] Y. Zeng, J. Xu, and R. Zhang. Energy minimization for wireless communication with rotary-wing UAV. *IEEE Transactions on Wireless Communications*, 18(4):2329–2345, 2019.

[71] E. Lutz, D. Cygan, M. Dippold, F. Dolainsky, and W. Papke. The land mobile satellite communication channel-recording, statistics, and channel model. *IEEE Transactions on Vehicular Technology*, 40(2):375–386, 1991.

[72] A. Al-Hourani, S. Kandeepan, and S. Lardner. Optimal LAP altitude for maximum coverage. *IEEE Wireless Communications Letters*, 3(6):569–572, 2014.

[73] M. Xia and S. Aissa. On the efficiency of far-field wireless power transfer. *IEEE Transactions on Signal Processing*, 63(11):2835–2847, 2015.

[74] X. Chen, Z. Zhang, S. Chen, and C. Wang. Adaptive mode selection for multiuser MIMO downlink employing rateless codes with qos provisioning. *IEEE Transactions on Wireless Communications*, 11(2):790–799, 2012.

[75] B. M. Hochwald, T. L. Marzetta, and V. Tarokh. Multiple-antenna channel hardening and its implications for rate feedback and scheduling. *IEEE Transactions on Information Theory*, 50(9):1893–1909, 2004.

[76] S. Boyd and L. Vandenberghe. *Convex Optimization*. Cambridge University Press, USA, 2004.

[77] X. Chen, X. Wang, and X. Chen. Energy-efficient optimization for wireless information and power transfer in large-scale MIMO systems employing energy beamforming. *IEEE Wireless Communications Letters*, 2(6):667–670, 2013.

[78] D. W. K. Ng, E. S. Lo, and R. Schober. Energy-efficient resource allocation for secure OFDMA systems. *IEEE Transactions on Vehicular Technology*, 61(6):2572–2585, 2012.

[79] Y. Nesterov. *Lectures on Convex Optimization*. Springer, 2018.

[80] S. Najmeddin, A. Bayat, S. Aïssa, and S. Tahar. Energy-efficient resource allocation for UAV-enabled wireless powered communications. In *IEEE Wireless Communications and Networking Conference*, pages 1–6, 2019.

[81] Z. Zhang, K. Long, A. V. Vasilakos, and L. Hanzo. Full-duplex wireless communications: Challenges, solutions, and future research directions. *Proceedings of the IEEE*, 104(7):1369–1409, 2016.

[82] T. Riihonen, S. Werner, and R. Wichman. Mitigation of loopback self-interference in full-duplex MIMO relays. *IEEE Transactions on Signal Processing*, 59(12):5983–5993, 2011.

[83] T. A. Zewde and M. C. Gursoy. NOMA-based energy-efficient wireless powered communications. *IEEE Transactions on Green Communications and Networking*, 2(3):679–692, 2018.

[84] Y. Sun, D. Ng, Z. Ding, and R. Schober. Optimal joint power and subcarrier allocation for full-duplex multicarrier non-orthogonal multiple access systems. *IEEE Transactions on Communications*, 65(3):1077–1091, 2017.

[85] M. S. Ali, H. Tabassum, and E. Hossain. Dynamic user clustering and power allocation for uplink and downlink non-orthogonal multiple access (NOMA) systems. *IEEE Access*, 4:6325–6343, 2016.

[86] J. Lyu and R. Zhang. Network-connected UAV: 3-D system modeling and coverage performance analysis. *IEEE Internet of Things Journal*, 6(4):7048–7060, 2019.

[87] W. Dinkelbach. On nonlinear fractional programming. *Management Science*, 13(7):492–498, 1967.

[88] Y. Zeng, Q. Wu, and R. Zhang. Accessing from the sky: A tutorial on UAV communications for 5G and beyond. *Proceedings of the IEEE*, 107(12):2327–2375, 2019.

[89] D. Romero and G. Leus. Non-cooperative aerial base station placement via stochastic optimization. In *IEEE International Conference on Mobile Ad-Hoc and Sensor Networks*, pages 131–136, 2019.

[90] S. Najmeddin, S. Aïssa, and S. Tahar. Energy-efficient resource allocation for UAV-enabled information and power transfer with NOMA. In *IEEE Global Communications Conference*, pages 1–6, 2020.

[91] M. Mohammadi, B. K. Chalise, H. A. Suraweera, and Z. Ding. Wireless information and power transfer in full-duplex systems with massive antenna arrays. In *IEEE International Conference on Communications*, pages 1–6, 2017.

[92] H. Ngo, H. Suraweera, M. Matthaiou, and E. Larsson. Multipair full-duplex relaying with massive arrays and linear processing. *IEEE Journal on Selected Areas in Communications*, 32(9):1721–1737, 2014.

[93] Y. He, H. Zhao, W. Guo, S. Shao, and Y. Tang. A time-robust digital self-interference cancellation in full-duplex radios: Receiver design and performance analysis. *IEEE Access*, 8:185021–185031, 2020.

[94] C. Yan, L. Fu, J. Zhang, and J. Wang. A comprehensive survey on UAV communication channel modeling. *IEEE Access*, 7:107769–107792, 2019.

Biography

Education

- **Concordia University**: Montreal, Quebec, Canada

  Ph.D., Electrical and Computer Engineering, (Jan. 2017 - Aug. 2021)

- **King Fahd University of Petroleum and Minerals**, Dhahran, Saudi Arabia

  M.Sc, Electrical and Computer Engineering, (Sep. 2012 - May. 2015)

- **Palestine Polytechnic University**: Al-Khalil, Palestine

  B.Sc, Computer Engineering (Jan. 2007 - Jun. 2011)

Awards

- Mitacs Research Training Award, Canada (2020).
- GCS Conference Travel Award, Canada (2019).
- Concordia University Conference and Exposition Award, Canada (2019).
- Concordia University Tuition Award of Excellence, Canada (2017-2019).
- KFUPM full PhD Scholarship, Saudi Arabia (2016, Declined)
- KFUPM full Master's Scholarship, Saudi Arabia (2012-2015)

Work History

- **Research Assistant**, Dept. of Electrical and Computer Engineering, Concordia University, Montreal, Quebec, Canada (2017-2021)
- **Teaching Assistant**, Dept. of Electrical and Computer Engineering, Concordia University, Montreal, Quebec, Canada (2020-2021)
- **Research Assistant**, Dept. of Electrical Engineering, King Fahd University of Petroleum and Minerals University, Dhaharan, Saudi Arabia (2012-2016)
- **Teaching Assistant**, Dept. of Electrical Engineering, King Fahd University of Petroleum and Minerals University, Dhaharan, Saudi Arabia (2013-2015)
- **Network Engineer**, Home Plaza Company, Al-Khalil, Palestine (2011-2012)

Publications

- **Journal Papers**
  - **Bio-Jr1** S. Najmeddin, S. Aïssa, and S. Tahar. "Resource Allocation Optimization for UAV-Enabled Simultaneous Information and Power Transfer with NOMA, OMA and Hybrid Access Schemes", IEEE Transactions on Vehicular Technology, *Submitted*, 2021.
  - **Bio-Jr2** S. Najmeddin, S. Aïssa, and S. Tahar. "Energy-Efficient Resource Allocation in Multi-UAV Networks with NOMA", IEEE Transactions on Green Communications and Networking, 10.1109/TGCN.2021.3101200, July 2021.

- **Refereed Conference Papers**

  - **Bio-Cf1** S. Najmeddin, S. Aïssa, and S. Tahar. "Energy-Efficient Wireless Powered Communications with NOMA in Multi-UAV Aided Networks". IEEE Vehicular Technology Conference (VTC-Fall'21), pages 1–6, September 2021.

  - **Bio-Cf2** S. Najmeddin, S. Aïssa, and S. Tahar. "Energy-Efficient Resource Allocation for UAV-Enabled Information and Power Transfer with NOMA". Proc. IEEE Global Communications Conference (GLOBECOM'20), pages 1–6, December 2020.

  - **Bio-Cf3** S. Najmeddin, A. Bayat, S. Aïssa, and S. Tahar. "Energy-Efficient Resource Allocation for UAV-Enabled Wireless Powered Communications", Proc. IEEE Wireless Communications and Networking Conference (WCNC'19), pages 1–6, April 2019.

  - **Bio-Cf4** S. Najmeddin, and O. Hammi. "Novel Single-Input Single-Output Two-Box Polar Behavioral Model for Envelope Tracking Power Amplifiers", Proc. IEEE International Midwest Symposium on Circuits and Systems (MWSCAS'15), pages 1–4, August 2015.

  - **Bio-Cf5** M. Abusubaih, S. Najmeddin, and A. Khamayseh. "IEEE 802.11n Dual Band Access Points for Boosting the Performance of Heterogeneous WiFi Networks", Proc. ACM workshop on Performance Monitoring and Measurement of Heterogeneous Wireless and Wired Networks (PM2HW2N'13), pages 1–4, November 2013.